DOKUZ EYLÜL UNIVERSITY
GRADUATE SCHOOL OF NATURAL AND APPLIED SCIENCES

ANALYSIS OF MACHINERY FAULTS BY CURVE LENGTH AND WAVELET TRANSFORMS

by
Olcay KURBAK

September, 2010
İZMİR

ANALYSIS OF MACHINERY FAULTS BY CURVE LENGTH AND WAVELET TRANSFORMS

A Thesis Submitted to the
Graduate School of Natural and Applied Sciences of Dokuz Eylül University
In Partial Fulfillment of the Requirements for the Degree of Master of Science
in Mechanical Engineering, Machine Theory and Dynamics Program

by
Olcay KURBAK

September, 2010
İZMİR

M.Sc THESIS EXAMINATION RESULT FORM

We have read the thesis entitled **"ANALYSIS OF MACHINERY FAULTS BY CURVE LENGTH AND WAVELET TRANSFORMS"** completed by **OLCAY KURBAK** under supervision of **ASSOC.PROF.DR. ZEKİ KIRAL** and we certify that in our opinion it is fully adequate, in scope and in quality, as a thesis for the degree of Master of Science.

Assoc. Prof. Dr. Zeki KIRAL

Supervisor

Prof. Dr. Hira KARAGÜLLE

(Jury Member)

Asst. Prof. Dr. Nalan ÖZKURT

(Jury Member)

Prof.Dr. Mustafa Sabuncu
Director
Graduate School of Natural and Applied Sciences

ACKNOWLEDGMENTS

I would like to thank my supervisor, Assoc. Prof. Dr. Zeki KIRAL for his very valuable guidance, his support and his critical suggestions throughout my master thesis.

Also, I wish to express special thanks to Mr. Munur Akay, who is the research and development manager of the firm Klemsan Electric Electronics Inc., for his support during the design of the test apparatus.

I would like to thank also to Klemsan mold shop team for their helps during the manufacture of design apparatus.

I would like to thank also to my friend Serkan Guler for his support during the literature research and test apparatus design .

Finally, I wish to dedicate this thesis to my parents who have always supported to me.

Olcay KURBAK

2010

ANALYSIS OF MACHINERY FAULTS BY CURVE LENGTH AND WAVELET TRANSFORMS

ABSTRACT

Rotation is a basic motion which is widely used in machinery and equipments of industry and energy production sites. The continuity of the motion is very important necessity. An unpredictable fault causing a stop or decrease of the performance in the system cause serious financial losses. For that reason, the necessity of predicting the fault arises. Considering the rotating machinery it can be concluded that the system basically consists of a shaft, housings and rolling element bearings. The basic faults are basically run-out, unbalanced masses and rolling element faults in such a kind of rotating machinery. The prediction of these faults and taking the corresponding precautions before the failure causes big financial savings. The most important method for this purpose is condition monitoring. Vibration measurements are mainly and widely used tool for condition monitoring.

With the help of this point of view, the corresponding studies are worked on an experimental setup which can simulate the situation in the real life applications. The common faults such as run-out, unbalance and inner race defect cases were configured on the system and the condition was monitored by using vibration data. Run-out fault was performed with the help of movable housings, unbalance fault was created with the help of a circular plate, which has holes in the radial direction for mass fixing and roller bearing fault (especially inner race fault) was created with the help of electrical discharge machine (creating defects on the outer surface of inner race of bearing). Vibration measurements were performed with a portable vibration analyzer at a wide range of shaft speeds. Velocity and acceleration data were recorded. Vibration signals which were taken from healthy and faulty system were investigated in time domain by using statistical parameters such as rms, kurtosis and peak to peak. In the further step, curve length transform, which is a nonlinear time domain transform, was applied to vibration signals and again healthy and faulty system, were investigated in time domain by using statistical parameters such as rms,

kurtosis and peak to peak. In addition to this process, effect of scale factor on curve length transform was examined. In the next step, fast Fourier transform (FFT) and short time Fourier transform (STFT) were applied on the vibration signals and frequency spectrum was investigated with aiming to get the characteristic fault frequencies. In the final step, continuous wavelet transform was applied to vibration signals and corresponding spectrums were created for giving more information about the fault frequency, fault time and fault amplitude.

Keywords: Condition monitoring, vibration signal analysis, curve length transform, wavelet transforms.

MAKİNA HATALARININ EĞRİ UZUNLUĞU VE WAVELET DÖNÜŞÜMLERİ İLE ANALİZİ

ÖZ

Dönme hareketi endüstride ve enerji üretiminde kullanılan makina ve ekipmanlardaki en temel hareket biçimidir. Bu hareketin sürekliliği oldukça önemli bir gereksinimdir. Zira beklenmeyen hatalardan dolayı sistemin durması veya performansının düşmesi gibi durumlar ciddi maliyet kayıplarına yol açmaktadır. Bu sebeple, hatanın tahmin edilmesi ihtiyacı doğmuştur. Bir döner sistem düşünüldüğünde, sistemin temel olarak bir mil, milin dönme hareketini destekleyecek yataklar ve rulmanlardan oluştuğu gözlenecektir. Böyle bir modelde oluşabilecek temel hatalar incelenecek olursa, mildeki eksen kaçıklığı, mil üzerindeki dengelenmemiş kütle ve dönme hareketini destekleyen yataklarda kullanılan rulmanlardaki hatalar ilk planda öne çıkmaktadır. Bu hataların kritik hata seviyesine gelmeden önce belirlenip gerekli önlemlerin alınması ciddi kazanımlar sağlamaktadır. Bu amaçla kullanılan metotlardan en önemlisi durum izleme yöntemidir. Durum izleme yönteminde temel olarak titreşim sinyallerinin izlenmesi yaygın olarak karşımıza çıkmaktadır.

Bu gerçeklikten yola çıkılarak ilgili çalışma, pratikteki durumu temel anlamda simule edecek bir deney düzeneğinin üzerinde gerçekleştirilmiştir. Eksen kaçıklığı, dengelenmemiş kütle ve rulman hatası gibi pratikte oldukça karşılaşılan hata biçimleri sistem üzerinde oluşturulmuş ve titreşim ölçümü ile sistemin durumu izlenmeye çalışılmıştır. Eksen kaçıklığı deney düzeneğinin yataklarının hareket edebilir ve istenen pozisyonda sabitlenebilirliğiyle, dengelenmemiş kütle oluşumu deney düzeneği üzerindeki dairesel plakaya radyal yönde ek kütlelerin sabitlenmesiyle ve rulman hataları masuralı rulmanın iç bileziğine dalma erezyon tezgahında oluşturulan çukur ile oluşturulmuştur. Titreşim ölçümleri taşınabilir bir titreşim analizörü ile hız ve ivme cinsinden geniş bir mil hızı aralığında gerçekleştirilmiştir. Hatasız ve hatalı sistemlerden elde edilen titreşim sinyalleri, öncelikle rms, kurtosis, tepe tepe gibi bazı istatiksel göstergeler ile zaman ortamında

incelenmiştir. Daha sonra eğri uzunluğu dönüşümü olarak adlandırılan lineer olmayan bir zaman ortamı dönüşmü yine titreşim sinyallerine uygulanmış ve bu dönüşümün etkinliği istaiksel parametreler yardımıyla gözlemlenmiştir. Buna ek olarak ilgili dönüşümdeki skala faktörünün eğri uzunluğuna etkisi incelenmiştir. Bir sonraki aşamada titreşim sinyallerine FFT ve STFT dönüşümleri uygulanarak frekans ortamında karakteristik hata frekanslarının yakalanması amaçlanmıştır. Son bölümde ise çalışmanın ana merkezini oluşturan yeni bir sinyal işleme yöntemi kullanılmıştır. Sürekli wavelet dönüşümü ismindeki bu sinyal işleme yöntemi ile hatanın hangi zaman içerisinde, hangi frekansta ve hangi şiddette oluştuğu gibi detaylı bilgilere de ulaşılmıştır.

Anahtar Kelimeler: Durum izleme, titreşim sinyal analizi, eğri uzunluğu dönüşümü, wavelet dönüşümleri

CONTENTS

Page

M.Sc. THESIS EXAMINATION RESULT FORM ii
ACKNOWLEDGEMENTS.....iii
ABSTRACT.....iv
ÖZ vi

CHAPTER ONE – INTRODUCTION.....1

CHAPTER TWO – CONDITION MONITORING AND ROLLING ELEMENT BEARING.....7

2.1 Condition Monitoring 7
2.2 Condition Monitoring of Rotating 7
2.3 Application Areas of the Condition Monitoring for Rotating Machinery 10
2.4 Condition Monitoring of Roller Bearings 12
2.5 Rolling Element Bearings 12
2.5.1 Brief History.....12
2.5.2 Bearing Theory 13
2.5.3 Bearing Components 15
2.5.3.1 Inner Ring 16
2.5.3.2 Outer Ring.....16
2.5.3.3 Rolling Elements.....16
2.5.3.4 Cage 17
2.5.3.5 Seals.....17
2.5.3.5 Guide Ring.....17
2.5.4 Types of the Bearing Failures and the Causes.....17

CHAPTER THREE – EXPERIMENTAL SETUP.....21

3.1 Test Aparatus.....21
3.2 Instrumentation.....23
3.3 Measurement Conditions.....24

CHAPTER FOUR – TIME DOMAIN PARAMETERS.....26

4.1 Mean.....26
4.2 Standard Deviation.....26
4.3 Peak to Peak.....27
4.4 Root Mean Square.....27
4.5 Skewness.....27
4.6 Kurtosis 1.....28
4.7 Crest Factor.....28
4.8 GM^3_{av}.....28
4.9 Kurtosis 2.....29
4.10 6th Normalized Moment of Probability Density Function.....29

CHAPTER FIVE – TIME DOMAIN ANALYSIS.....30

5.1 Single Fault Experiment.....30
5.1.1 Shaft Misalignment Experiment.....30
5.1.2 Unbalance Experiment.....33
5.1.3 Inner Race Fault Experiment.....35
5.2 Combined Fault Experiments.....38
5.2.1 Shaft Misalignment and Inner Race Fault Experiment.....38
5.2.2 Unbalance and Inner Race Fault Experiment.....39

CHAPTER SIX – THE CURVE LENGTH TRANSFORM.....41

6.1 Definition of Curve Length Transform.....41

6.2 Curve Length Transform Application 42
6.3 Effect of Scale Factor on Curve Length Transform 55
6.3.1 Misalignment Fault 55
6.3.2 Unbalance Fault 56
6.3.3 Inner Race Fault 58
6.4 Comparisons of 6^{th} Moment & Kurtosis on Vibration Signal 59

CHAPTER SEVEN – FREQUENCY DOMAIN ANALYSIS 62

7.1 Bearing Characteristic Frequency 62
7.2 The Fast Fourier Transform 64
7.3 The Fast Fourier Transform Application For Inner Race Defect Case 64
7.4 The Short Time Fourier Transform (STFT) 71
7.5 STFT Application For Inner Race Defect Case 71
7.5.1 STFT of Velocity Signal For Inner Race Defect Case 72
7.5.2 STFT of Acceleration Signal For Inner Race Defect Case 75

CHAPTER EIGHT – WAVELET ANALYSIS 79

8.1 The Definition of Wavelet 79
8.2 Scale Frequency Relationship 81
8.3 CWT Application for the Healthy Case 82
8.4 CWT Application for Inner Race Fault Case 88
8.5 CWT Application for Inner Race Fault with Unbalance Case 94

CHAPTER NINE – CONCLUSION 98

REFERENCES 101

APPENDICES 105

CHAPTER ONE
INTRODUCTION

Importance of the condition monitoring techniques used in rotating machinery is increasing. This is because of the fact that implementation of these techniques brings considerable financial savings by reducing scheduled maintenance costs, and improving the productivity and safety. Moreover, early detection of incipient fault prevents major component failures. The malfunctions, which are mainly shaft misalignment, unbalance and rolling element bearing faults may cause serious failures in the rotating machinery process. To detect and diagnose the defect in rotating machinery, various condition monitoring techniques have been developed. The most powerful and commonly used method is the vibration analysis. There are many examples on the application of the vibration analysis for condition monitoring in the literature.

Hariharan & Srinivasan (2009) presented vibration analysis of the misaligned shaft-ball bearing system. In their study, experiments were performed on a rotor dynamic test apparatus to predict the vibration spectrum for shaft misalignment. The accelerations of the system were measured with a dual channel vibration analyzer under the misalignment condition. Moreover, numerical frequency spectra were obtained with the help of software, ANSYS. The results from the experiment and software were compared and it was seen that the results were in agreement. Both results showed that misalignment can be characterized primarily two times shaft running speed. However, if the misalignment characteristic frequency is not close enough to one of the system natural frequencies, the corresponding fault cannot excite the system appreciably. Therefore, there are cases where the misalignment response is hidden.

Tandon & Choudhury (1999) presented a review of vibration and acoustic measurement methods for the detection of defects in rolling element bearings. In their study, vibration measurements in both time and frequency domains along with signal processing techniques such as the high-frequency resonance technique were

covered. Acoustic measurement techniques such as sound pressure, sound intensity, and acoustic emission were reviewed. Detection of both localized and distributed categories of defect were explained. They observed vibration in the time domain that can be measured through the parameters such as RMS level, crest factor, probability density, and kurtosis. Kurtosis was mentioned as the most effective method. Vibration measurement in the frequency domain has the advantage that it can detect the location of the defect. However, the direct vibration spectrum from a defective bearing may not indicate the location of the defect especially at the initial stage. This problem has been overcome by some signal processing techniques. The high-frequency resonance technique is the most popular among the other techniques. The sound intensity, which is one of the acoustic techniques, was reported to be better than sound pressure measurements for bearing diagnostics. They observed in the related studies that, acoustic emission measurements are better than vibration measurements for detecting defects in rolling element bearings. In addition, acoustic emission signals can detect a defect even before it appears on the surface.

Kıral & Karagulle (2006) modeled the loading mechanism in a bearing structure, which houses a deep groove ball bearing having different localized defects and carrying an unbalanced force rotating with the shaft. The finite element vibration analysis was employed to simulate the bearing vibration signals. They proposed the use of the finite element vibration analysis with the proper loading model, which produces simulated vibration signals including the structural information in order to find the most efficient analysis method. The effects of different parameters such as the rotational speed, sensor location, angular position, and number of the outer ring defects, defect type (inner ring defect and rolling element defect) on the vibration monitoring methods were examined by using the time and frequency domain parameters. They reported that the envelope method can be used efficiently in order to detect the outer and inner ring defects, but rolling element defects were not easy to detect via envelope and band energy ratio procedures.

Orhan, Aktürk, & Çelik (2006) investigated diagnosis techniques of the ball and cylindrical roller element bearing defects by vibration monitoring and spectral

analysis. The vibration of a huge centrifugal pump with nine vanes was monitored. The experimental study had included three different cases. In case 1, the ball bearing has looseness on the housing. The vibration amplitudes were in low level at the initial stage. The vibration monitoring was continued and after a few weeks, they reported the increase in vibration levels indicating development in the looseness. In case 2, inner bearing vibration of a fan motor, which is supported by cylindrical rolling element bearing, was monitored. Existence of multipliers of outer race defect frequency in the spectrum was attributed to an outer race defect. In case 3, outer bearing vibration of the fan motor, which is supported by ball bearing, was monitored. Vibration frequencies in the frequency spectrum are matched to the ball bearing outer race defect frequency and its harmonics. In the study, ball bearing looseness, a ball bearing outer race defect, and a cylindrical bearing outer race defect were successfully diagnosed. They observed that ball and cylindrical rolling bearing defects were progressed in identical manner without depending on the type of rolling element.

Tao, Zhu, Ding & Xiong (2006) improved an alternative time-domain index for condition monitoring of rolling element bearings. In the time domain analysis, the kurtosis and Honarvar third moment are the major parameters. In this study, a new statistical moment was derived from the viewpoint of Renyi entropy. The comparisons were made by using both experimental data and simulations. As a result, it was seen that new moment called S_α has less sensitivity to the changing shaft speed than kurtosis and close to Honavar third moment. Furthermore, new statistical parameter is less susceptible to spurious vibrations than the others are.

Takeyasu & Higuchi (2006) derived 6th normalized moment as an alternative time parameter to the 4th normalized moment of probability density function which is also called kurtosis. In their survey, they proved that 6th normalized moment is much more sensitive than the kurtosis by using numerical examples.

Zong, Moody & Jiang (2006) studied on curve length transform such that used corresponding transform for the analysis of the heart beat signals and feature

extraction from body surface electrocardiograms (ECGs). The curve length transform is applied to the rolling element bearing diagnostics in this thesis.

Oztürk, Yeşilyurt and Sabuncu (2010) presented the use of vibration analysis in the early detection and monitoring of distributed pitting faults in gear trains. In this experimental study, the pits were seeded on all of the gear tooth surfaces in different degrees of severity. The gears were tested with each fault severity and resulting vibration data were recorded. Different kind of vibration analysis methods such as time, frequency, and wavelet transform (scalogram and its mean frequency variation) to each set of experimental data were presented. In the results it was seen that, presence of the pitting cannot be seen clearly unless fault severity is significant large. However, in the wavelet analysis the scalogram and especially its mean frequency variation provided early indication of presence of the pitting faults.

Khalid, Asok, K.P., D.K., & Steven (2007) investigated an alternative approach for detecting localized faults in the outer and inner races of a rolling element bearing using the envelope power spectrum of the Laplace Wavelet. The vibration model for a rolling element bearing with outer and inner race faults was given. The implementation of a proposed approach for the detection of localized ball bearing defects for both simulated and actual bearing vibration signals was presented. The wavelet shape parameters (damping factor and the center frequency) were optimized by maximizing the kurtosis value for the wavelet transform coefficients vibration signal. The application of this technique for both of the simulated and real bearing vibration signals showed the effectiveness of the wavelet power spectrum in extraction of the bearing characteristic frequencies and its harmonics for outer and inner race defective bearings from noisy vibration signals.

Mazanoğlu (2004) presented a study on the detection of a localized defect in a roller bearing using vibration analysis. The real roller bearing that was in both of healthy and faulty conditions was tested under different loads. The acquired vibration signals from experimental set was processed in time, frequency, and combined time and time- frequency domains. In conclusion, the presence of a fault was observed to

reveal clearly by time and frequency analyses when severity of fault was large. Frequency peaks that were the results of application of envelope analysis were observed at characteristic frequency of fault component. When the application of combined time-frequency analysis, indications of fault were observed in the combined time-frequency maps as local increases in the energy levels of vibration only where components of bearing came into contact with defect.

Chebil, Noel, Mesbah & Deriche (2009) presented a wavelet-based analysis technique for the diagnosis of faults in rotating machinery in terms of mechanical vibration. The choice between the discrete wavelet transform and the discrete wavelet packet transform was discussed with the choice of the mother wavelet and some of the common extracted features. In this work, it was seen that the peak locations in the spectrum of the vibration signal could also be used in the detection of a fault in ball bearings. For the identification of fault location and its size, the rms extracted from the terminal nodes of a wavelet tree can be reliably used as discriminating feature. It was found that the choice of the mother wavelet sym6 combined with the use of the rms feature produces excellent classification results.

Liu, Ling, and Gribonval (2002) proposed matching pursuit that is a new approach for detection of localized defects of rolling element bearings. Matching pursuit is an adaptive approach of time-frequency analysis unlike Short Time Fourier Transform and Wavelet Transform. They used vibration signals, which were collected from a test rig for different test configuration such as normal bearing, the bearing with an outer race defect, the bearing with an inner race defect. They processed vibration signals via matching pursuit approach. At the same time, they applied a typical traditional method, envelope detection to detect defects. They observed that matching pursuit approach was more sensitive than envelope detection.

The aim of this study is to detect the behavior of the rotating system having cylindrical roller bearing under different fault conditions such as run out, unbalance and inner race defect by using vibration signals. For this aim, an experimental test apparatus was designed and manufactured. The corresponding apparatus includes

two types of roller bearing (cylindrical roller bearing and spherical roller bearing). The housings in which the roller bearings are fixed are movable in the perpendicular direction to the rotation axis. Moreover, circular plate on the shaft is designed to create different unbalance forces on the system. Cylindrical roller bearing faults were generated artificially by using electrical discharge machine. Tests were performed for different fault conditions both separately and their combinations with each other for varying shaft speeds. Vibration signals were measured by a piezoelectric accelerometer located on the cylindrical bearing housing. This thesis is organized as follows. In Section 2, condition-monitoring systems on detecting rolling element faults and rolling bearing elements are described. In Section 3, experimental setup and vibration measurements are introduced. In Section 4, the statistical indices used in this study are described. In Section 5, the results of the time domain indices for the corresponding fault cases are given. In section 6, effect of curve length transform on the time domain analysis are described. Results of the frequency domain analyses are given in Section 7. The formulation of the wavelet transform and the results are given in Section 8. The concluding remarks are given in Section 9.

CHAPTER TWO
CONDITION MONITORING AND ROLLING ELEMENT BEARINGS

2.1 Condition Monitoring

Condition monitoring is the process of monitoring a parameter of condition in machinery, such that a significant change is indicative of a developing failure. It is a major component of predictive maintenance. The use of conditional monitoring allows maintenance to be scheduled, or other actions to be taken to avoid the consequences of failure, before the failure occurs. Nevertheless, a deviation from a reference value (e.g. temperature or vibration behavior) must occur to identify impeding damages. Predictive maintenance does not predict failure. Machines with defects are more at risk of failure than defect free machines. Once a defect has been identified, the failure process has already commenced and condition monitoring systems can only measure the deterioration of the condition. Intervention in the early stages of deterioration is usually much more cost effective than allowing the machinery to fail. Serviceable machinery includes rotating equipment and stationary plant such as boilers and heat exchangers.

2.2 Condition Monitoring of Rotating Machinery

Rotating machinery's condition monitoring is the process of monitoring the condition of a machine with the intent to predict mechanical wear and failure. Vibration, noise, and temperature measurements are often used as key indicators of the state of the machine. Trends in the data provide health information about the machine and help detect machine faults early, which prevent unexpected failure and costly repair.

The most commonly used method for rotating machines is called vibration analysis. Measurements can be taken on machine bearing casings with seismic or piezo-electric transducers to measure the casing vibrations, and on the vast majority of critical machines, with eddy-current transducers that directly observe the rotating

shafts to measure the radial (and axial) vibration of the shaft. The level of vibration can be compared with historical baseline values such as former starts and shutdowns, and in some cases established standards such as load changes, to assess the severity.

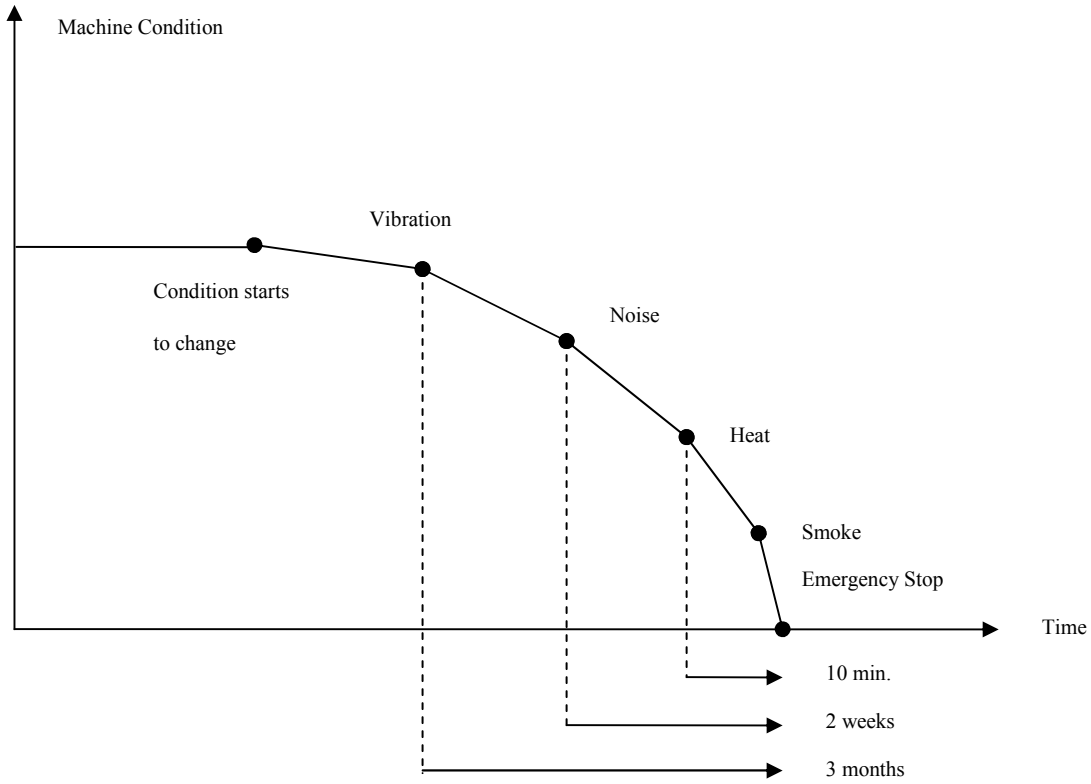

Figure 2.1 Machine condition vs time diagram

As shown in the Figure 2.1, vibrations are the first warning sign that a machine is prone to failure. This warning signs can provide 3 months of lead time before the actual failure date. Monitoring this data with vibration analysis allows predicting this failure early and scheduling proper maintenance.

Interpreting the obtained vibration signal is a complex process that requires specialized training and experience. There are many techniques for interpretation of vibration signals. The main techniques are the time domain analysis, the frequency domain analysis, and the time-frequency domain analysis. The easiest and fastest

method is time domain analysis of vibration signal. In the time-domain analysis, rotating system's faults are detected by monitoring the variation of some statistical indices such as the crest factor, skewness, root mean square, and kurtosis. A bearing is believed to be damaged when a monitoring index exceeds threshold values; however, it is usually difficult to determine the healthy condition values so the ratio between the healthy and faulty condition can be compared.

Frequency domain analysis is the most commonly used approach in the condition monitoring of the rotating machinery. In this method, defect detection is based on the analysis of the spectral information. The main advantage of this analysis is that it is relatively easier to identify and isolate certain frequency compent of interest (Tandon & Chouldhury, 1999). Frequency-based techniques, however, are not suitable for the analysis of non-stationary signals that are generally related to machinery defects (Jardine, Lin & Banjevic, 2005).

Non-stationary or transient signals can be analyzed by applying joint time-frequency domain techniques such as the short-time Fourier transform and wavelet transform (Liu, Wang, Golnaraghi, Liu, 2007). The short time Fourier transform (STFT) can be employed to detect the localized transient. Unfortunately, the fixed windowing used in the STFT implies fixed time-frequency resolution in the time frequency plane (Wadhwani, Gupta, Kumar, 2005). The difficulty is that the accuracy of extracting frequency information is limited by window relative to the duration of the interesting signal. To overcome the fixed time-frequency resolution problem, the recently developed wavelet based analysis becomes an efficient alternative in dealing with non-stationary type of machinery transient signal (Yen & Lin, 2000). The wavelet transform approach allows the detection of short-lived time component in the signals. This method is logical since high frequency components such as short bursts need high time resolution as compared with low-frequency components, which requires low frequency resolution (Wadhwani, Gupta, Kumar, 2005). Shortly, in fault detection, wavelet transform is the most popular time-frequency domain technique because of its more flexible multi-resolution (Luo,Osypiw, Irle, 2000).

2.3 Application Areas of the Condition Monitoring for Rotating Machinery

The condition monitoring technique is applied many types of rotary machines including machines that are vital to the plant or process and without which the plant or process cannot function such as the steam or gas turbines in a power plant, crude oil export pumps on an oil rig, the cracker in an oil refinery, and applied to machinery that is a key part of the process. However, if it fails the process can still operates such as boiler feed pumps in a power plant, wind turbines, air compressors and export pumps on an oil refinery.

Figure 2.2 Offshore wind turbines (Siemens, 2010).

Wind turbines as in the Figure 2.2 may be a good example for the application area of the condition monitoring process. Their vibration monitoring is one of the most important aspects because it helps determine the condition of rotating equipment. In a wind turbine, this equipment consists of the main bearing, gearbox, and generator.

Figure 2.3 shows where you can place vibration sensors to read data in the axial and radial directions. Depending on the applicable frequency range, you can use either position sensors (low range), velocity sensors (mid range), or accelerometers (high range) for this measurement. These vibration sensors are rigid mounted to the component of interest and return an analog signal proportional to the instantaneous local motion. An acquisition device that has a high sampling rate, high dynamic range, and anti-aliasing is ideal for this type of measurement.

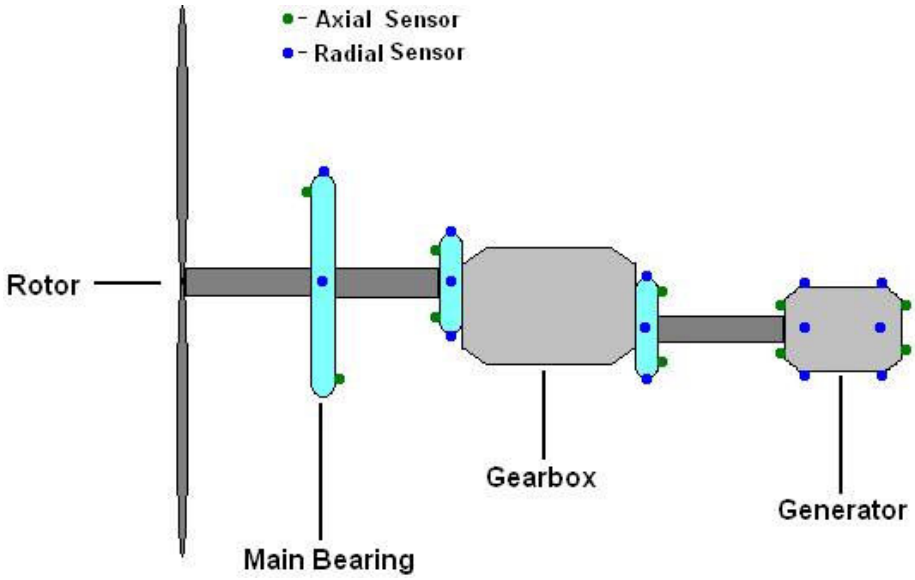

Figure 2.3 Vibration sensor positions for wind turbine model (National Instrument, 2010).

The principle of the condition monitoring system is based on the recording of structure-borne vibrations caused, for example, by bearings and gear tooth. The signals are received by means of special acceleration sensors attached to defined measuring points on the individual drive train components.

In a three-month start-up phase an individual vibration picture is drawn, the so-called "fingerprint" for the turbine and its components. The values measured are stored as parameters in a "black box." When the turbine is in operation, the actual

values measured are automatically compared online by means of measuring routines and measuring methods, such as frequency, envelope, and order analysis, with the reference values stored in the system. If there are discrepancies or limits are exceeded, the system automatically sends a warning or alarm message to the central remote monitoring center. There it is possible to draw accurate conclusions on the degree of change or wear based on experience gained over years and to initiate service activities in good time (Nordex Service, 2010).

2.4 Condition Monitoring of Roller Bearings

Roller bearing, by design, has extremely small clearances which do not allow a significant amount of shaft motion; forces from the shaft are transferred through the rolling elements to the bearings outer race and then ultimately to the bearing housing. Because of this transmission, a casing (bearing housing) measurement is normally acceptable for monitoring machines with rolling element bearings. Since the most of the machinery in a predictive maintenance program contains rolling element bearings, it is important to understand firstly to rolling element theory deeply.

2.5 Rolling Element Bearings

2.5.1 Brief History

Ancient man was forced to push or pull heavy objects to long distances just to make basic improvements to his life. This effort to move objects was reduced considerably when he discovered simple forms of lubrication such as mud or water.

With the invention of the wheel, it became obvious that rolling motion requires less effort and is less damaging to surfaces than sliding motion. It is not surprising therefore, that bearings, using only rolling motion, were eventually developed for use in machines, where metal sliding on metal causes considerable wear.

In fact, the first machine designs used journal (plain) bearings, which consisted of steel shafts running in wooden blocks, impregnated with lubricant. Eventually as steel improved and manufacturing techniques improved, two steel rings with rolling elements between, replaced them. First precision steel rolling element was designed by Friedrick Fisher in 1883. This resulted in a bearing with greatly reduced friction and extended service life.

2.5.2 Bearing Theory

Bearings can be categorized as two types, sliding bearings and rolling bearings. Sliding bearings includes linear bearings and journal bearings. Linear bearings are generally used for precise applications by precision engineering industries. Journal bearings can tolerate axial displacement of the shaft within certain limits.

All bearings that transfer loads via rolling elements are denoted rolling bearings. Depending on the type of rolling elements that are used rolling element bearings are divided into ball bearings and roller bearings. The balls in a ball bearing transfer the load over a very small surface point contact (Figure 2.4a) with the raceway. The load carrying capacity is therefore lower than for a roller bearing, where rollers transfer the load via line contact (Figure 2.4b) with the raceways.

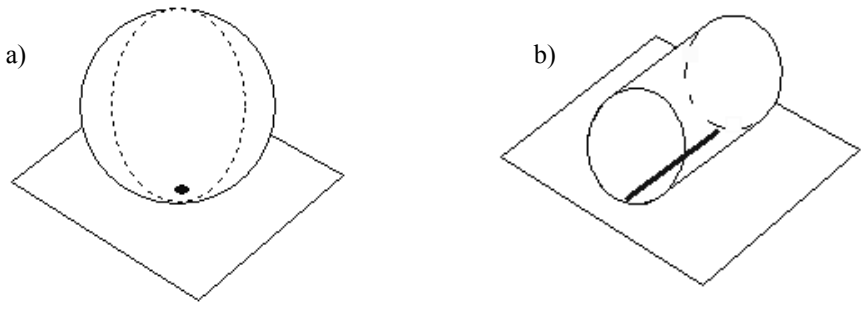

Figure 2.4 Type of contacts a) point contact b) line contact (SKF, 1996).

One of the factors which make the rolling element bearings so popular for most types of machinery is their very low friction. In a rolling element bearing the, inner ring rolls via the rolling elements in the outer ring. Under the same load conditions, the friction in a plain bearing is greater than that of a rolling bearing. Furthermore, the friction in a plain bearing varies with the rotational speed but is practically constant for a rolling bearing as shown in Figure 2.5.

There are two basic families, that is, ball and roller bearings, which are categorized according to the shape of the rolling elements. Each family includes a variety of bearing designs, depending on requirements such as available space for bearing, magnitude of load, direction of load, misalignment, speed, precision, quiet running, stiffness and axial displacement. Ball bearings are usually used in light to moderately loaded applications and are suited for high-speed operations. Roller bearings are able to support heavier loads than ball bearings. Rolling element bearings can also be classified into radial bearings and thrust bearings based on the direction of applied load. These types of direction-wise bearings are designed to transfer pure radial loads, pure thrust loads, or a combination of the radial and thrust loads.

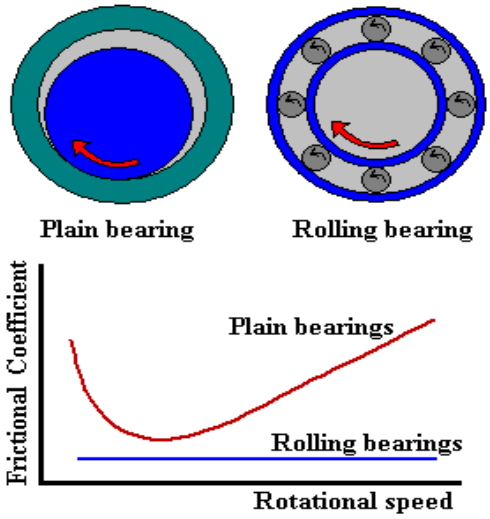

Figure 2.5 Frictional behaviour of plain and rolling bearings (SKF,1996).

A radial bearing is designed primarily for carrying a radial load. A thrust bearing is mainly intended to carry a thrust load (also called axial load) that is pushing force

against the bearing parallel to the shaft axis. Since most rolling bearings, both radial and thrust bearing, can also carry some radial and axial load**,** there is no clear distinction between them. However, bearings with a contact angle α<= 45° (shown in Figure 2.6) are considered radial bearings and their ratings are given by radial load. Bearings with a contact angle α >45° are considered thrust bearing and are rated by axial load.

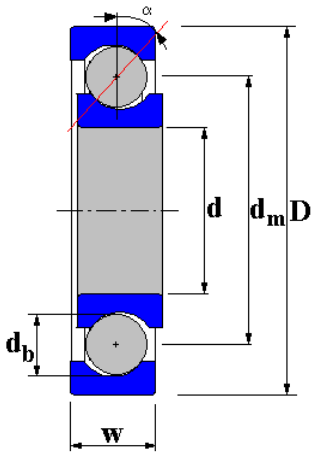

D : Outer diameter

d_m : Pitch diameter

d : Bore diameter

d_b : Ball diameter

w : Raceway width

α : Contact angle

Z : Number of ball

Figure 2.6 Bearing geometry.

2.5.3 Bearing Components

All rolling bearings are composed of four basic parts: inner ring, outer ring, rolling elements, and cage or separator as seen in Figure 2.7.

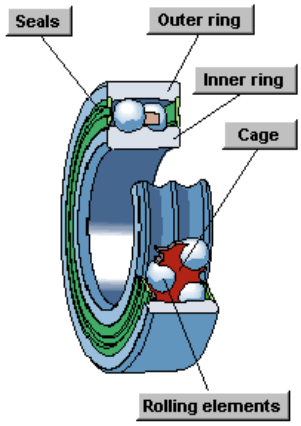

Figure 2.7 Components of the rolling bearing (SKF, 1996).

2.5.3.1 Inner Ring

The inner ring is mounted on the shaft of the machine and is mostly the rotating part. The bore can be cylindirical or tapered. The raceways against which the rolling elements run have different forms such as spherical, cylindirical or tapered, depending on the type of rolling elements.

2.5.3.2 Outer Ring

The outer ring is mounted in the housing of the machine and in most cases it does not rotate. The raceways against which the rolling elements run have different forms depending on the type of rolling elements. The forms of the raceways may be spherical, sylindirical or tapered.

2.5.3.3 Rolling Elements

The rolling elements may have different forms as shown in Figure 2.8. The forms of the rolling elements may be balls, cylindirical rollers, spherical rollers, tapered rollers or needle “rollers. They rotate against the inner and outer ring raceways and transmit the load acting on the bearing via small surface contacts separated by a thin lubricating film. The rolling elements are made of carbon chromium steel, also called bearing steel.

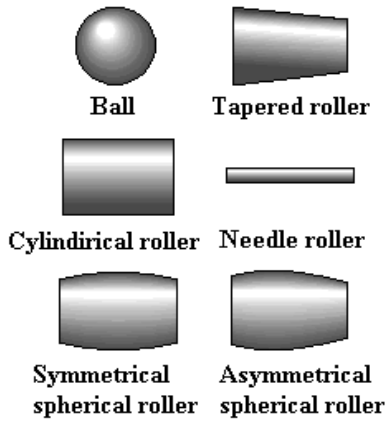

Figure 2.8 Types of rolling elements (SKF, 1996).

2.5.3.4 Cage

The cage separates the rolling elements to prevent metal-to-metal contact between them during operation that would cause poor lubrication conditions. With many bearing types the cage holds the bearing together during handling. Cages are made from cold rolled steel strip.

2.5.3.5 Seals

Seals are essential for a long and reliable life of the bearing. They protect the bearing from contamination and keep the lubricant inside the bearings.

2.5.3.6 Guide Ring

Guide rings are used in some spherical roller bearings that demand extremely high quality. The main function of the guide rings is to guide the rollers in the bearings so that they can rotate parallel to the shaft and distribute the load evenly to the raceways.

2.5.4 Types of the Bearing Failures and the Causes

Rolling element bearings are among the most important and popular components in the vast majority of machines. Additionally, the component most likely to cause machine downtime is the bearing, because all machine forces are transmitted through the bearings. Therefore, rolling element bearings have been the subject of extensive research over the years to improve their reliability. However, since a large number of bearings are associated with any critical process, system failure due to any individual bearing failing can occur in a short period. There are many reasons for early failure, such as heavy loading, inadequate lubrication, careless handling, ineffective sealing, or insufficient internal bearing clearance due to tight fits. Each of these factors results in its own particular type of damage and leaves its own special imprint on the bearing.

Rolling bearing damage may result in a complete failure of the rolling bearing at least, however, in a reduction in operating efficiency of the bearing arrangement. Only if operating and environmental conditions as well as the details of the bearing arrangement (bearing surrounding parts, lubrication, sealing) are completely in tune, can the bearing arrangement operate efficiently. Bearing damage does not always originate from the bearing alone. Damage due to bearing defects in material or workmanship is exceptional.

The types of mechanical bearing failure and their frequencies are categorized in Table 2.1. The most frequent bearing failure category is corrosion, which is lubrication related. Chemical reaction occurs between the oil and the surface of the bearing, generally from water or other corrosive materials present in the oil. Dimensional discrepancies of rolling element bearings are a consequence of damage prior to or during service. The causes of dimensional discrepancies could be manufacturing flaws, improper handling or installation, and severe overloading during service. Foreign objects, carried by contaminated lubricant, are trapped inside the bearing between the rolling element and the raceway, and are overloaded. Understanding the underlying reason for the defects and their consequences in terms of failures gives the diagnostic clues to detect early failures.

Table 2.1 The distribution of the bearing failure (Lee, 2000).

Reason	**Failure percent**
Corrosion	35 %
Dimensional Discrepancies	29 %
Foreign Objects	24 %
Other	10 %
Fatigue	2 %

Bearing failures that are not responsible for material fatigue are generally classified as premature. Typical reasons for rolling bearing damage (FAG, 1985):

Inexpert mounting:

- incorrect mounting method, wrong tools
- contamination
- too tight fit
- too loose fit
- misalignment

Abnormal conditions during operation:

- overload, absence of load
- vibrations
- excessive speeds

Unfavorable environmental influences:

- external heat
- dust, dirt
- passage of electric current
- humidity
- aggressive media

Inadequate lubrication:

- unsuitable lubricant
- lack of lubricant
- over lubrication

Each of the different causes of bearing failure generates its own characteristic damage. Such damage is also known as primary damage, which, in turn, creates secondary, failure-inducing damages, such as spalling and cracks. Most failed bearings frequently display a combination of primary and secondary damage. The types of damage are summarized in Table 2.2 (Afshari, 1998).

Table 2.2 Types of bearing damages (Afshari, 1998).

	DAMAGE TYPE		
	Primary Damages	**Secondary Damages**	**Other Damages**
DAMAGE CASES	Indentations Corrosion Wear Electric current damage Surface distress	Spalling Cracks Cage damage Score marks	Roll out

CHAPTER THREE
EXPERIMENTAL SETUP

3.1 Test Apparatus

Test apparatus used in this study is a simplified model of rotating machinery. The test set up includes basically a shaft, two housings with roller bearings (one is ball bearing and the other one is cylindrical roller bearing) and a circular disc. The corresponding apparatus as seen from Figure 3.1 is designed to allow monitoring three different types of faults in the system such as unbalance, shaft misalignment (run-out), and bearing faults.

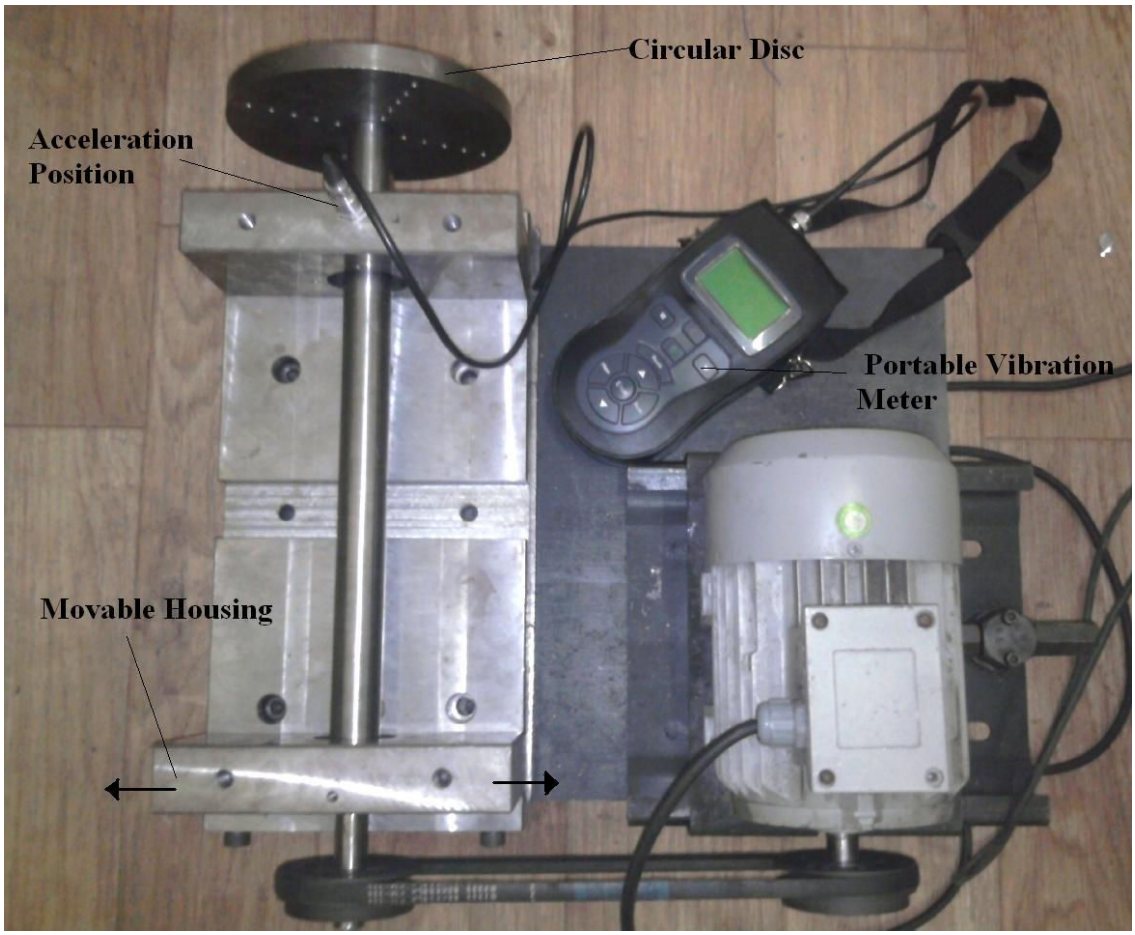

Figure 3.1 Top view of the experimental setup.

For creating unbalance forces on the rotating system, a circular disc, which have equally spaced holes in the radial direction, is designed. Circular disc is assembled to the shaft with the help of retaining rings. The unbalance condition is provided by adding masses on the circular discs through the holes.

The test apparatus is designed in such a way that its housings have ability of moving in the direction perpendicular to the shaft rotation axis. These movable housings give the opportunity of controlling the run-out distance in the system. Moreover after setting the housing position for creating the desired run-out, housing are fixed in that position with the help of bolts and nuts. In the corresponding experiments, 3 mm run out is created on the system.

The housings in the test apparatus have roller bearings inside. In this study, two different type of test bearings are chosen, one as deep groove ball bearing and the other one is FAG Cylindrical roller bearings NU306-E-TVP2 type. The corresponding roller bearings are assembled inside the housings without causing any damage. The deep groove ball bearing is in healthy condition. However, the cylindrical roller bearing has two versions (healthy one and faulty one). The fault in the cylindrical roller bearing is inner race fault. The predefined cavity is artificially generated on the outer surface of the inner race with the help of an electrical discharge machine. Corresponding fault can be seen in the Figure 3.2.

Experimental setup is configured each time for the desired fault type. After the configuration, the system is started to run and the vibration data are collected for each shaft speed. The experiments are performed between 750 rpm – 1750 rpm shaft speed. The velocity and acceleration of the vibrations are collected from the test set up with the help of a piezoelectric type of accelerometer. The measurements are taken from the rear side housing (one with cylindrical roller bearing) and outer surface of the cylindrical roller bearing.

The front side of the shaft where the healthy bearing is mounted is extended in order to attach a pulley for driving the shaft by an electrical motor with a V-shaped

belt. The motor provided by AC power supply is monophase. Power of the motor is 0.55 kW. The speed of the motor is controlled by a speed controller. All of the components are put on a heavy plate. Rubber foots were mounted under the plate in order to reduce the vibration transmission from ground to test bearing. Schematic view of the experimental set-up is given in Figure 3.3.

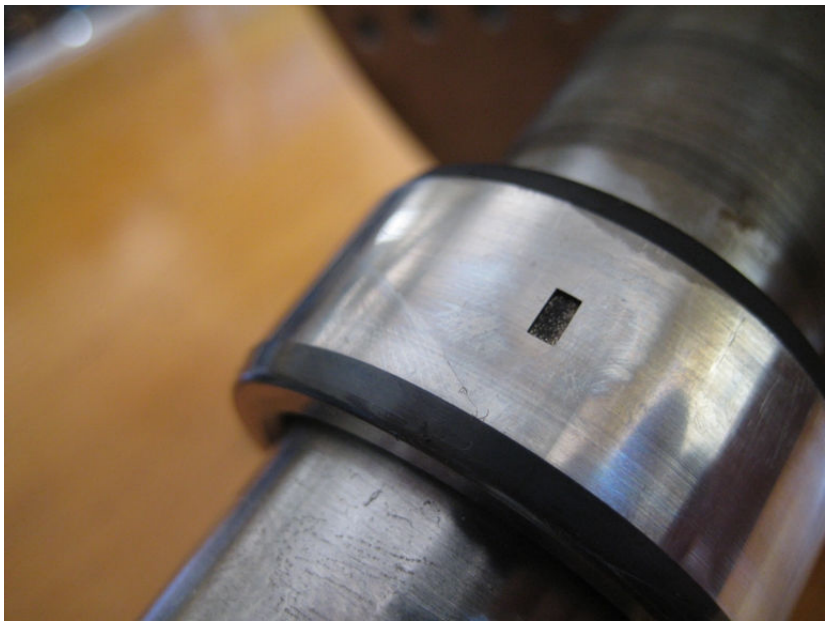

Figure 3.2 Inner race fault in the cylindrical roller bearing.

3.2 Instrumentation

In this thesis, vibration measurements are performed by a portable vibration meter, Sendig 911 as shown in Figure 3.1. The portable device has a piezoelectric accelerometer of the type L14A. The accelerometer sensitivity is 4.86 [pC/ms^{-2}] at 20 ^{0}C. The device can measure vibration signals in terms of acceleration, velocity, and displacement and can save these signals into its memory. These signals can be fetched from the device memory to the computer by RS-232 connection. Sendig 911 has its own data acquisition software, which is called as MCME2.0H. A sample screen shot of the software is given in Figure 3.4. The vibration signals gathered via the vibration meter can be processed in both time and frequency domains. The

sampling frequency of the vibration measurement is 2560 Hz and the total duration of measurement is 0.39 seconds.

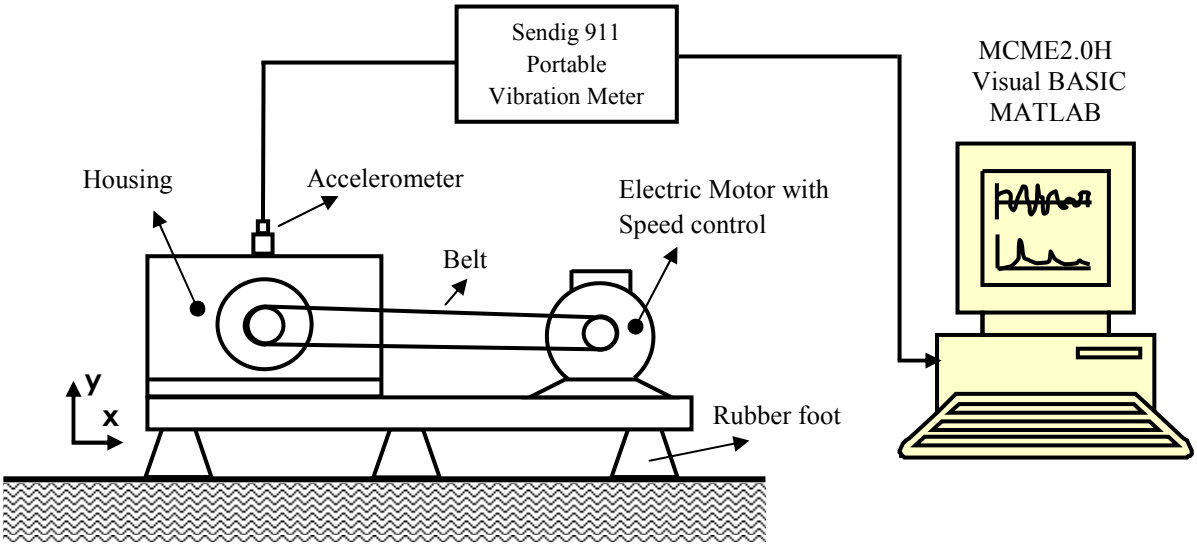

Figure 3.3 Schematic view of the experimental set-up.

3.3 Measurement Conditions

The vibration signals are measured firstly for the healthy condition, which means healthy roller bearings with balanced system and aligned shaft. The rotating system is started at 750 rpm and the corresponding velocity and acceleration data are recorded. The speed of the shaft is changed from 750 rpm to 1750 rpm by 250-rpm increment after each measurement. The vibration signals with velocity and acceleration parameters are recorded. In the second step, one of the movable housing is shifted 3 mm in the perpendicular direction to the shaft axis and fixed its position with the help of a nut and bolt for creating a misalignment condition and same measurement procedure is repeated. In the third step, system is returned to the aligned condition configuration and an unbalance mass (14 gr x 10 mm) is added to the circular plate and same measurement procedure is repeated.

In the forth step, unbalanced mass is removed and faulty roller bearing is changed with the healthy bearing and same measurement procedure is repeated. The defect of

the bearing is inner race fault, which is generated artificially by using electrical discharge machine as seen in Figure 3.2. In other steps, additional faults (unbalance & run-out) to the inner race fault are generated and measurements are recorded. In all of the experiment, the vibration signals are taken from the outer surface of cylindrical roller bearing. The velocity and acceleration parameters are recorded.

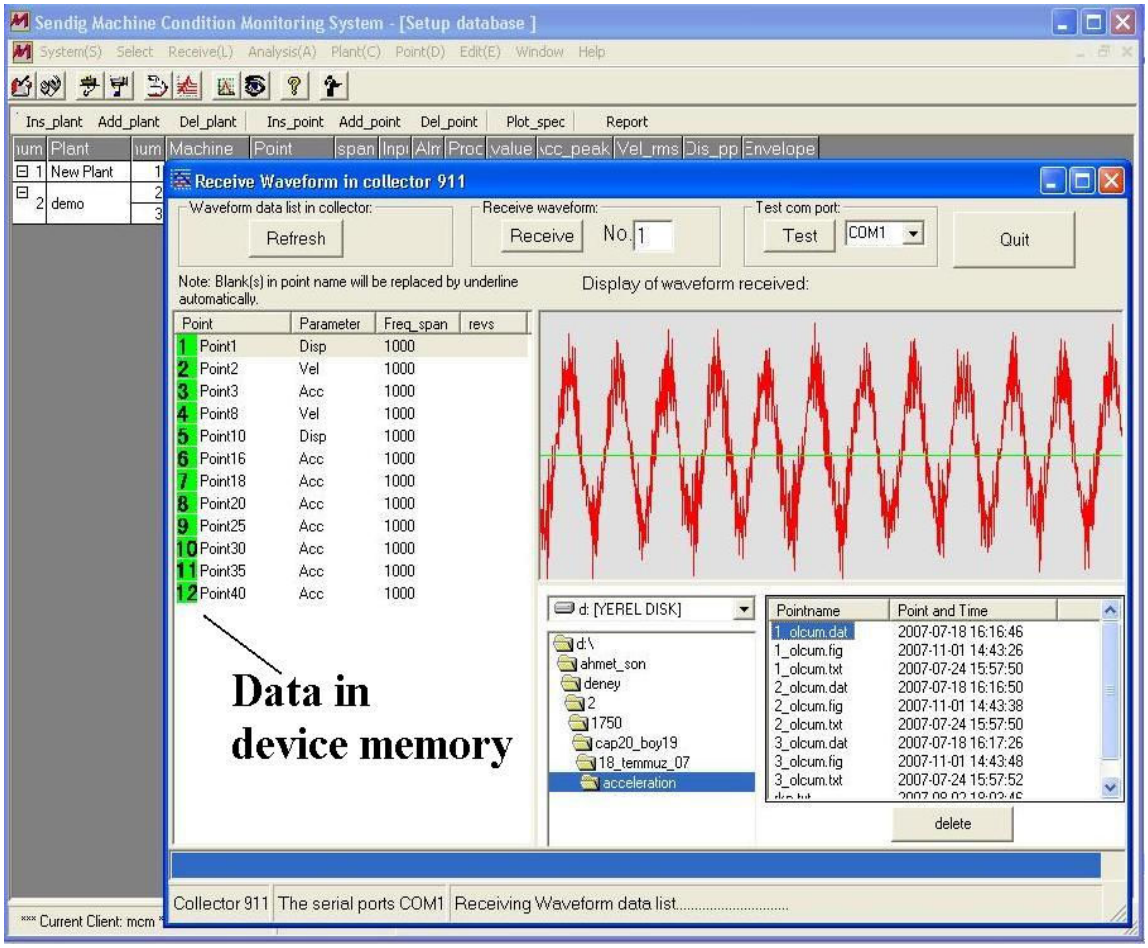

Figure 3.4 Screen shot of the software.

CHAPTER FOUR
TIME DOMAIN PARAMETERS

In this study, different statistical indices derived from the experimental vibration signals are used to identify the condition of the rotating system by taking measurement from outer ring of the cylindrical rolling element bearing. Different moments of the vibration signals for different faulty conditions such as run out, unbalance and rolling element fault (inner race fault) are calculated and then compared with the reference values obtained for balanced, aligned, and healthy bearing system. The statistical indices used in the time domain analysis are described in this section.

4.1 Mean

The mean value is the arithmetic mean of the vibration signal. The mean value of a discrete time signal x having N samples is calculated (Neter, Wasserman, & Whitmore,1988) as

$$\bar{x} = \frac{1}{N}\sum_{i}^{N} x_i \tag{4.1}$$

Generally, the mean value does not give useful knowledge about a widely distributed signal.

4.2 Standard Deviation (σ)

Standart deviation gives useful knowledge about a widely distributed signal. If the values of signal are close to the mean, standart deviation is low, otherwise standart deviation is high. It is equal to square root of variance (Heperkan, Kesgin, 2002). The standart deviation of a signal x is calculated as,

$$\sigma = \sqrt{\frac{1}{N-1}\sum_{i}^{N}(\bar{x} - x_i)^2} \tag{4.2}$$

4.3 Peak to Peak (p2p)

Peak to peak is another statistical index. Peak to peak is denoted as the difference between the maximum value and the minimum value of the signal. It is given as

$$p2p = x_{max} - x_{min} \tag{4.3}$$

4.4 Root Mean Square (rms)

The root mean square (rms) value of a vibration signal shows the energy content of the signal (Miettinen, Leinonen, 1999). For a vibration signal the rms values is calculated as

$$rms = \sqrt{\frac{1}{N}\sum_{i=1}^{N} x_i^{\,2}} \tag{4.4}$$

4.5 Skewness

The 3rd standardized moment of the vibration signal is called as the skewness. Its value indicates the asymmetry of a distribution around its mean. Positive skewness denotes a distribution with an asymmetric tail extending toward values that are more positive. In consideration of negative skewness, a distribution with an asymmetric tail extending toward values that are more negative is observed. A symmetrical distribution is observed when skewness value is zero (Miettinen, Leinonen, 1999). The skewness value of a vibration signal is calculated as

$$\text{skewness} = \frac{1}{N\sigma^3}\sum_{i=1}^{N}(x_i - \bar{x})^3 \tag{4.5}$$

4.6 Kurtosis 1 (kurt1)

The 4th standardized moment is named as kurtosis. Kurtosis indicates peakeness or flatness of a distribution compared with the normal distribution. Positive kurtosis denotes a relatively peaked distribution. Negative kurtosis denotes a relatively flat distribution. The kurtosis value of a vibration signal is calculated (Neter, Wasserman,& Whitmore, 1988) as

$$kurtosis = \frac{1}{N\sigma^4}\sum_{i=1}^{N}(x_i - \bar{x})^4 \tag{4.6}$$

4.7 Crest factor (cf)

The peak amplitude of a vibration waveform divided by the rms value determines the crest factor. Crest factor value is expected to be between 2 and 6 in healthy situation. This value increases when a fault appears (Lebold, McClintic, Campell, Byington, & Maynard, 2000). Crest factor value is given by the following equation

$$cf = \frac{x_{\max} - x_{\min}}{rms(x)} \tag{4.7}$$

4.8 GM^3_{av} (S_α)

New statistical moment is derived from the viewpoint of Renyi entropy. According to comprehensive comparisons of kurtosis, Honarvar third moment ($S_{r)}$ and this moment, a new moment has a better overall performance than kurtosis and S_r. On the one hand, this moment behaves much like kurtosis but is less susceptible to spurious vibrations, which is considered to be one of the main shortcoming of higher statistical moments including kurtosis. On the other hand, from the viewpoint of sensitivity to incipient faults, which is the major drawback of lower statistical moments including S_r, the new moment is superior to S_r. Moreover, the sensitivity of

this new moment to changes of bearing speed and load is also less than kurtosis and is close to that of S_r. (Tao, Zhu, Ding, & Xiong, 2006)

$$s_\alpha = \frac{1/N\sum_{i=1}^{N}(x_i)^3}{\left[1/N\sum_{i=1}^{N}|x_i|\right]^3} \tag{4.8}$$

4.9 Kurtosis 2 (kurt2)

In the literature, another approach to kurtosis is also available. (Tao, Zhu, Ding & Xiong, 2006). The corresponding kurtosis is symbolized as $GM^2{}_{sv}$ and formulated as below:

$$GM^2{}_{sv} = \frac{1}{N\sigma^4}\sum_{i=1}^{N}(x_i)^4 \tag{4.9}$$

4.10 6th Normalized Moment of Probability Density Function

6^{th} normalized moment of probability density function which is given below is shown as more sensitive parameter than kurtosis (Takeyasu, Higuchi, 2006)

$$Q = \frac{1}{N\sigma^6}\sum_{i=1}^{N}(x_i - \bar{x})^6 \tag{4.10}$$

CHAPTER FIVE
TIME DOMAIN ANALYSIS

In this section rms, kurtosis, peak to peak (p2p), skewness, crest factor, standard deviation, S_α and 6^{th} normalized moment values of raw velocity and acceleration signals are examined under different faulty conditions such as shaft misalignment, unbalance, rolling element fault (inner race defect) and their combinations at various shaft speeds ranging from 750 rpm to 1750 rpm. In the first step, vibration measurements are performed for the healthy system and corresponding statistical indices are calculated at each shaft speed. In the second step, system is configured for the corresponding faulty condition, vibration measurements are performed and statistical indices for faulty condition are calculated at each shaft speed. In the final step, the ratios of faulty/healthy are calculated for each statistical parameter and ratios versus shaft speed figures are obtained.

5.1 Single Fault Experiments

5.1.1 Shaft Misalignment Experiment

In the shaft misalignment experiments, the test set up is configured in such a way that, cylindrical roller bearing (healthy) housing position is fixed at the center and the spherical bearing housing is shifted 3 mm to the left side and fixed there. The vibration measurements are taken from the outer race of the cylindrical roller bearing for each shaft speeds. The ratio of the vibration amplitudes of faulty (shaft misalignment) to healthy condition is calculated for each statistical parameter with the changing rotation speed. The corresponding curves are obtained as from Figure 5.1 to Figure 5.4.

Sample vibration velocity signal (for run out experiment at 1250 rpm shaft speed) can be seen in Figure 5.1.

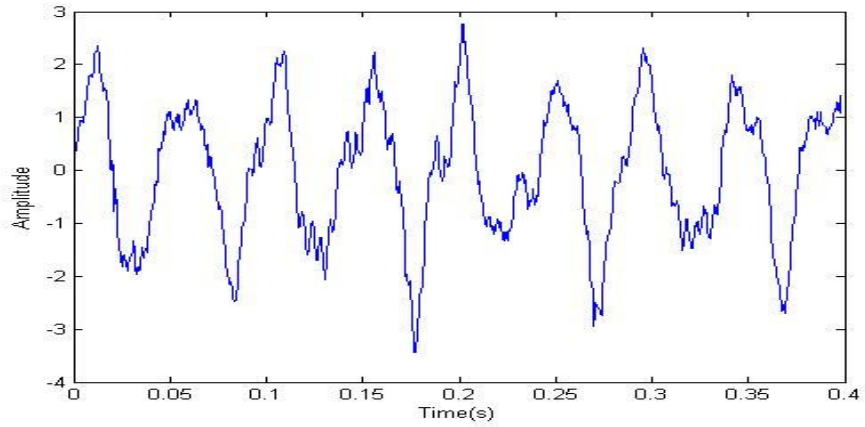

Figure 5.1 Vibration velocity signal of raw data for run out experiment at 1250 rpm.

The statistical parameters are calculated for run out fault. In the raw data of vibration velocity signals (Figure 5.2), two statistical indices, standard deviation, and peak to peak values are above the healthy condition ratio. They show similar behavior to changing shaft speed. Their ratio increase up to 1250 rpm and gets 1.2 as a peak value at that shaft speed and then stay constant come with the increasing shaft speed.

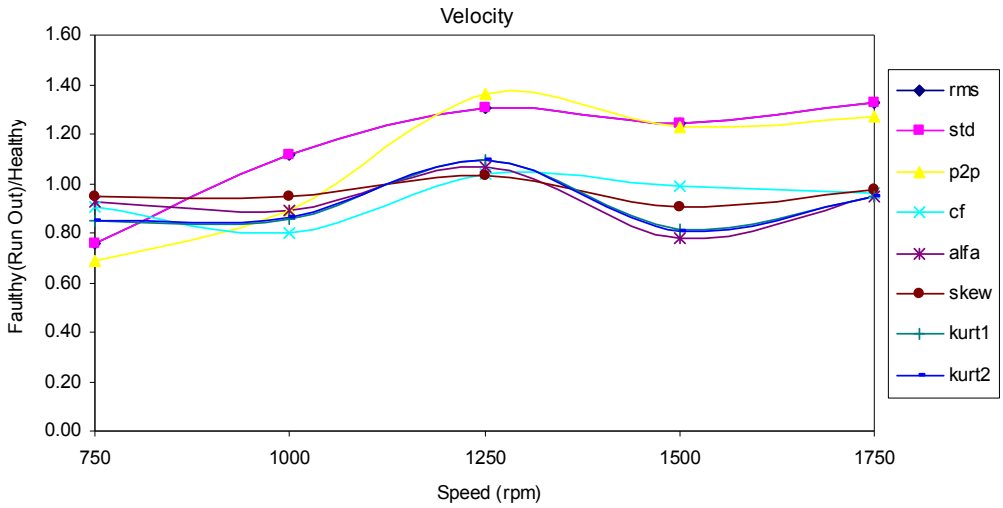

Figure 5.2 Statistical indices of raw velocity data for 3 mm run out error.

Same analysis is performed for the vibration acceleration data. The sample acceleration signal for the run out experiment at 1250 rpm can be seen in Figure 5.3.

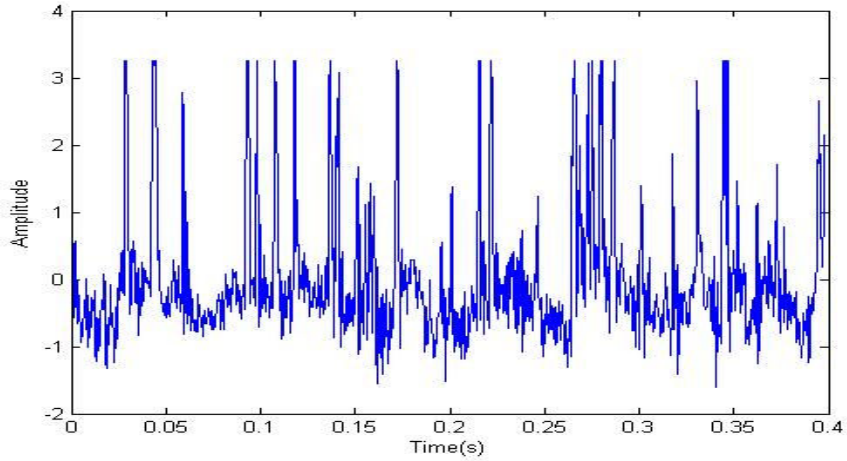

Figure 5.3 Acceleration signal of raw data for run out experiment at 1250 rpm.

In the raw data of vibration acceleration signals (Figure 5.4), all the statistical indices have constant values up to 1250 rpm. Up to this shaft speed, they take nearly healthy condition ratio values. Starting from 1250 rpm, all the statistical indices have increasing trend up to 1500 rpm. All of them make a peak at that shaft speed and decrease for further increasing shaft speeds. The kurtosis (kurt 2) and alfa indices take the highest values at the 1500-rpm shaft speed.

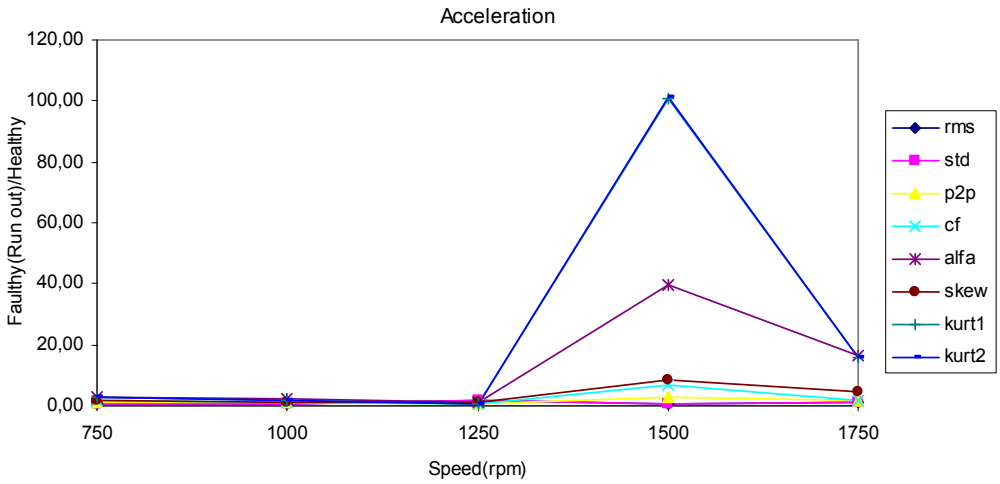

Figure 5.4 Statistical indices of raw acceleration data for 3 mm run out error.

5.1.2 Unbalance Experiment

In the unbalance experiments, spherical roller bearing and cylindrical roller bearing housing positions are fixed in concentric position. The unbalanced mass is added on symmetrically drilled circular plate in the system. The vibration measurements are taken from the outer race of the cylindrical bearing. The ratio of the vibration amplitudes of faulty (unbalance) to healthy condition is calculated for each statistical parameter with the changing rotation speed. The corresponding curves are obtained as in the Figure 5.5 and Figure 5.8.

Sample vibration velocity signal (for unbalance experiment at 1500 rpm shaft speed) can be seen in Figure 5.5

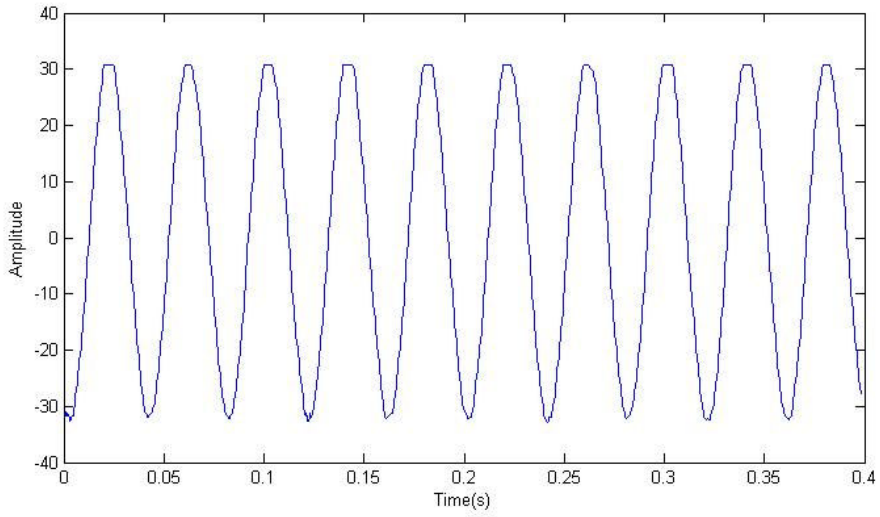

Figure 5.5 Velocity signal of raw data for unbalance experiment at 1500 rpm.

In the raw velocity data two statistical indices (Figure 5.6), standard deviation, and peak to peak values are above the healthy condition. The statistical indices (standard deviation and peak to peak values) show a nearly sinusoidal behavior with the changing shaft speed. However in every cycle, faulty/healthy ratio increases.

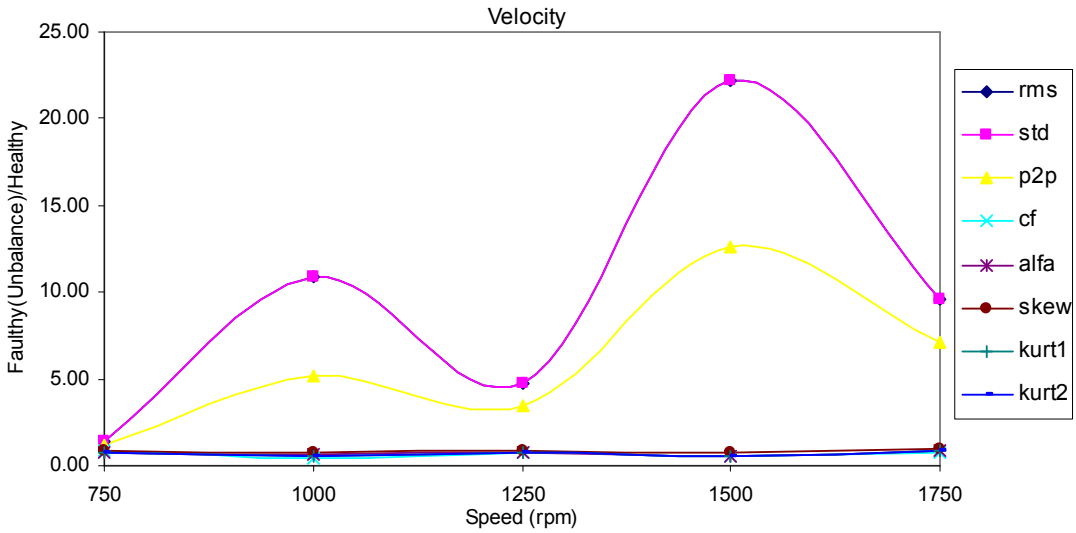

Figure 5.6 Statistical indices of raw velocity data for unbalance.

Same analysis is performed for the vibration acceleration data. The sample acceleration signal for the unbalance experiment at 1500 rpm can be seen in Figure 5.7.

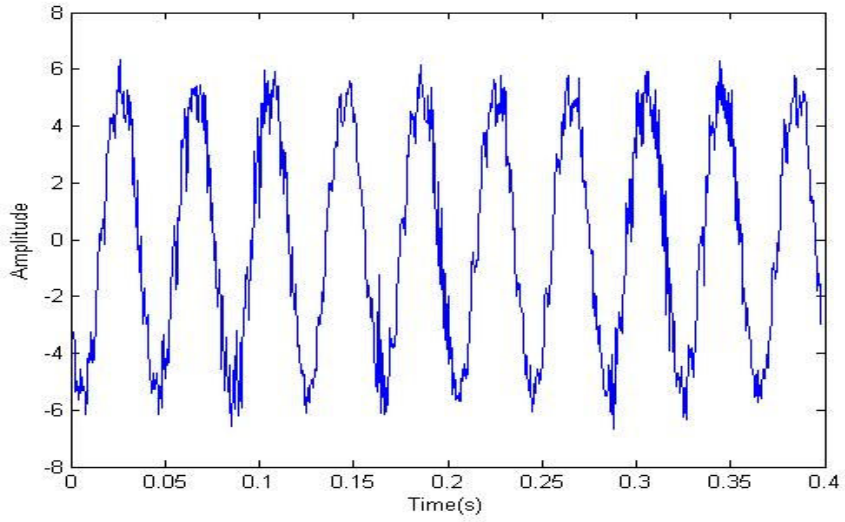

Figure 5.7 Acceleration signal of raw data for unbalance at 1500 rpm.

In the raw acceleration data, two statistical indices (Figure 5.8), standard deviation, and peak to peak values are above the healthy condition. Standard deviation has a constant value up to 1000 rpm shaft speed. With the further increase

in shaft speed, standard deviation values increases. Moreover, peak to peak index also shows faulty condition after 1250 rpm shaft speed and its ratio values increases with the increasing shaft speed.

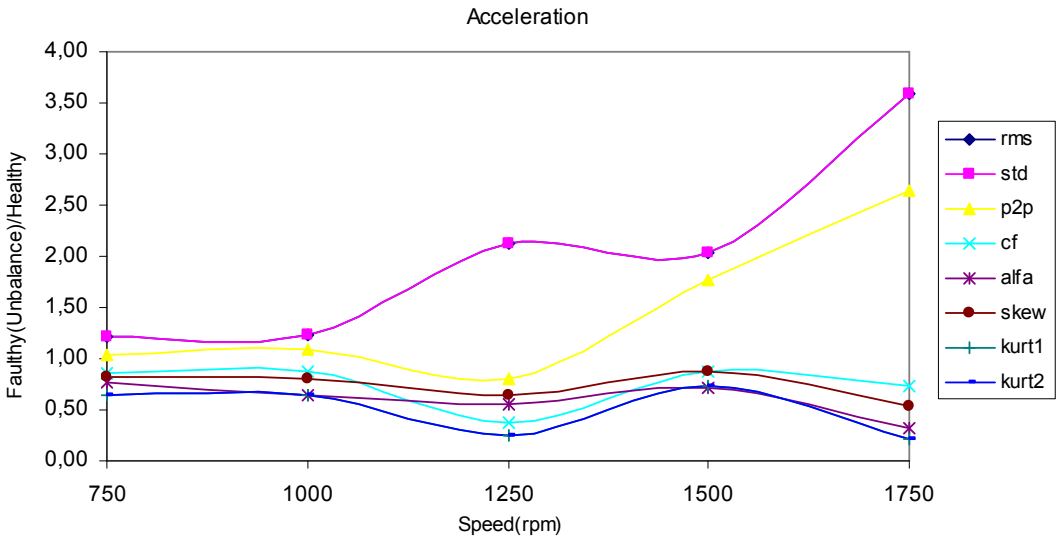

Figure 5.8 Statistical indices of raw acceleration data for unbalance.

5.1.3 Inner Race Fault Experiment

In the inner race fault experiment, the healthy cylindrical roller bearing is changed with the faulty one. Fault on the outer surface of the inner race was created by electrical discharge machine. The vibration measurements are taken from the outer race of the cylindrical bearing. The ratio of the vibration amplitudes of faulty (inner race defect) to healthy condition is calculated for each statistical parameter with the changing rotation speed. The corresponding curves are obtained from Figure 5.9 to Figure 5.12.

Sample vibration velocity signal (for inner race fault experiment at 1250 rpm shaft speed) can be seen in Figure 5.9.

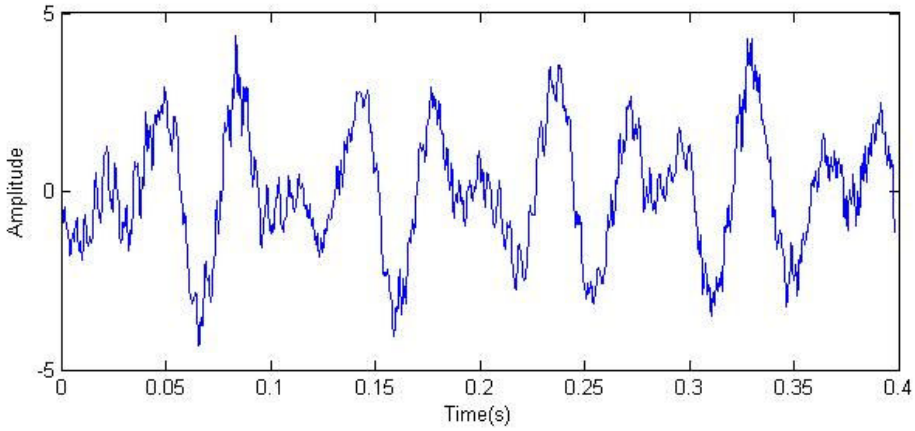

Figure 5.9 Velocity signal of raw data for inner race fault condition at 1250 rpm.

In the raw velocity data, two statistical indices (Figure 5.10), standard deviation and peak to peak values are above the healthy condition up to 1500 rpm. As the shaft speed increases from 1500 rpm, standard deviation and peak to peak values decrease. Moreover, all the other statistical indices start to increase at 1500 rpm.

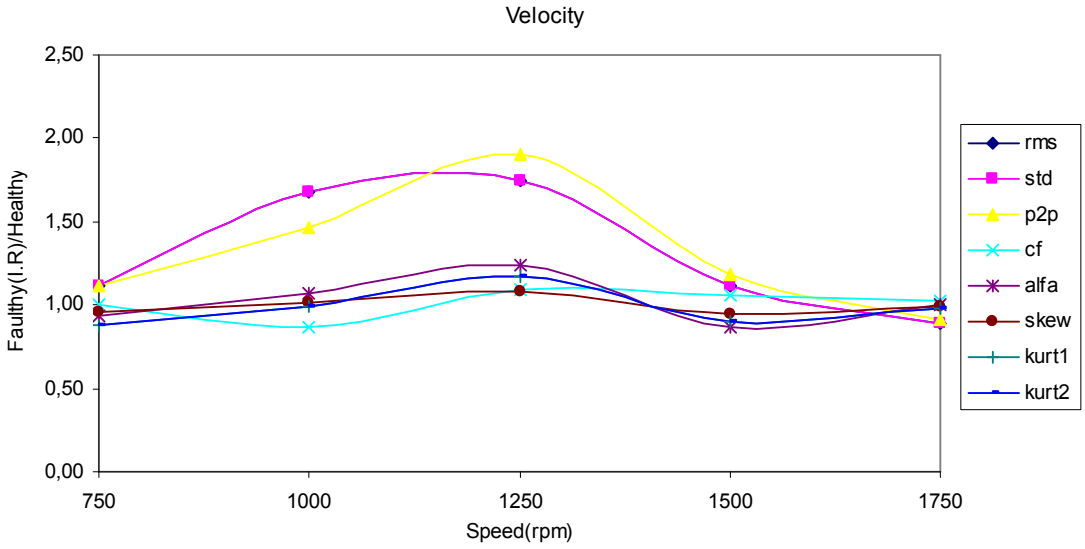

Figure 5.10 Statistical indices of raw velocity data for inner race defect.

In the next step, same analysis is performed for the acceleration data. The acceleration signal for the run out fault at 1250 rpm can be seen in Figure 5.11.

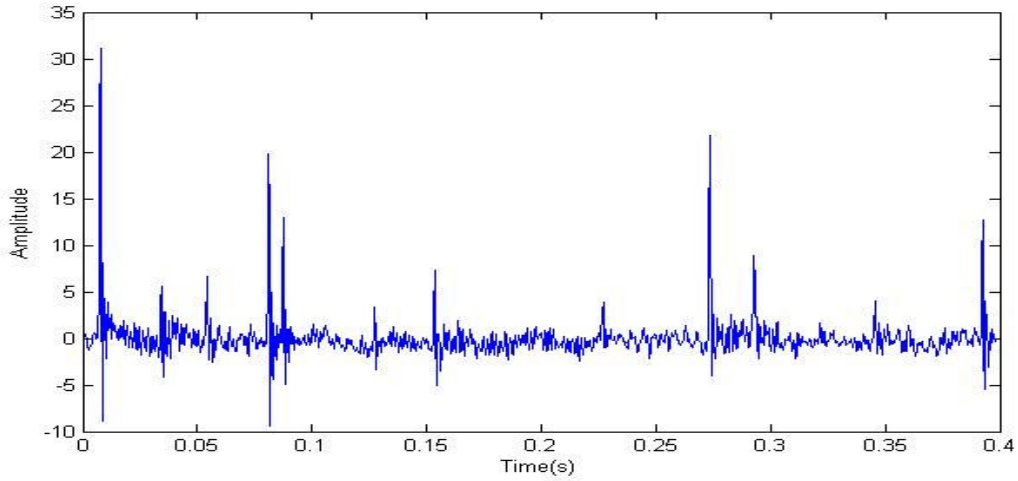

Figure 5.11 Acceleration signal of raw data for inner race fault condition at 1250 rpm.

In the raw acceleration data, four statistical indices (kurt1,kurt2,alfa and p2p) show the faulty condition. Their faulty/healthy ratio amplitudes show sinusoidal behavior with the changing shaft speed which can be seen from Figure 5.12. The indices take their higher values at 1500 rpm shaft speed.

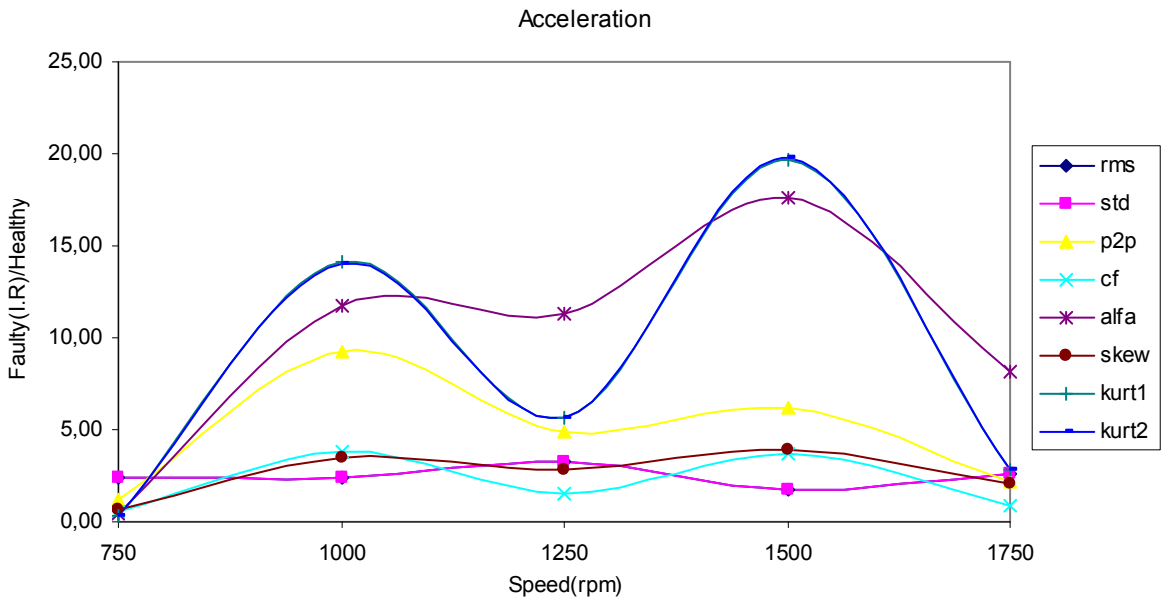

Figure 5.12 Statistical indices of raw acceleration data for inner race defect

5.2 Combined Fault Experiments

In the combined fault experiments, the effect of two-faulthy condition on the vibration signals is investigated. Two types of combinations are tried in the experiment: Inner race fault and shaft misalignment and inner race fault and unbalance conditions are analyzed.

5.2.1 Shaft Misalignment & Inner Race Fault Experiment

In the raw velocity data, two statistical indices (Figure 5.13), standard deviation, and peak to peak values are above the healthy condition and have increasing trend as the shaft speed increases up to 1250 rpm. Further, increase in shaft speed cause these two indices to decrease. Moreover, crest factor starts to increase with the shaft speed of 1250 rpm and make its peak value at 1750 rpm. Crest factor takes unhealthy condition ratio after the 1500 rpm shaft speed.

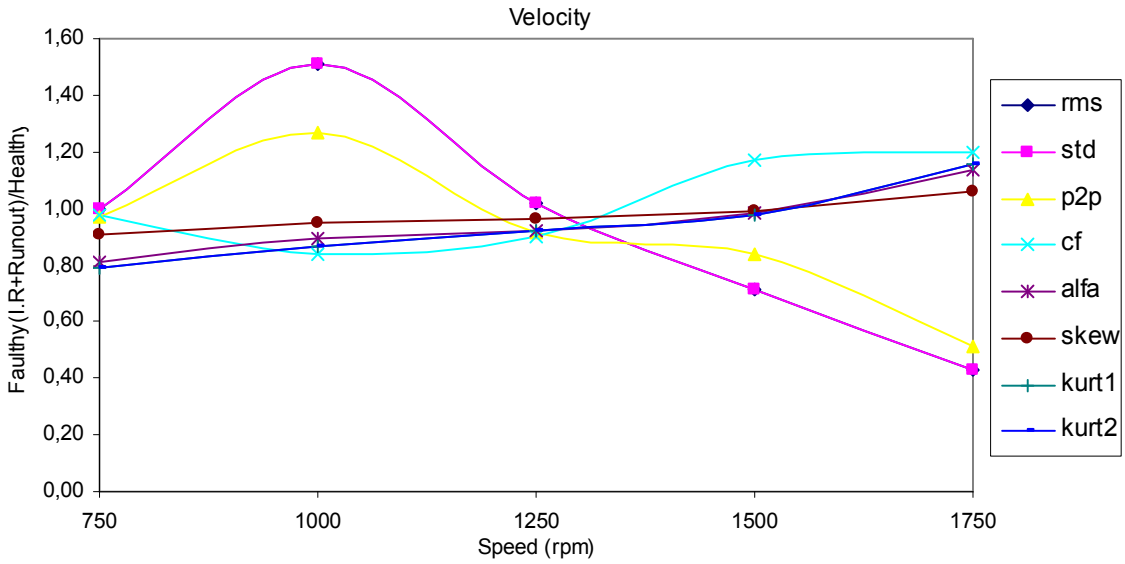

Figure 5.13 Statistical indices of raw velocity data for inner race defect + 3mm run out.

In the raw acceleration data, most of the statistical indices (Figure 5.14) have a sinusoidal behavior with the changing shaft speed. Among them standard deviation

has an opposite sinusoidal behavior to the other indices such that between 750 rpm – 1000 rpm shaft speed, all of the indices' values increase except standard deviation which has a decreasing trend. Between 1000 rpm – 1250 rpm shaft speed, all of the indices decrease except standard deviation, which has a increasing trend. Moreover, most of the indices take their highest ratio value in the 1500 rpm shaft speed and among them kurtosis (kurt1 and kurt2) has the maximum value at that speed.

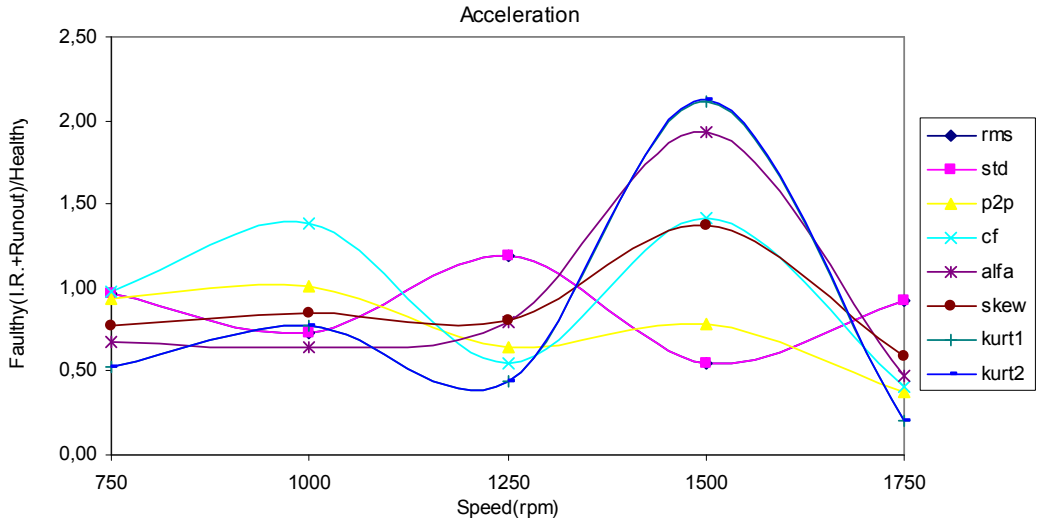

Figure 5.14 Statistical indices of raw acceleration data for inner race defect + 3mm run out.

5.2.2 Unbalance & Inner Race Fault Experiment

In the raw velocity data, two statistical indices (standard deviation and peak to peak values) are above the healthy condition as can be seen from Figure 5.15. These two statistical indices' values increase as the shaft speed increases.

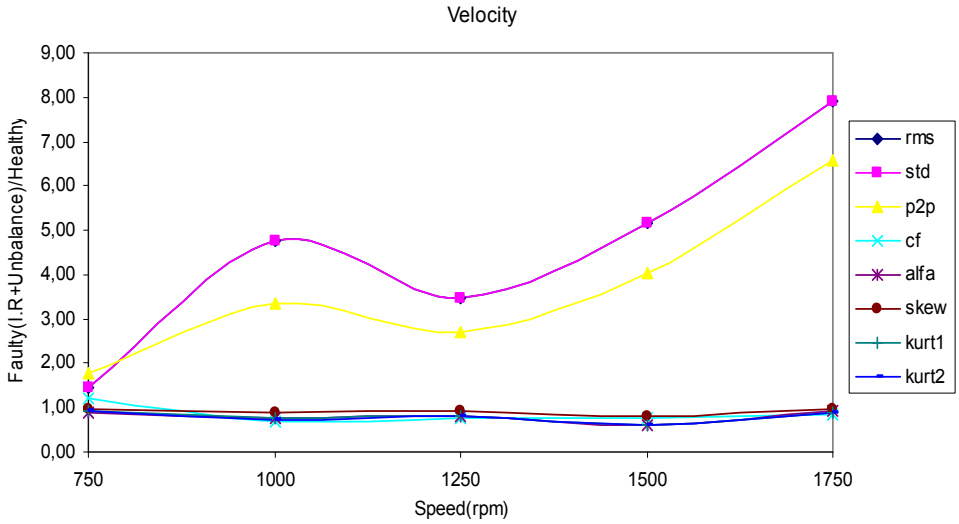

Figure 5.15 Statistical indices of raw velocity data for inner race defect + unbalance.

In the raw acceleration data, all the statistical indices (Figure 5.16) have different behavior to shaft speed changes. Four statistical indices (alfa, kurt2, p2p & std) show the faulty condition. The alfa and kurtosis start to increase from 1000 rpm shaft speed to 1500 rpm. At 1500 rpm both of the indices take the peak value. Peak to peak and standard deviation indices have sinusoidal behavior with changing shaft speed.

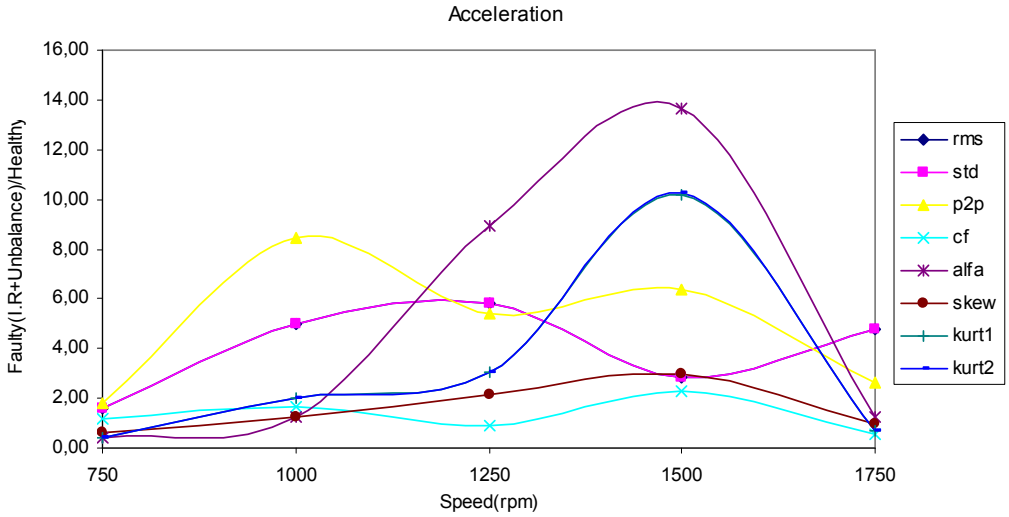

Figure 5.16 Statistical indices of raw acceleration data for inner race defect + unbalance.

CHAPTER SIX
THE CURVE LENGTH TRANSFORM

6.1 Definition of the Curve Length Transform

In this study, the vibration responses collected from the test setup for healthy and faulty cases are processed by a time-based transform named as the Curve Length Transform (CLT).

The curve length transform is a nonlinear time based transform in which the discrete values of a time signal are used. The total curve length, which is the sum of the lengths of the straight lines defined between the adjacent measurement points, is calculated for a specified window length w as shown in Figure 6.1. The curve length transform is generally used for QRS complex detection and feature extraction in ECG analysis (Zong, Moody & Jiang, 2006).

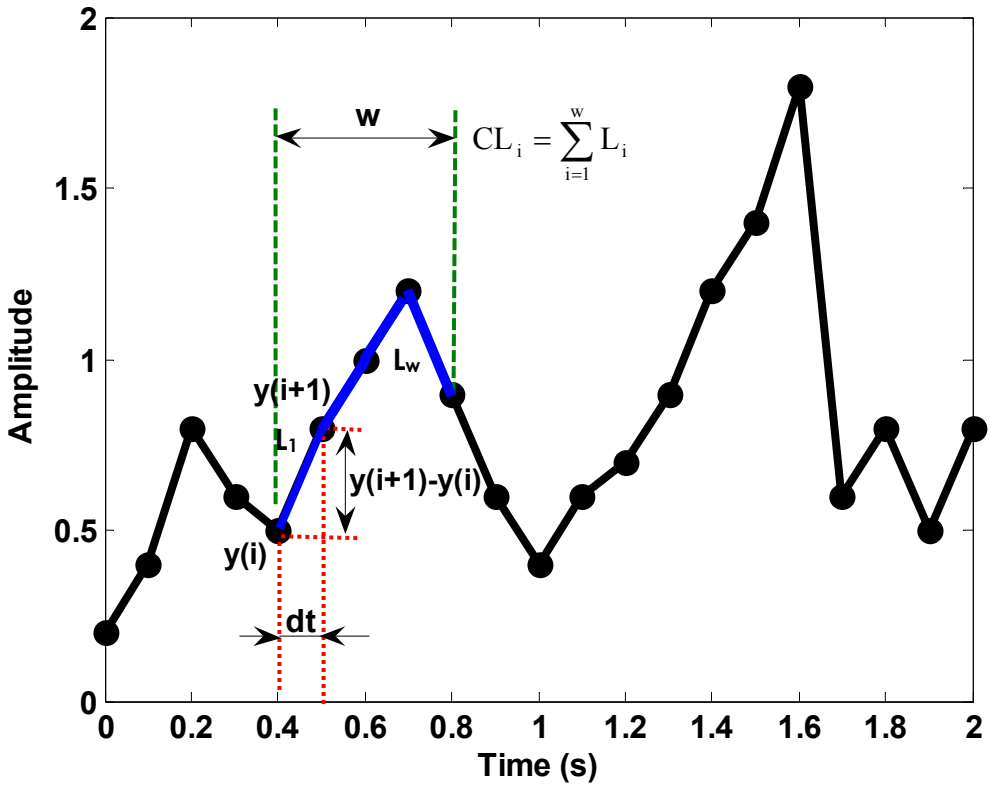

Figure 6.1 Definition of the curve length transform.

The curve length transform is used in this study for diagnostic purpose of rolling element bearings. The curve length transform of a vibration signal having N samples is calculated for the window length w as

$$CL_k = \sum_{i=1}^{w} \sqrt{dt^2 + (x_{i+1} - x_i)^2} \qquad (k=1, N-w) \tag{6.1}$$

where dt is the sampling period of the vibration signal x. Due to the nature of the faulty vibration signal, it is expected that the curve length at the ball-defect impact corresponding to the examined defect is generally longer than the other parts of the signal. The curve length transform is also defined using a scaling factor C as

$$CL_k = \sum_{i=1}^{w} \sqrt{C + (x_{i+1} - x_i)^2} \tag{6.2}$$

In the following pages, the curve length transform is applied to the raw velocity and acceleration vibration signals and effects are observed.

6.2 Curve Length Transform Applications

Curve length transforms are applied to the raw vibration signal data in the below analysis. In the transforms the scale factor C is taken as 1. In the further study, the effect of scale factor on the transform will also be investigated.

6.2.1 CLT on Shaft Misalignment Vibration Data

In the Figure 6.2, a sample raw velocity signal and the transformed (curve length transform) signal's graphs can be seen. In the transform scale factor "C" is taken as 1.

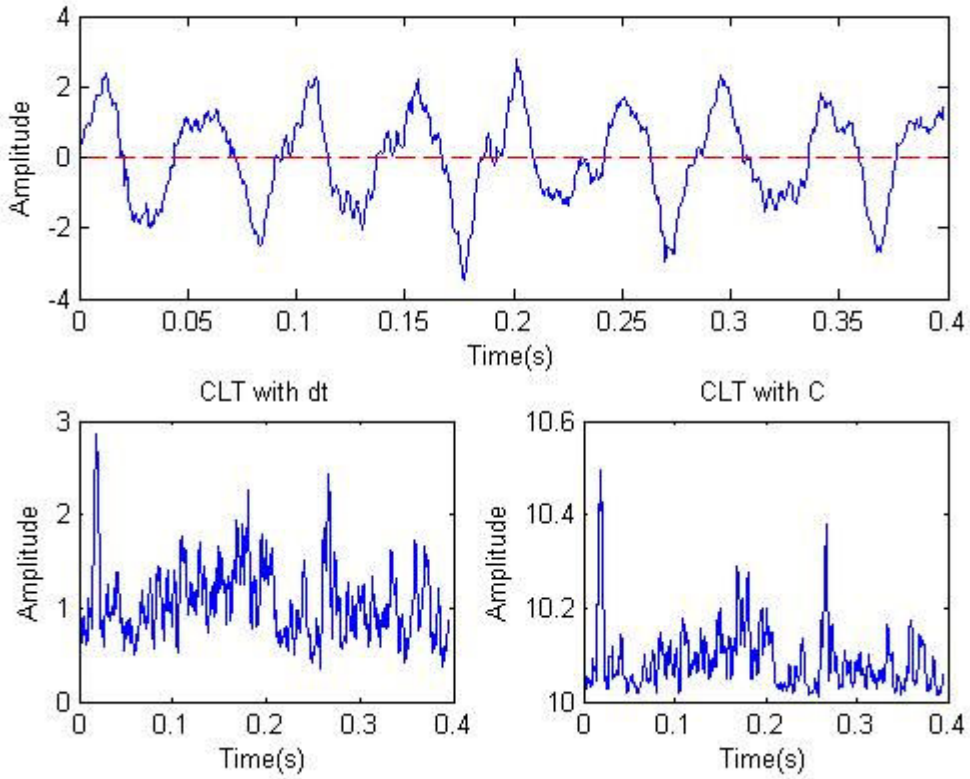

Figure 6.2 Curve length transform of velocity data for 3 mm run out error at 1250 rpm.

As it is seen from Figure 6.2 to Figure 6.7, after the curve length transform to the vibration velocity signal of shaft misalignment, kurtosis (kurt2) takes higher values and fault condition becomes more visible. Moreover, curve length transform to the vibration velocity signal has a negative effect on standard deviation and peak to peak values. Their values decrease after the transform.

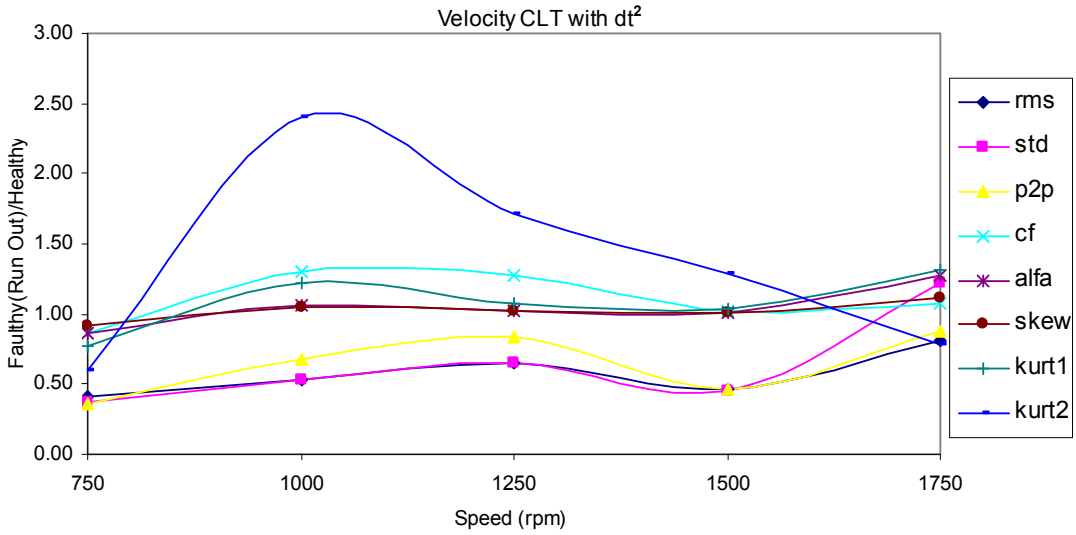

Figure 6.3 Statistical indices of CLT with dt^2 velocity data for 3 mm run out error.

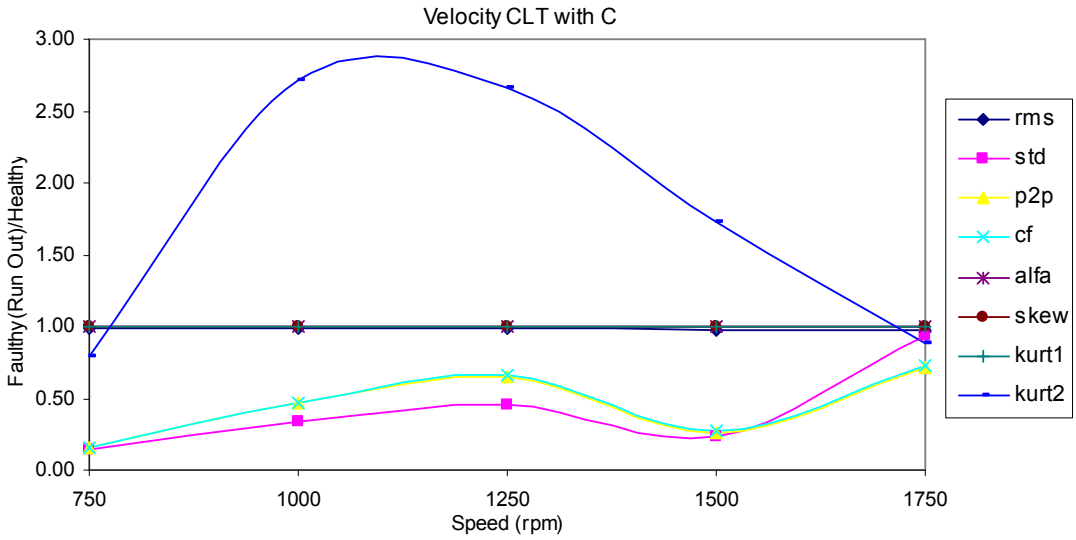

Figure 6.4 Statistical indices of CLT with C=1 velocity data for 3 mm run out error

In the Figure 6.5, a sample raw acceleration signal and the transformed (curve length transform) signal's graphs for shaft misalignment can be seen. In the transform scale factor "C" is taken as 1.

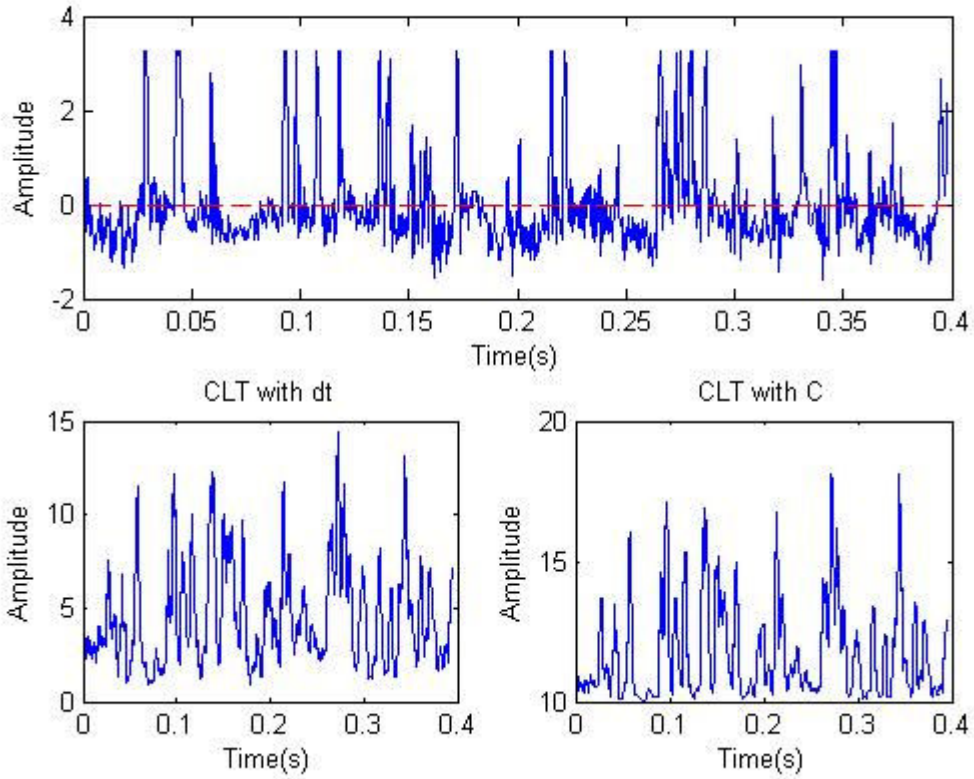

Figure 6.5 Curve length transform of acceleration data for 3 mm run out error at 1250 rpm.

Furthermore, as it is seen from Figure 6.6 and Figure 6.7, curve length transform to the acceleration signal causes a decrease in the faulty/healthy ratios when compared with the raw acceleration data. After the curve length transform with dt^2, kurtosis and alfa are main statistical indices showing the faulty condition best. Moreover, after the curve length transform with C, kurtosis becomes a good fault indicator when compared with others.

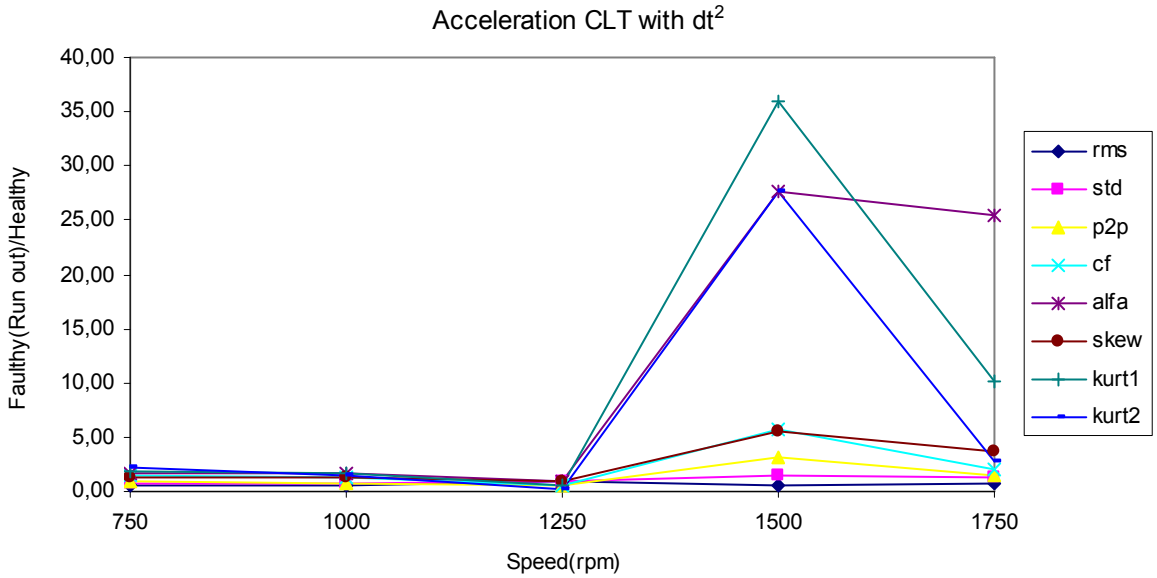

Figure 6.6 Statistical indices of CLT with dt^2 acceleration data for 3 mm run out error.

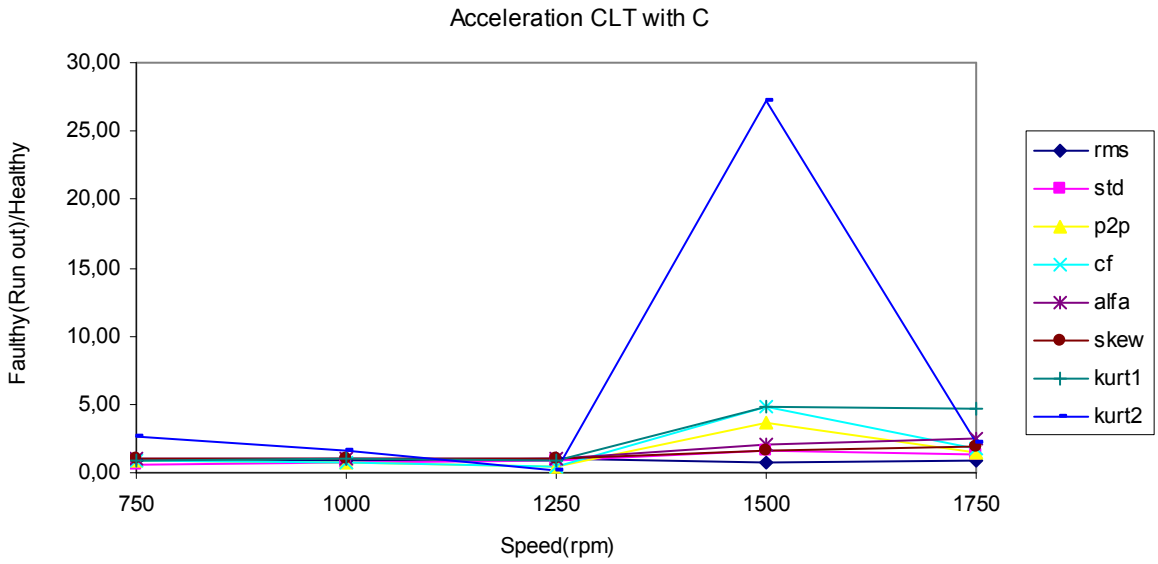

Figure 6.7 Statistical indices of CLT with C=1 acceleration data for 3 mm run out error.

6.2.2 CLT on Unbalance Vibration Data

In the Figure 6.8, a sample raw velocity signal and the transformed (curve length transform) signal's graphs for the unbalance condition (at 1500 rpm shaft speed) can be seen. In the transform, scale factor "C" is taken as 1.

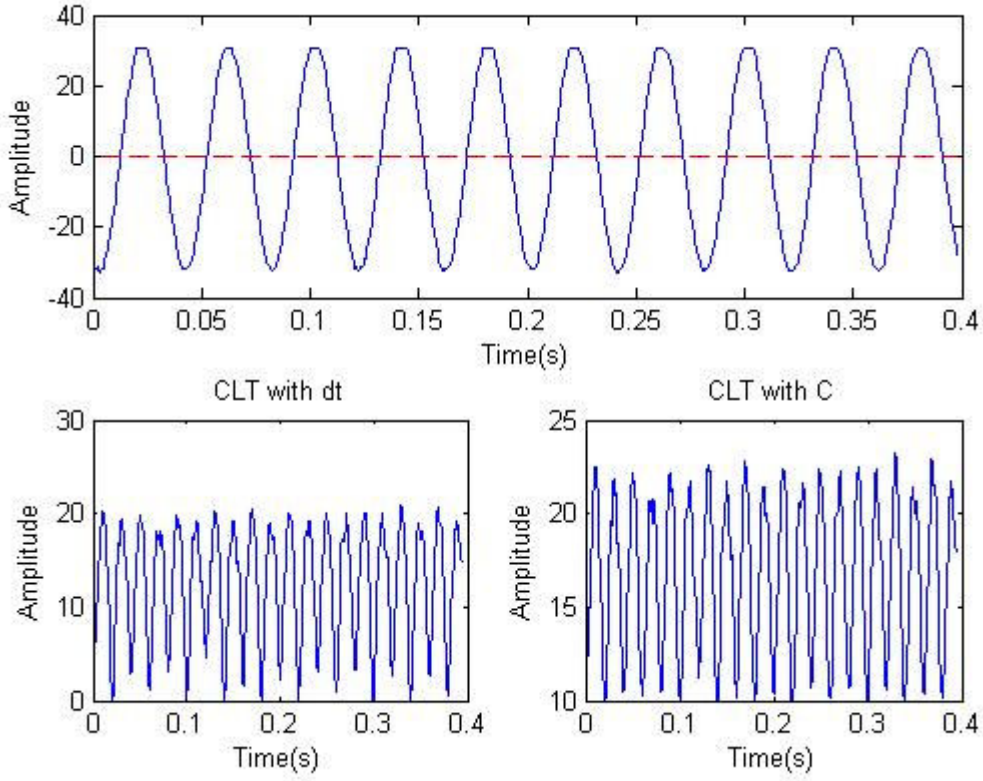

Figure 6.8 Curve length transform of velocity data for unbalance fault condition at 1500 rpm.

As it is seen from Figure 6.9 and Figure 6.10, after the curve length transform to the vibration velocity signal, the amplitudes of the indices decrease. Moreover, again after transform, standard deviation and peak to peak indices can be used to detect the faulty condition. Moreover, after the transform, rms and crest factor amplitudes increase and they also show the faulty condition. Their amplitudes increase as the shaft speed increases.

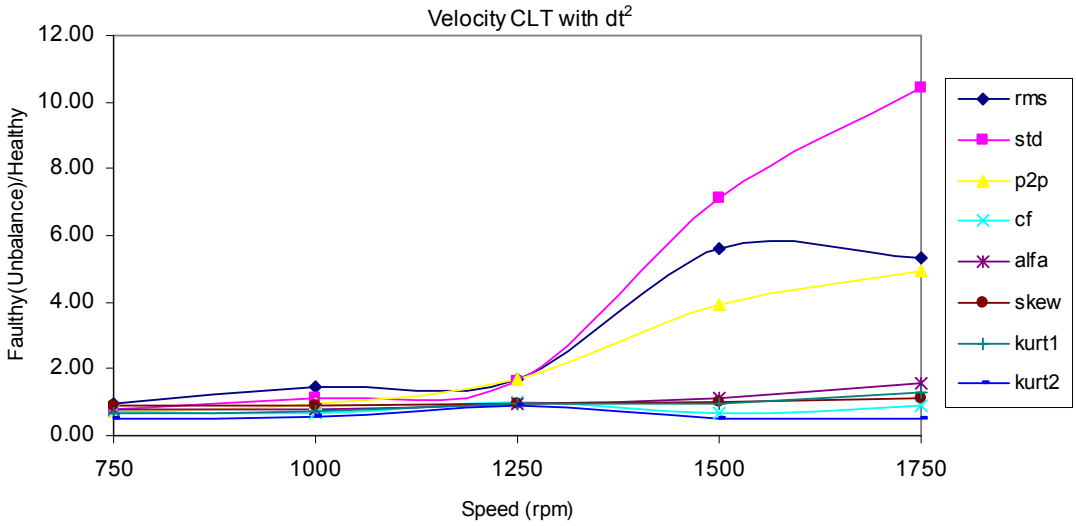

Figure 6.9 Statistical indices of CLT with dt^2 velocity data for for unbalance.

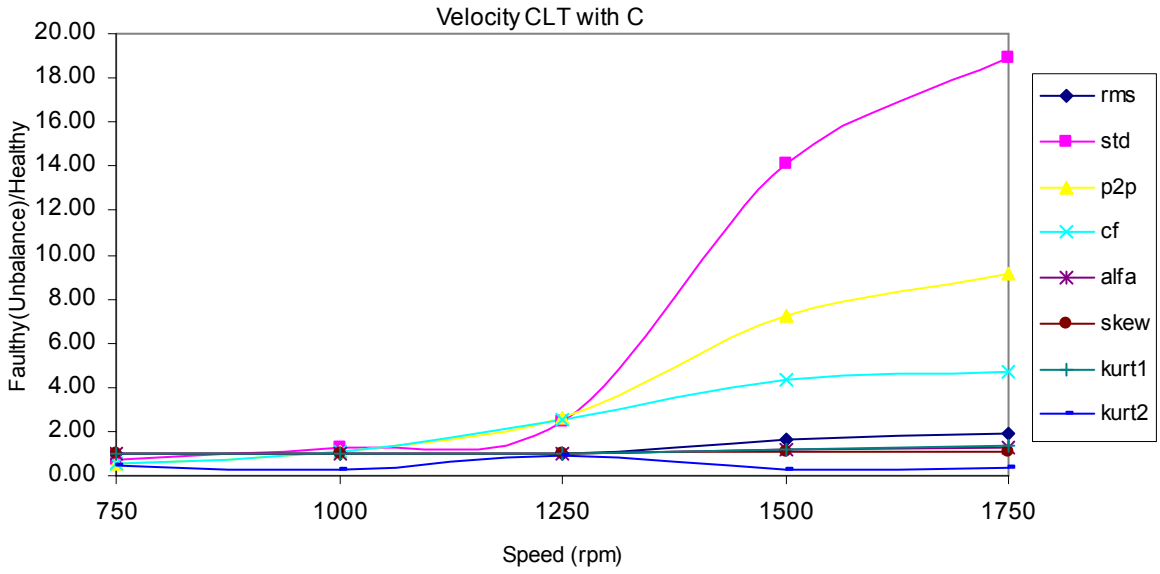

Figure 6.10 Statistical indices of CLT with C=1 velocity data for unbalance.

From the Figure 6.11, a sample raw acceleration signal and the transformed (curve length transform) signal's graphs for the unbalance condition (at 1500 rpm shaft speed) can be seen. In the transform scale factor "C" is taken as 1.

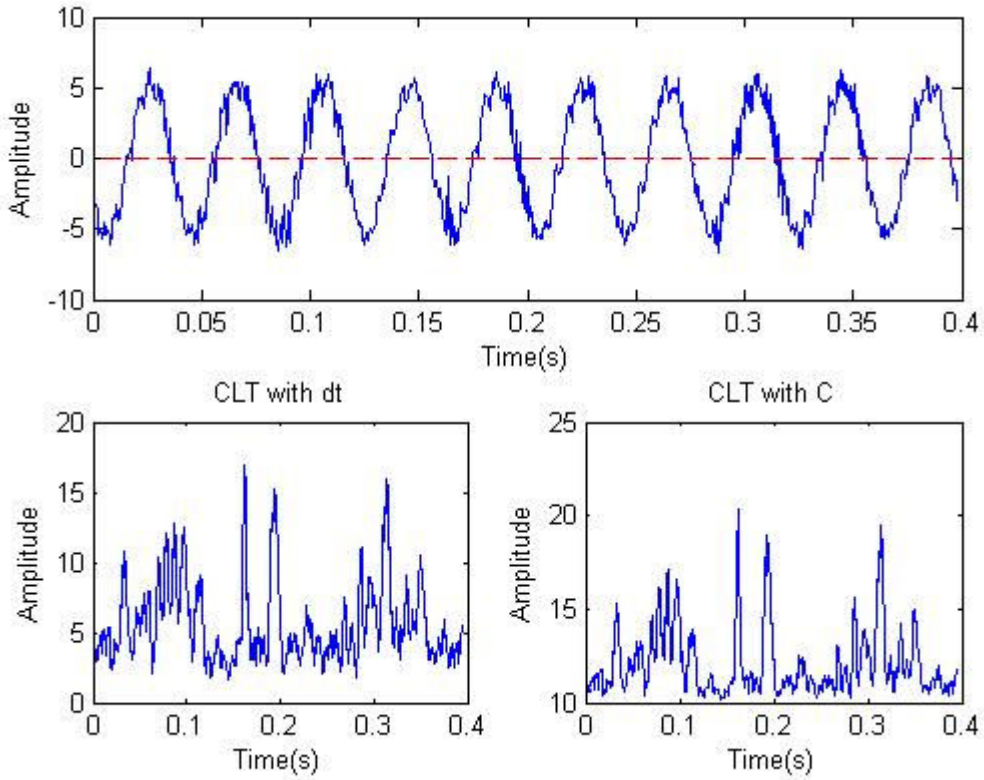

Figure 6.11 Curve length transform of acceleration data for unbalance fault condition at 1500 rpm

After the curve length transform to the vibration acceleration signal, the amplitudes of the indices increase as it is seen from Figure 6.12 and Figure 6.13. However, indices, which show faulty condition in the raw signal, change their behavior after the transform. Alfa and kurtosis (kurt1) indices take higher values after the transform.

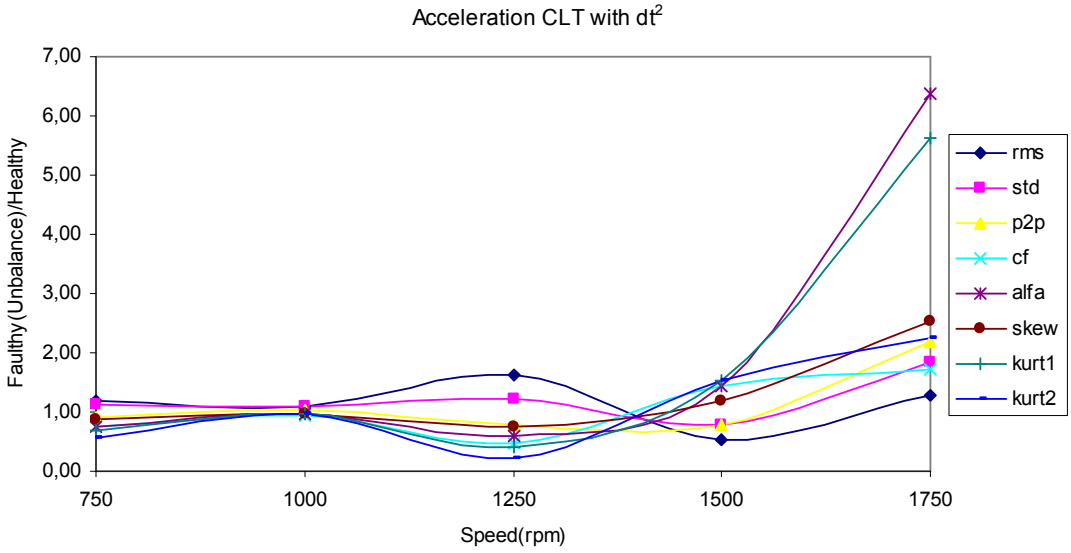

Figure 6.12 Statistical indices of CLT with dt^2 acceleration data for unbalance.

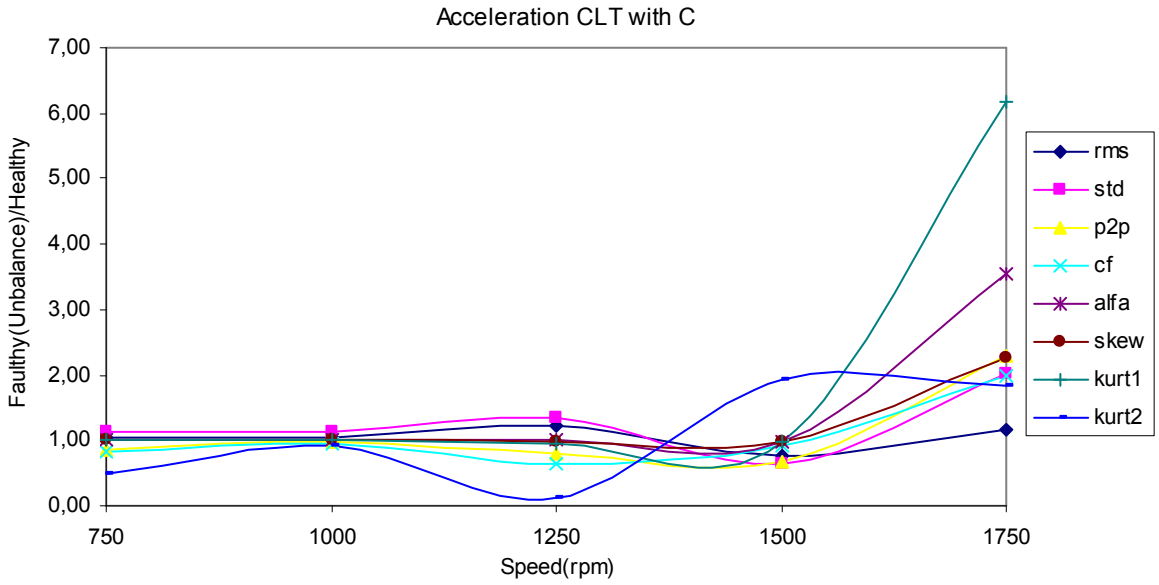

Figure 6.13 Statistical indices of CLT with C=1 acceleration data for unbalance.

6.2.3 CLT on Inner Race Fault Vibration Data

In the Figure 6.14, a sample raw velocity signal and the transformed (curve length transform) signal's graphs for the inner race fault (at 1250 rpm shaft speed) can be seen. In the transform scale factor "C" is taken as 1.

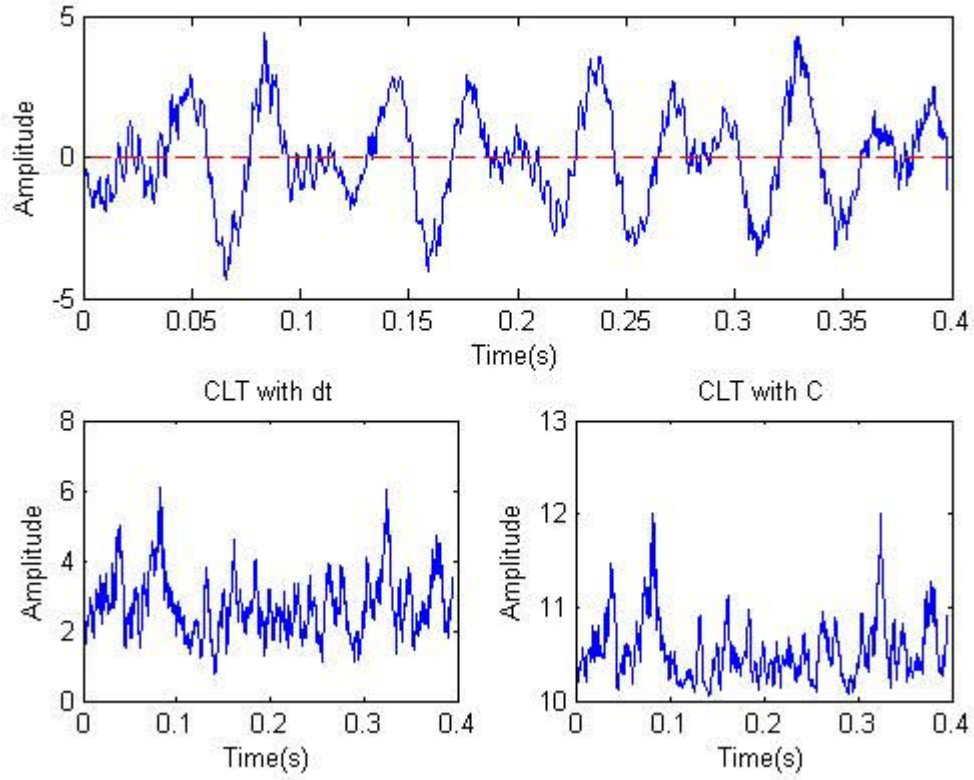

Figure 6.14 Curve length transform of velocity data for inner race fault condition at 1250 rpm

As it is seen from Figure 6.15 and Figure 6.16, after the curve length transform to the vibration velocity signal of inner race fault, the amplitudes of the indices increase. Root mean square and crest factor become good faulty condition indicators after the curve length transform. The indices' ratio values are increasing until the 1250 rpm shaft speed. After the corresponding shaft speed, indices are decreasing with the increasing shaft speed.

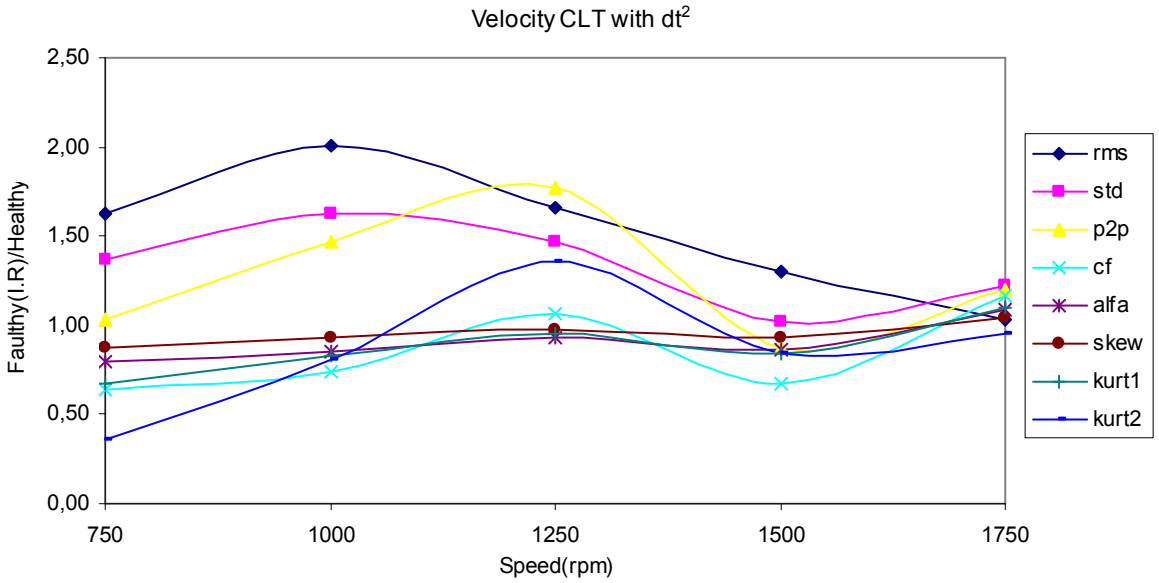

Figure 6.15 Statistical indices of CLT with dt^2 velocity data for inner race defect.

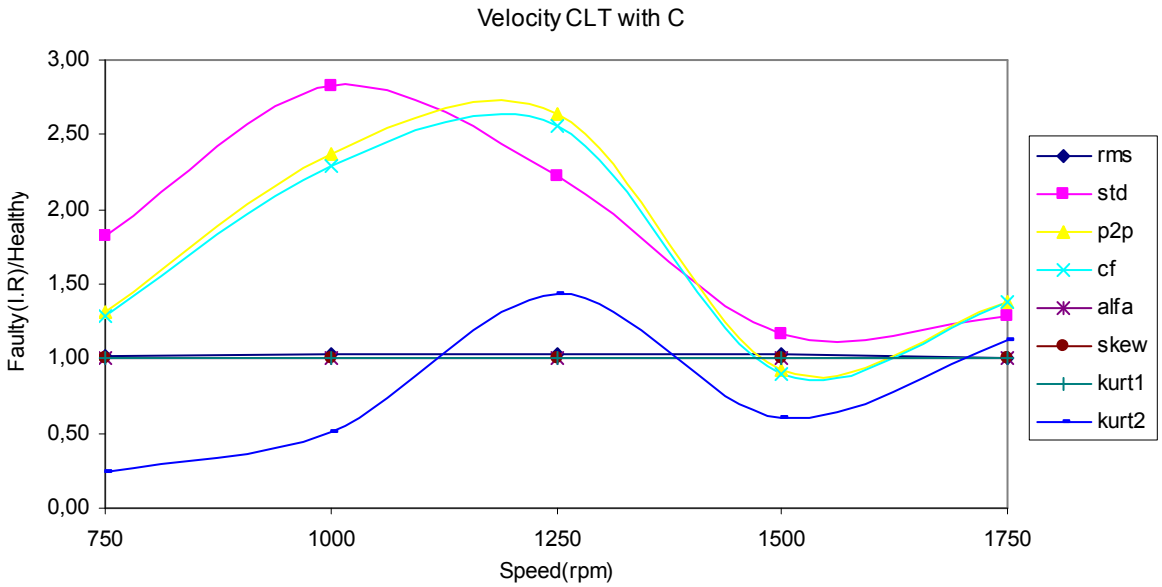

Figure 6.16 Statistical indices of CLT with C velocity data for inner race defect.

In the Figure 6.17, a sample raw acceleration signal and the transformed (curve length transform) signal's graphs for the inner race fault (at 1250 rpm shaft speed) can be seen. In the transform scale factor "C" is taken 1.

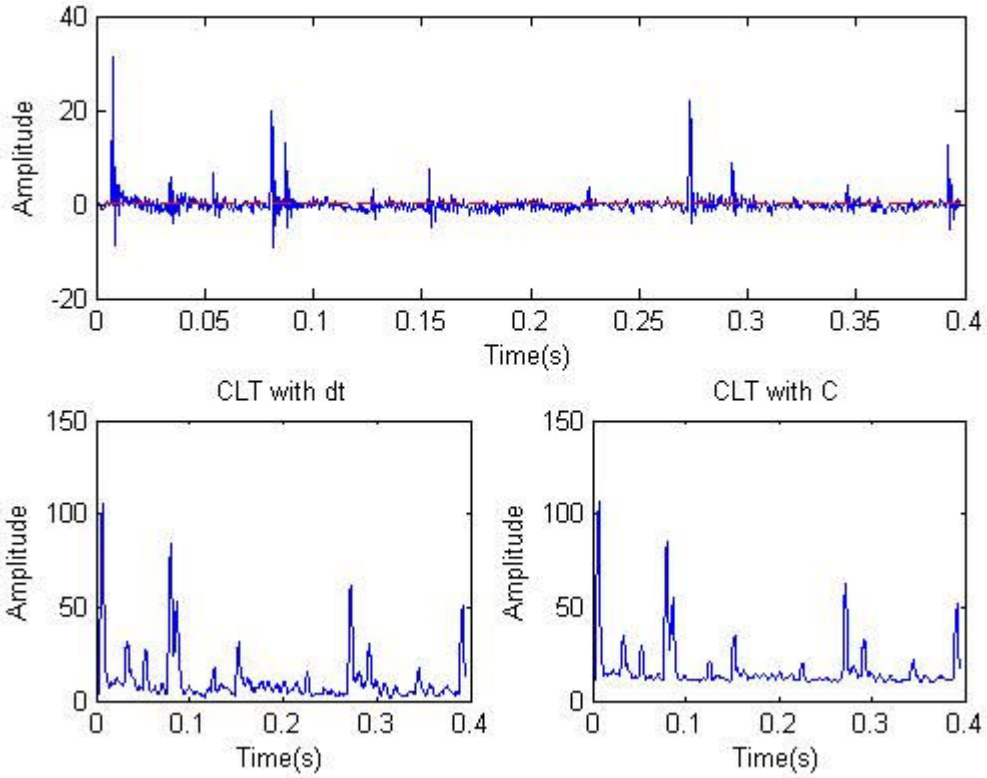

Figure 6.17 Curve length transform of acceleration data for inner race fault condition at 1250 rpm

After the curve length transform to the vibration acceleration signal, the amplitudes of the indices decrease as it is seen from Figure 6.18 and Figure 6.19. Alfa has the highest value in the transformed data with dt^2 . For the transform with C=1, the peak to peak and kurtosis (kurt 1) become good fault indicators. Moreover, all of the indices show a sinusoidal behavior to the shaft speed increase with decreasing amplitude.

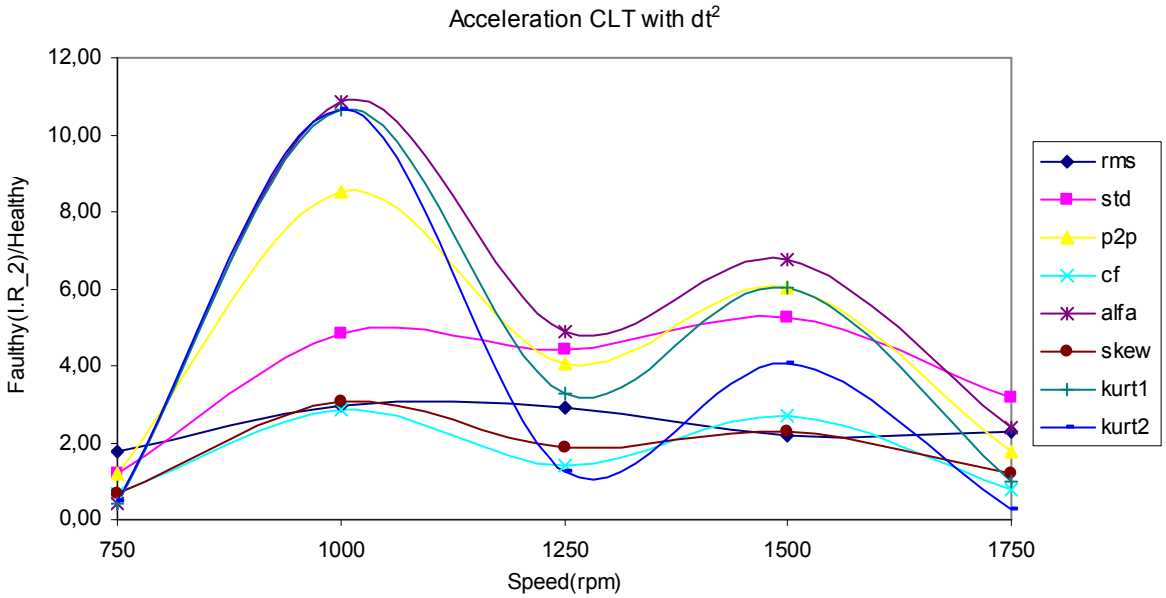

Figure 6.18 Statistical indices of CLT with dt^2 acceleration data for inner race defect.

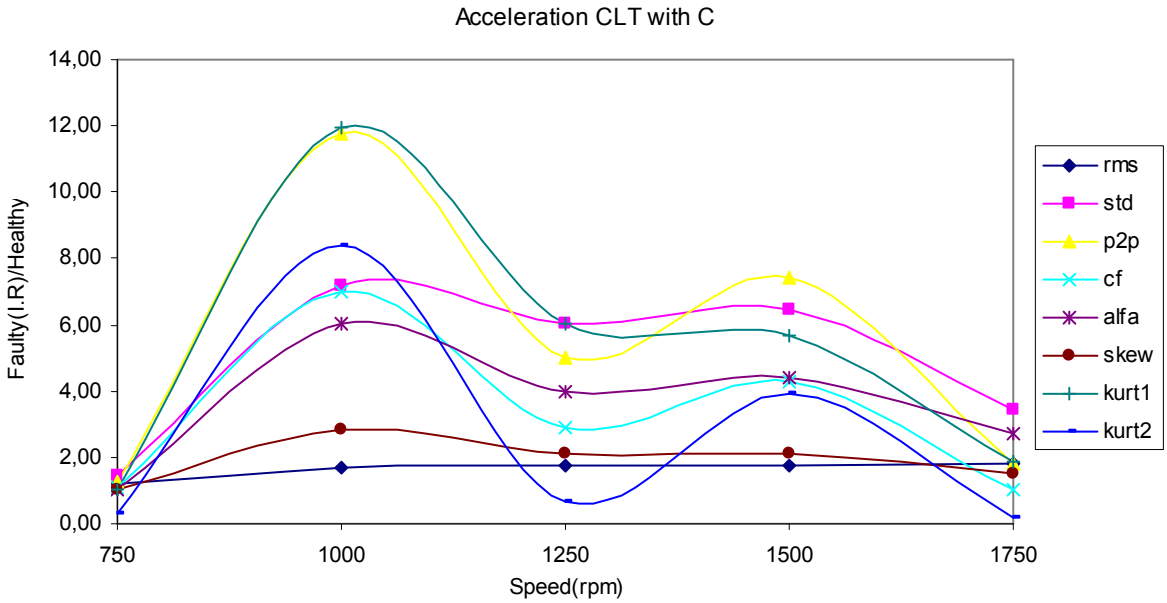

Figure 6.19 Statistical indices of CLT with C=1 acceleration data for inner race defect.

6.3 Effect of Scale Factor on Curve Length Transform

In this study, how the scale factor value affects the curve length transform is investigated. The curve length transform is applied to a raw vibration data to make the faults more visible in the system. In the above transforms scale factor C is taken as a constant value, 1. However, it is important to see whether the faulty / healthy condition's ratio changes with changing scale factor for a corresponding statistical parameter. For this reason in the below analysis, scale factor value is changed from 1 to 10 and its effects are investigated. Velocity of the vibration data is used in all of the analysis.

6.3.1 Misalignment Fault

In this study, the statistical indices are chosen according to their ability of showing the faulty condition. Two statistical indices (kurt2 & p2p) are investigated for the corresponding fault.

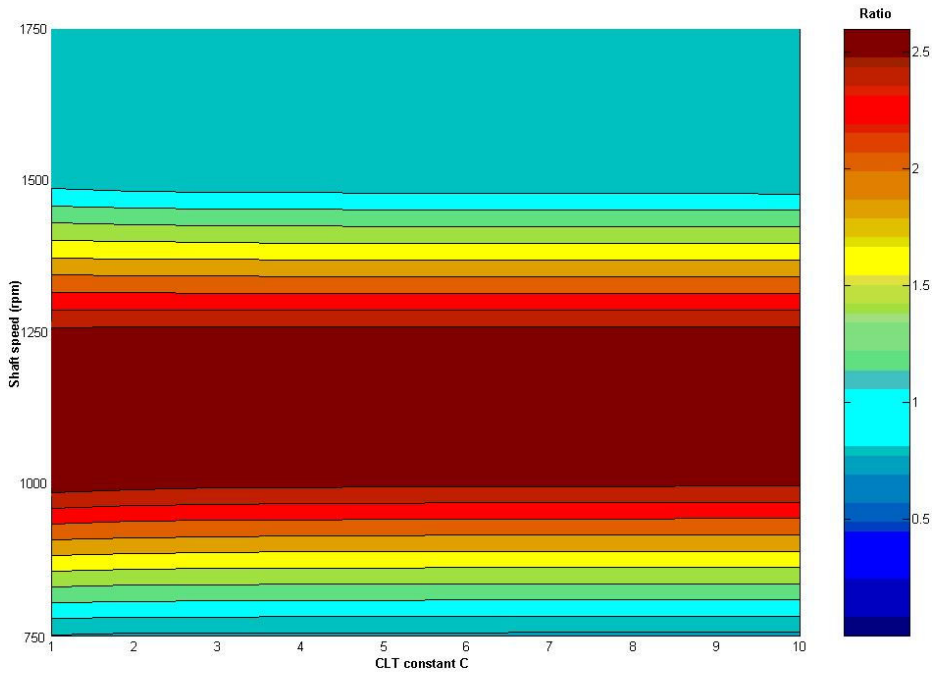

Figure 6.22 Scale factor effect on curve length transform (kurtosis).

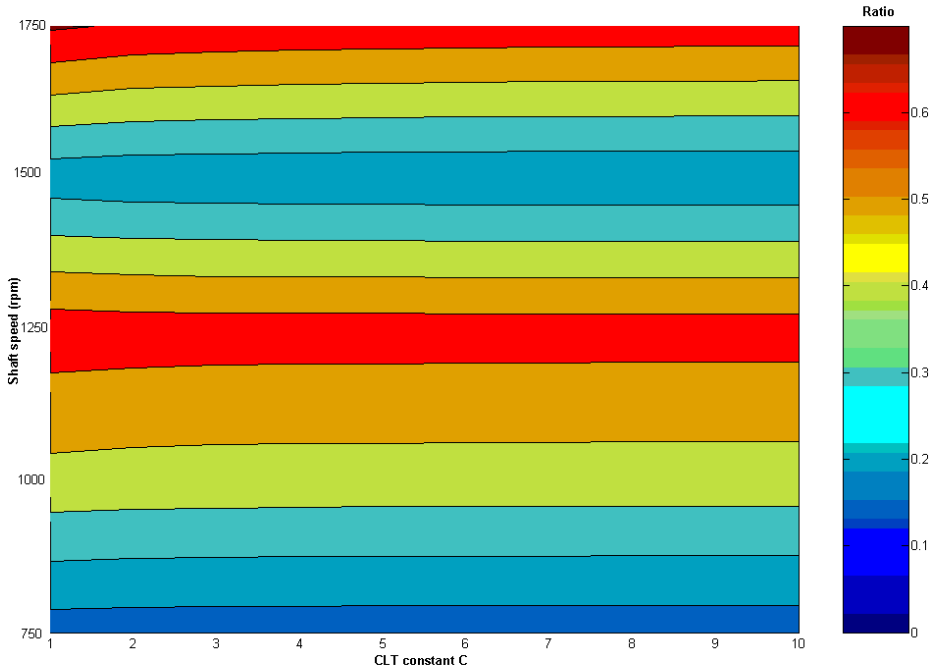

Figure 6.23 Scale factor effect on curve length transform (peak to peak).

As it is seen from Figure 6.22 & Figure 6.23, scale factor values does not affect the kurtosis and peak to peak values.

6.3.2 Unbalance Fault

Two statistical indices (standard deviation and peak to peak) are investigated for the corresponding fault.

As it is seen from Figure 6.24 and Figure 6.25, changing scale factor values does not affect the kurtosis and standard deviation values up to shaft speed of 1250 rpm. Further increase in the shaft speed changes the effect of scale factor. It can be concluded that increase in the scale factor value causes an increase in the ratio values at the speed that are higher than 1250 rpm.

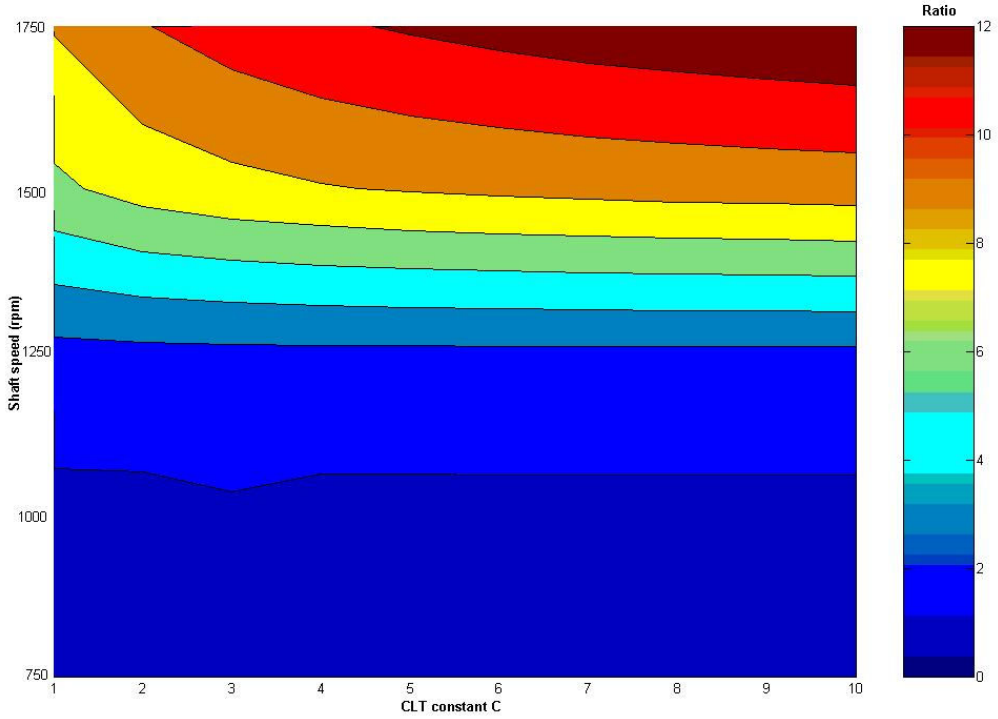

Figure 6.24 Scale factor effect on curve length transform (standard deviation).

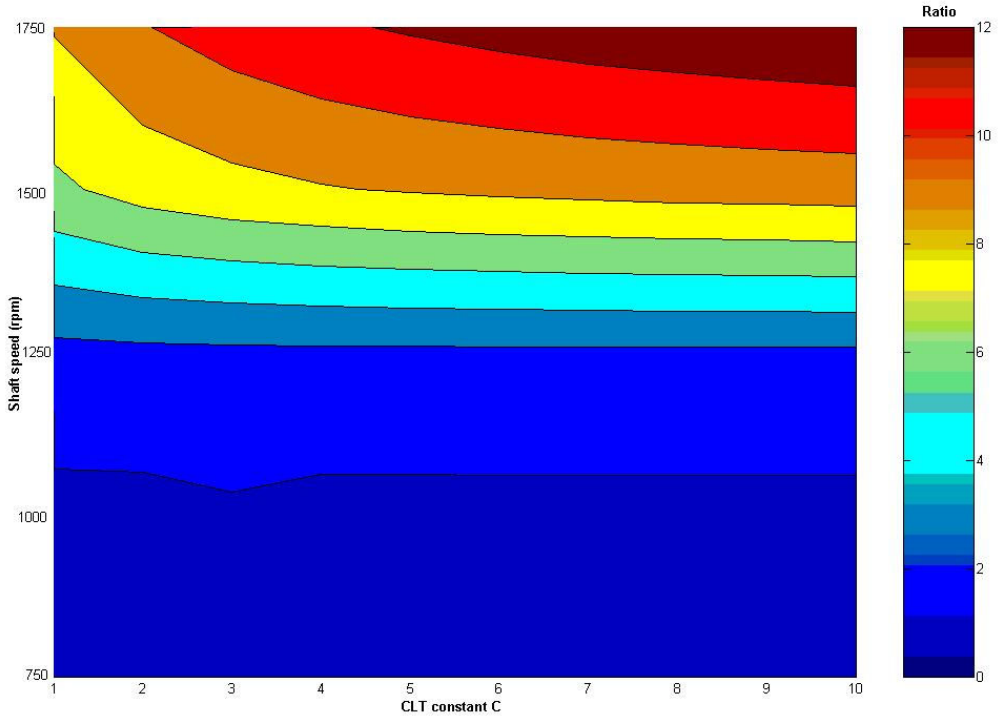

Figure 6.25 Scale factor effect on curve length transform (peak to peak).

6.3.3 Inner Race Fault

For the inner race fault velocity data, two statistical parameters (standard deviation and peak to peak) are investigated. The corresponding contours are obtained as shown in Figure 6.26 and Figure 6.27.

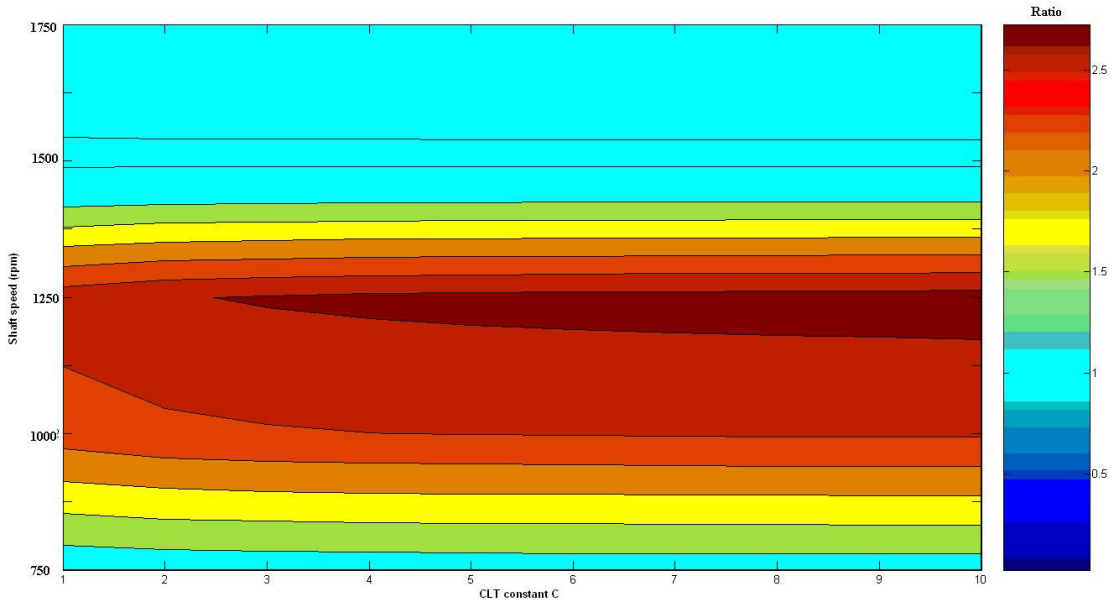

Figure 6.26 Scale factor effect on curve length transform (peak to peak).

From Figure 6.26, it can be observed that scale factor has different effects at different shaft speeds for the peak to peak values. At 1250 rpm until the scale value of 3, faulty/healthy ratio is constant. Further increase in the scale value causes the ratio to increase. At other shaft speeds as the scale factor increases faulty/healthy ratio stays constant.

From Figure 6.27, it can be observed that scale factor has same effect with peak to peak value of inner race fault. At 1250 rpm until the scale value of 7, faulty/healthy ratio is constant. Further increase in the scale value cases the ratio to increase. As the scale factor increases at other shaft speeds, faulty/healthy ratio stays constant.

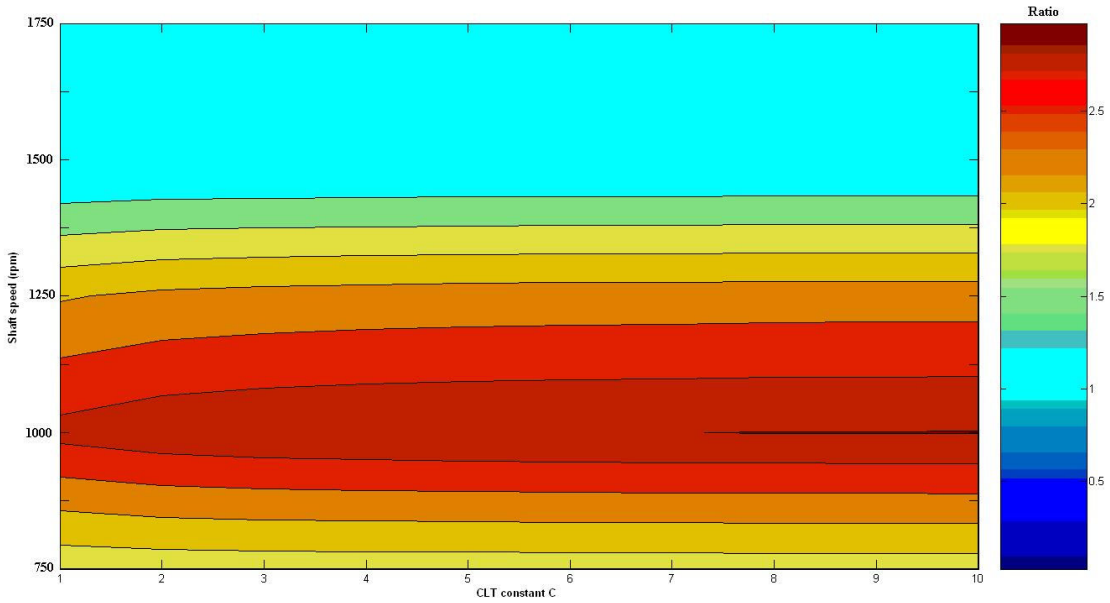

Figure 6.27 Scale factor effect on curve length transform (standard deviation).

6.4 Comparisons of 6th Moment & Kurtosis on Vibration Signal

In this study, 6th moment of the probability density function, which is more sensitive to the changes, is investigated on the run out vibration signals.

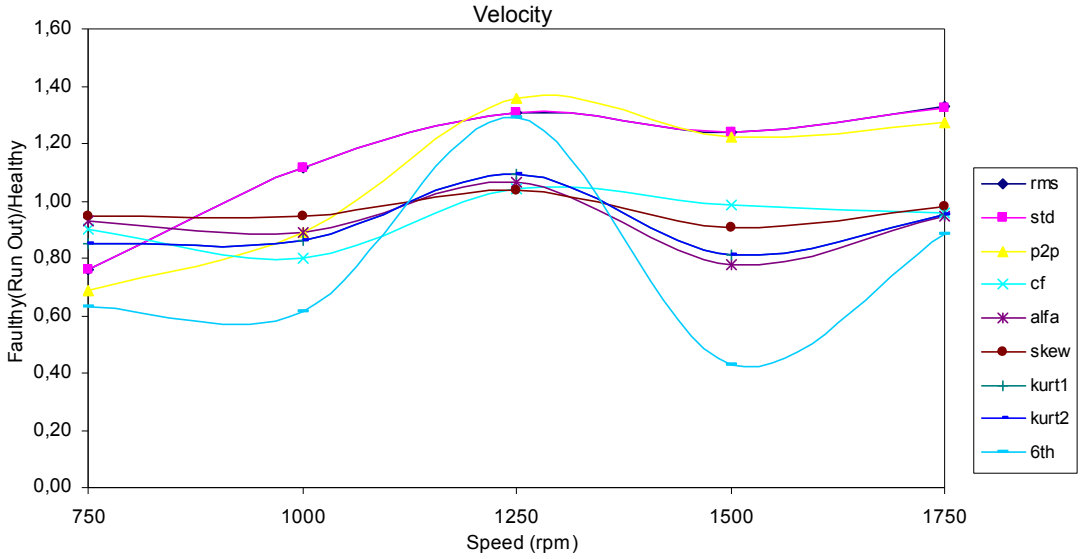

Figure 6.28 Statistical indices of raw velocity data for 3 mm run out error.

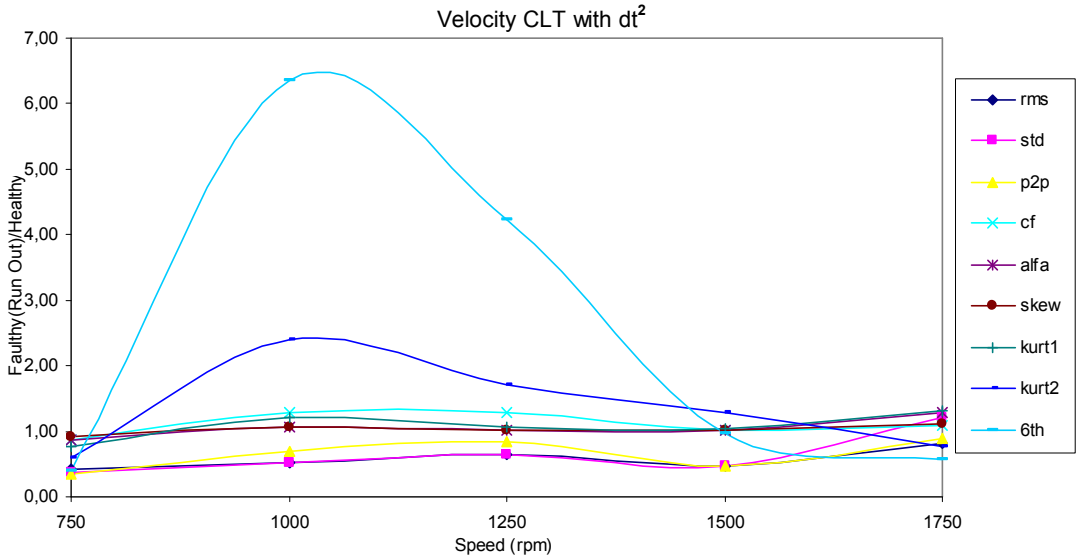

Figure 6.29 Statistical indices of CLT with dt^2 vel. data for 3 mm run out error.

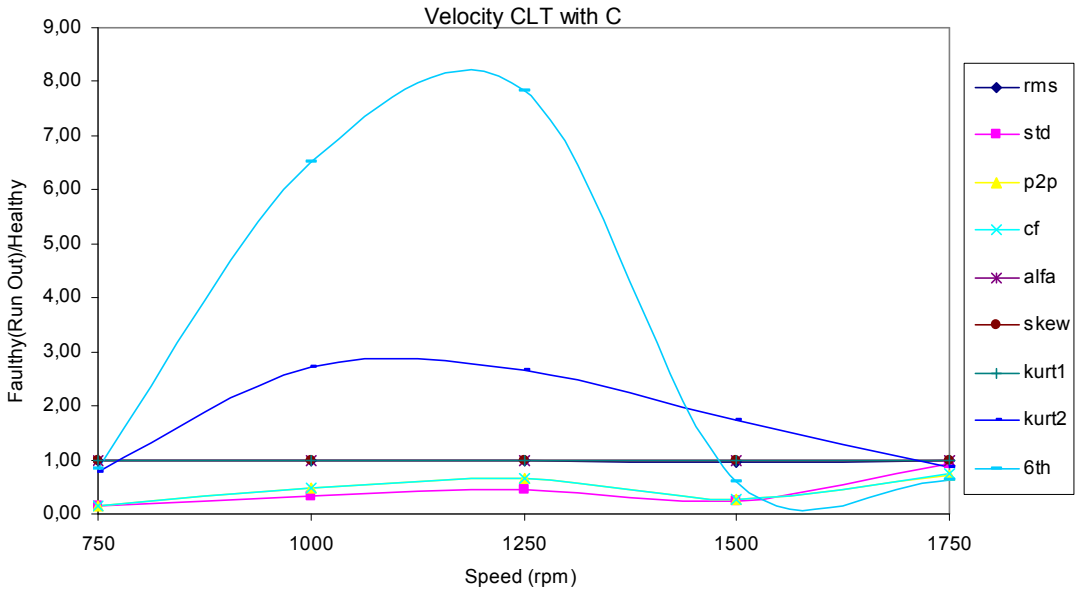

Figure 6.30 Statistical indices of CLT with C velocity data for 3 mm run out error.

From Figures 6.28-6.30, the behavior of the 6^{th} normalized moment for the shaft misalignment is investigated. In theory, Takeyasu and Higuchi derived 6^{th} normalized moment as an alternative time parameter to Kurtosis and in their survey and they proved that 6^{th} normalized moment is much more sensitive than the Kurtosis by using numerical examples. In the above two figures which are related

with curve length transform, 6^{th} normalized moment has a more sensitive behavior to a fault when compared with Kurtosis.

CHAPTER SEVEN
FREQUENCY DOMAIN ANALYSIS

In the experiments, three different types of faulty conditions (shaft misalignment, unbalance, inner race fault) are investigated. Each of the malfunctions has characteristic rotational frequency. These characteristics frequencies are used to identify the bearing defect (inner race), shaft misalignment and unbalance condition in the frequency spectrum of a time signal.

7.1 Bearing Characteristic Frequencies

Bearing characteristic frequencies are known as the defect frequencies. These frequencies indicate the location of faults, if there is as defect on any components of rolling element bearing. In the faulty situation, these frequencies are observed in the frequency spectrum. These frequencies depend on rolling element bearing geometry, number of rolling element and shaft rotational speed. Bearing characteristic frequencies were calculated by the formula given in equations 7.1. (Tandon, & Choudhury, 1999). The properties of the rolling element bearing used in this study are given in Figure 7.1. and Table 7.1.

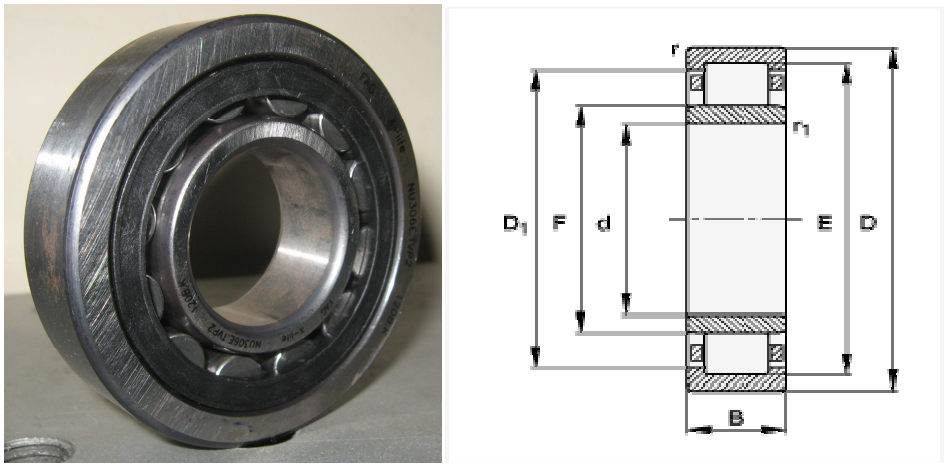

Figure 7.1 Geometry of rolling element bearing (FAG NU306-E-TVP2).

Table 7.1 Geometrical parameters of FAG NU306-E-TVP2.

d (inner diameter)	30 mm
D (outer diameter)	72 mm
B (width)	19 mm
D_1	59,2 mm
E	62,5 mm
F	40,5 mm
Z(#of rolling element)	12
Contact Angle(α)	0 degree

In this study inner race fault was investigated. Corresponding characteristic inner race fault frequency which is denoted by f_i is given below.

$$f_i = \frac{Zf_s}{2}\left(1+\frac{d_b}{d_m}\cos\alpha\right) \qquad (7.1)$$

The unkonwn symbols used in above equations are

f_s : shaft speed

f_i : characteristic frequency of inner race

d_m : pitch diameter

d_b : ball diameter

According to above equation, inner race fault frequency of FAG Cylindrical roller bearing NU306-E-TVP2 is calculated for each shaft speed. The bearing characteristic frequencies for different shaft speeds are given Table 7.2.

Table 7.2 Inner race defect frequencies of FAG NU306-E-TVP2.

Shaft speed(rpm)	f_i [Hz]
750	91,02
1000	121,36
1250	151,70
1500	182,04
1750	212,38

7.2 The Fast Fourier Transform

The frequency contents of the vibration signals are calculated by the Fast Fourier Transform (FFT). The FFT's of the experimental vibration signals are calculated by MATLAB software. For a continuous time signal, the Fourier transform is calculated by the equation given below.

$$F(i\omega) = \int_{-\infty}^{\infty} f(t)\, e^{-i\omega t} dt \tag{7.2}$$

If vibration signal is a discrete signal having n samples, the Fast Fourier Transform is calculated as

$$X(k) = \sum_{i=1}^{n} x(i)\, e^{-i\frac{2\pi(k-1)*(i-1)}{n}} \qquad 1<k<n \tag{7.3}$$

where n is the number of sample

7.3 The Fast Fourier Transform Application For Inner Race Defect Case

In the first step, the vibration velocity signals are examined. The fast Fourier transform is performed on the corresponding data and the frequency spectrum is

obtained. In the frequency spectrum, it is observed that characteristic inner race fault frequency cannot be seen for velocity data. For example, at 750 rpm shaft speed, inner race fault frequency is 91 Hz. However, there is no frequency component at that frequency as it can be seen from Figure 7.2. In the further step, vibration acceleration signals are examined and the fast Fourier transform is performed on data. It is observed that characteristic inner race fault frequency can be seen in the FFT of the acceleration data.

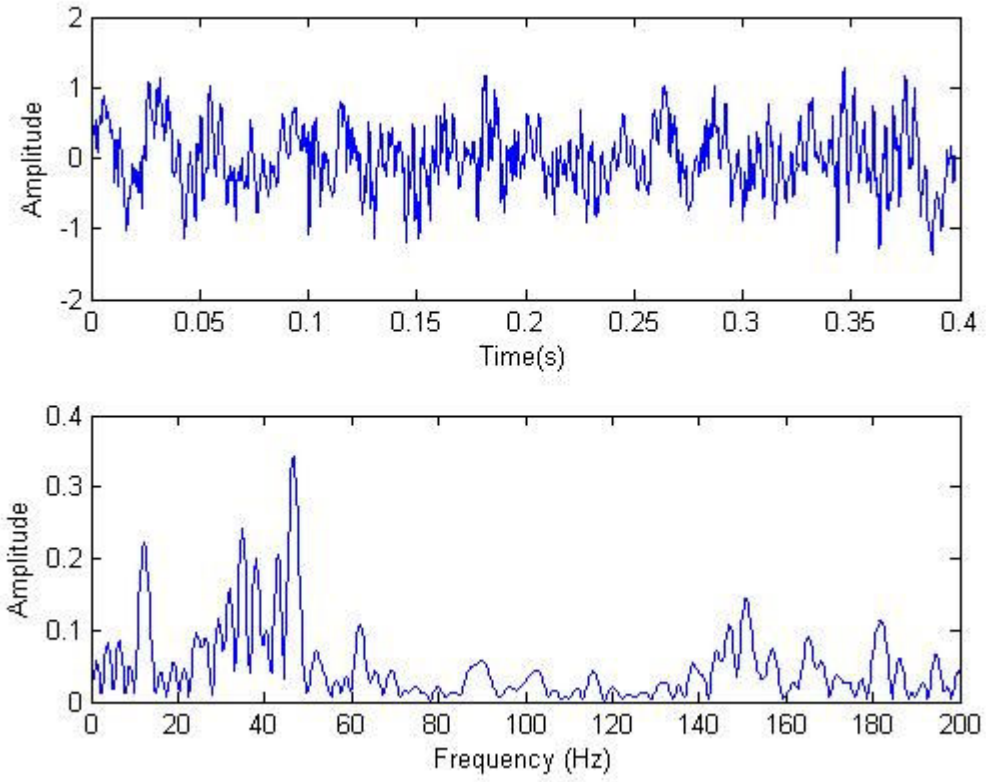

Figure 7.2 FFT of the velocity signal (shaft speed: 750 rpm).

As it is mentioned before, the characteristic fault frequencies can be seen in the vibration acceleration signals. Therefore, further analysis is focused on acceleration signals for the corresponding inner race fault for each shaft speed. Furthermore, FFT of the healthy condition vibration signals also are presented for comparison purposes below from the Figures 7.3 to Figure 7.12 repeatedly.

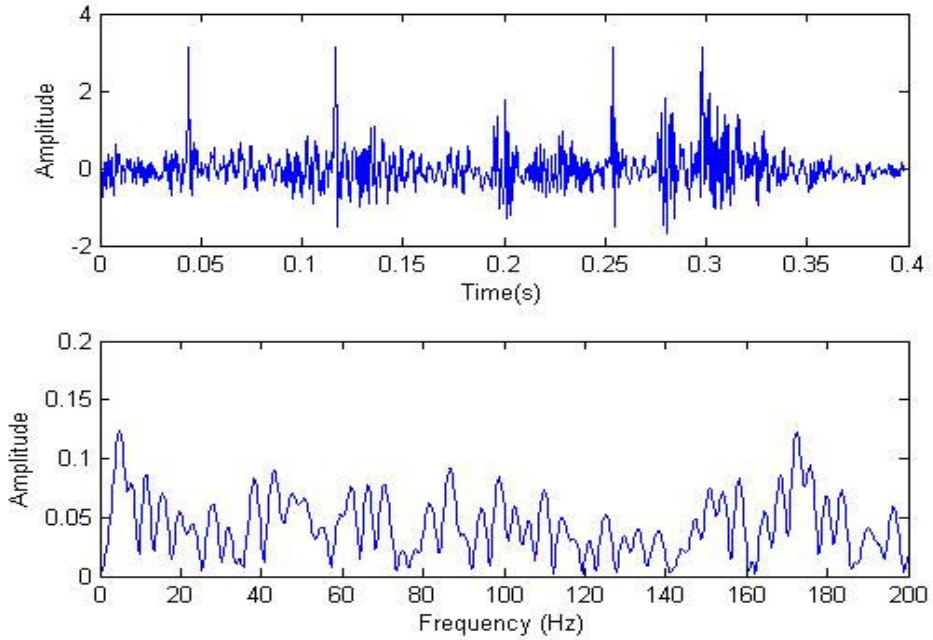

Figure 7.3 FFT of the healthy condition - acceleration signal (shaft speed: 750 rpm).

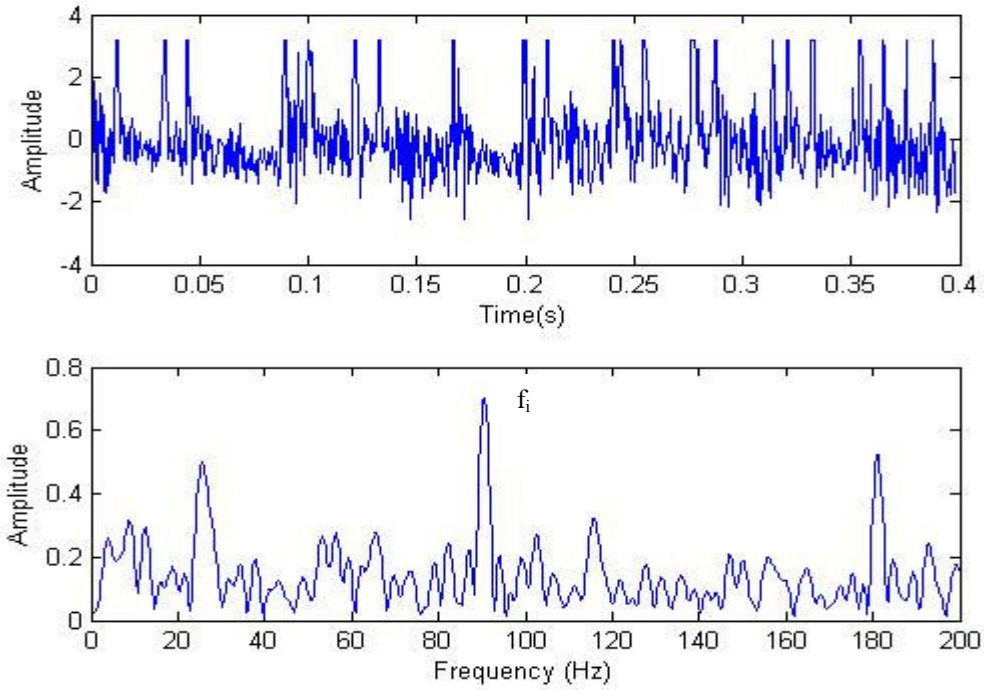

Figure 7.4 FFT of the inner race fault - acceleration signal (shaft speed: 750 rpm).

.

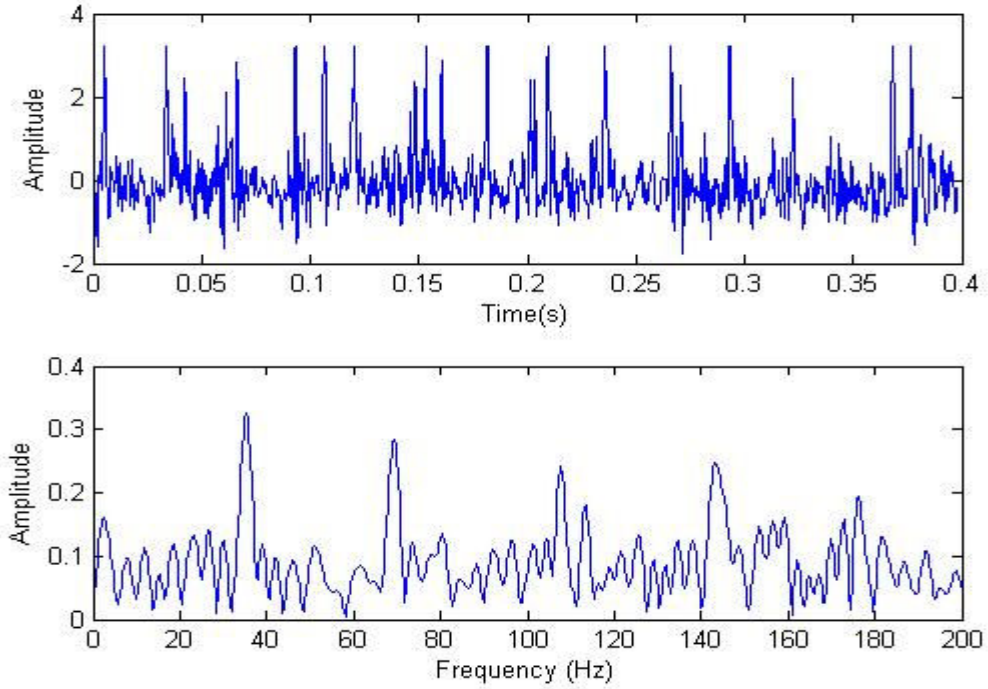

Figure 7.5 FFT of the healthy condition - acceleration signal (shaft speed: 1000 rpm).

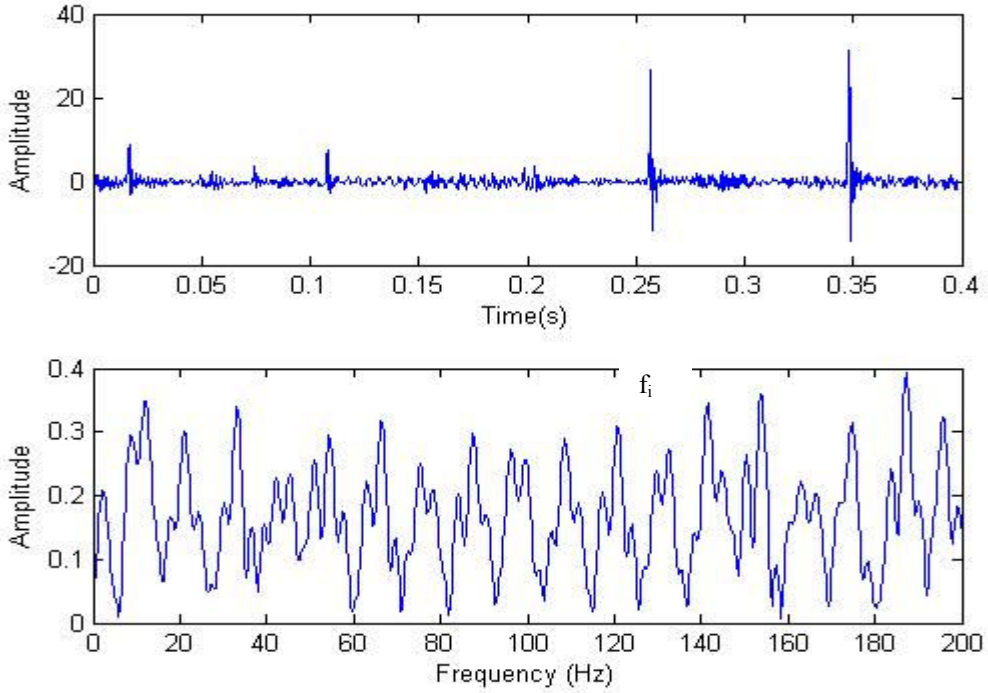

Figure 7.6 FFT of the inner race fault - acceleration signal (shaft speed: 1000 rpm).

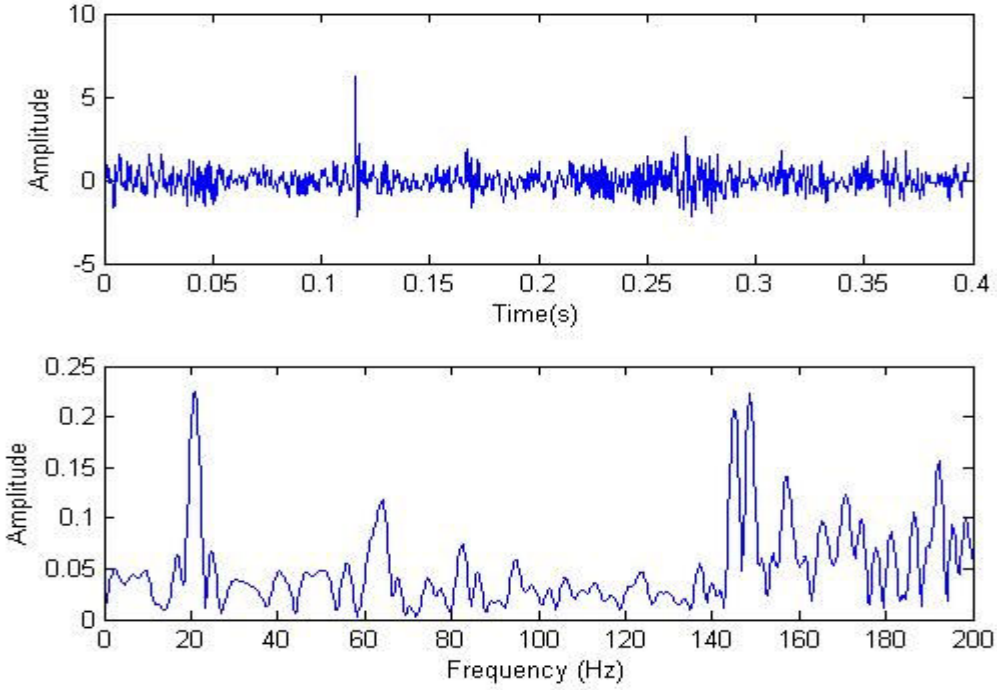

Figure 7.7 FFT of the healthy condition - acceleration signal (shaft speed: 1250 rpm)

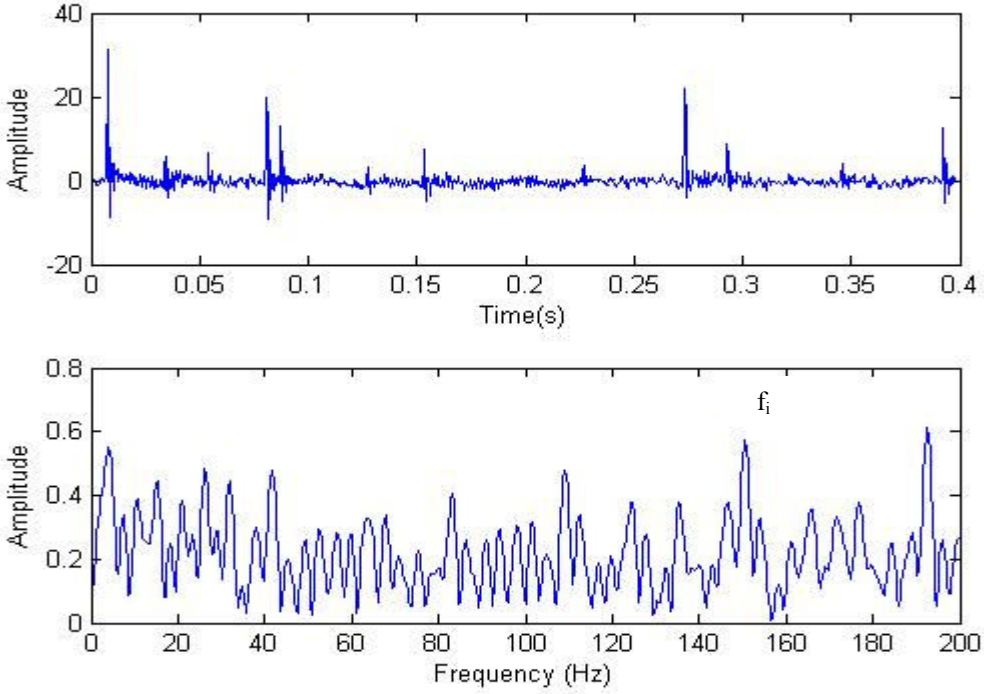

Figure 7.8 FFT of the inner race fault - acceleration signal (shaft speed: 1250 rpm).

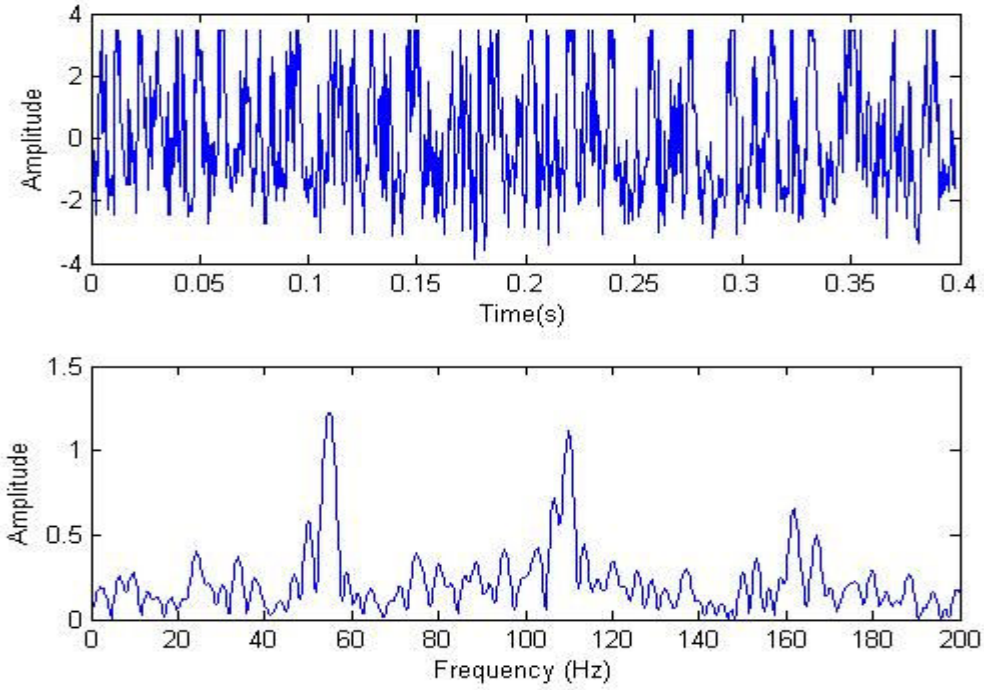

Figure 7.9 FFT of the healthy condition - acceleration signal (shaft speed: 1500 rpm)

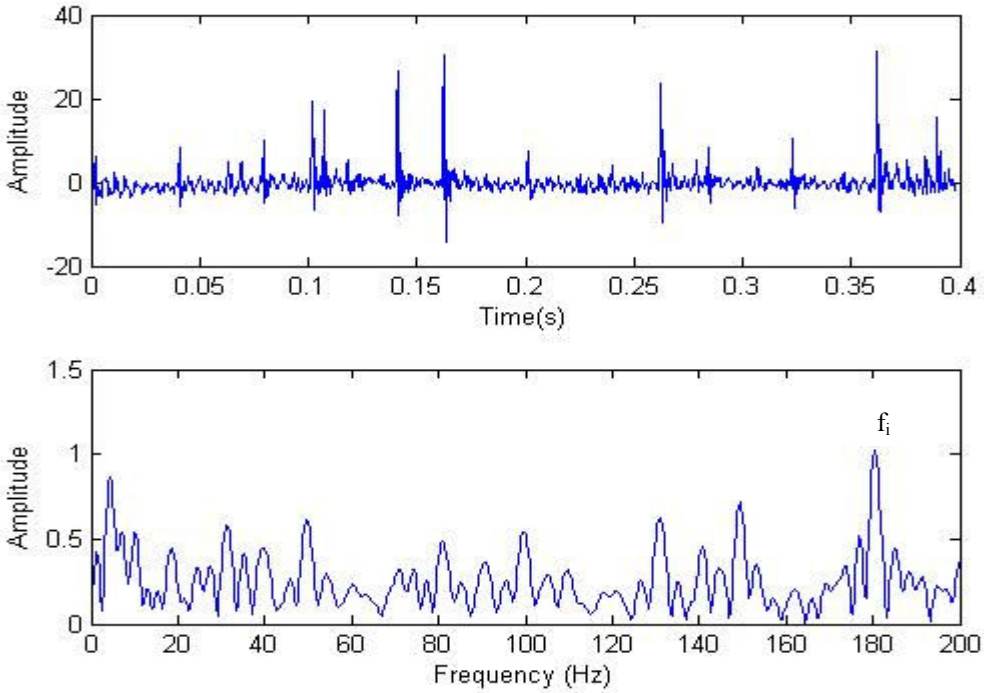

Figure 7.10 FFT of the inner race fault - acceleration signal (shaft speed: 1500 rpm).

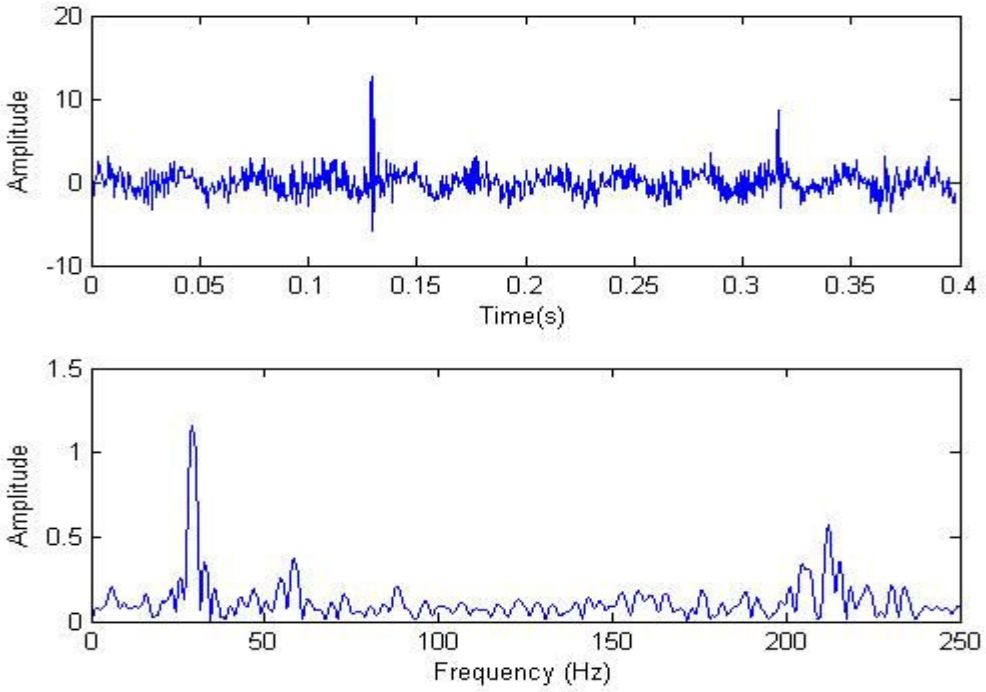

Figure 7.11 FFT of the healthy condition - acceleration signal (shaft speed: 1750 rpm).

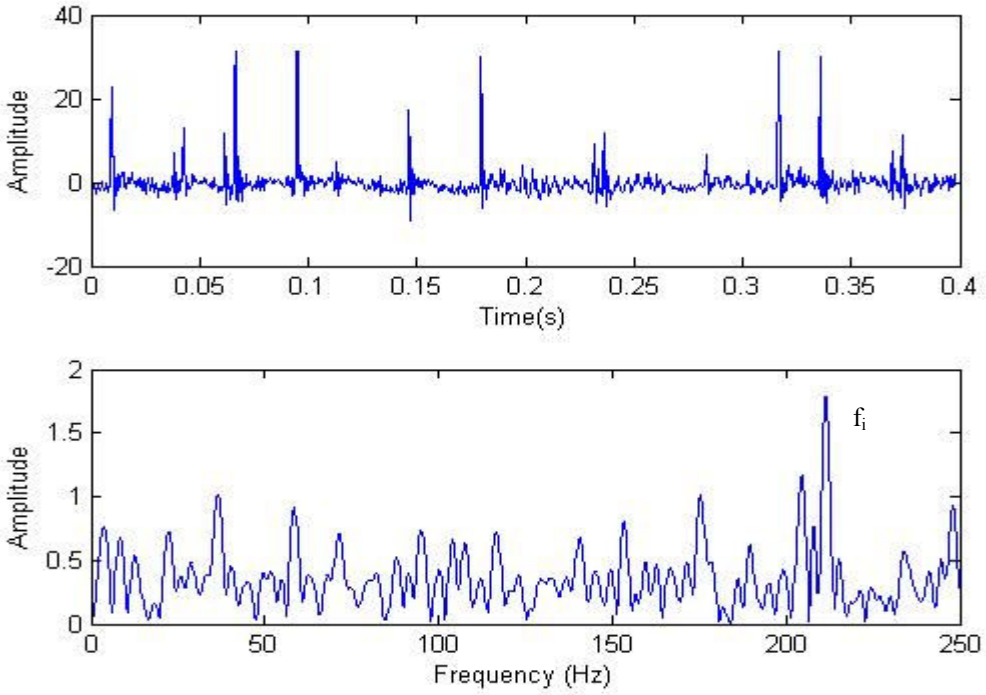

Figure 7.12 FFT of the inner race fault - acceleration signal (shaft speed: 1750 rpm).

From the Figures (from Figure 7.3 to Figure 7.12), time vs amplitude and frequency spectrums are given for both healthy cases and the inner race fault cases. From the corresponding figures, characteristic inner race frequency can be seen clearly. For example, for the shaft speed 1750 rpm the corresponding inner race fault frequency is 212 Hz. From the Figure 7.12, it is seen that there is a peak at that frequency.

7.4 The Short Time Fourier Transform (STFT)

The Short Time Fourier Transform of a time signal x(t) is described by Eq.(7.4) and further information about the STFT can be obtained from the study of Misiti M., Misiti Y., Oppenheim and Poggi (1997).

$$X(\tau,\omega) = \int_{-\infty}^{\infty} x(t)\omega(t-\tau)e^{-j\omega t}dt \tag{7.4}$$

where ω is the window used in the transformation. The STFT is a joint time-frequency transformation and gives the frequency contents of a time signal with their occurrence times.

The Short Time Fourier Transforms (STFT) of experimental vibration signals are calculated by MATLAB's spectrogram command in order to show the time dependence of the frequency components.

7.5 STFT Application For Inner Race Defect Case

The short time Fourier transform is applied on the vibration data for inner race fault. Both the velocity and the acceleration signals are investigated.

7.5.1 STFT of Velocity Signal For Inner Race Defect Case

The short time Fourier transform of velocity responses for the inner race defect case are given from Figure 7.13 to Figure 7.16. In the transform, window length is chosen to get the optimum time and frequency resolution.

At 750 rpm shaft speed, characteristic inner race fault frequency is 91 Hz. From Figure 7.13., it is not clear to see corresponding characteristic frequency component. There is no dark red area which shows the highest amplitude at that frequency in the spectrum. In the FFT of the same data (Figure 7.2), there is a high amplitude frequency component near 50 Hz. This situation is also observed from Figure 7.13.

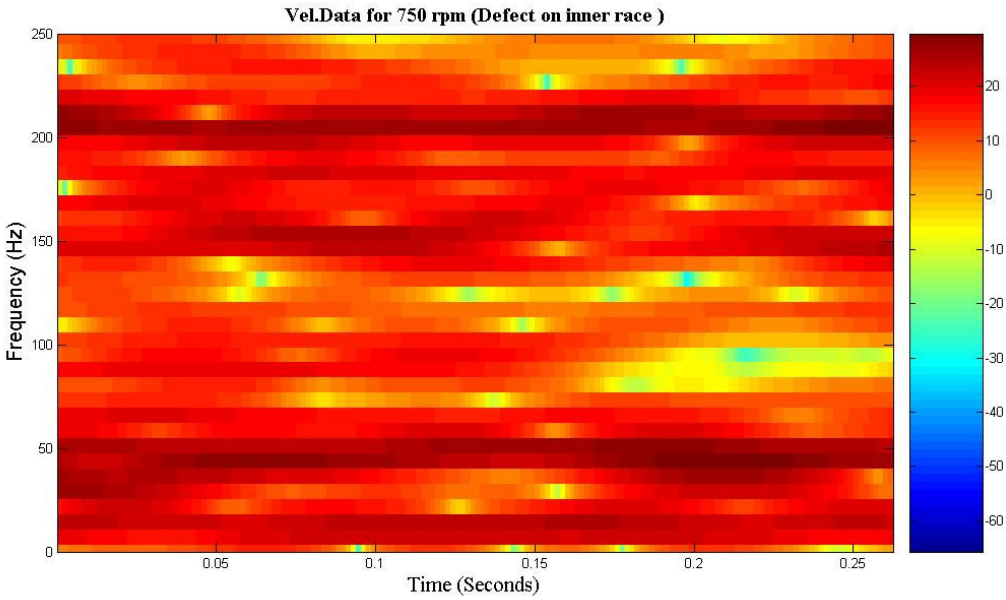

Figure 7.13 STFT of the velocity signal (shaft speed: 750 rpm).

At 1000 rpm shaft speed, characteristic inner race fault frequency is 121 Hz. From Figure 7.14, it is not clear to see corresponding characteristic frequency component. There is no dark red area at that frequency in the spectrum.

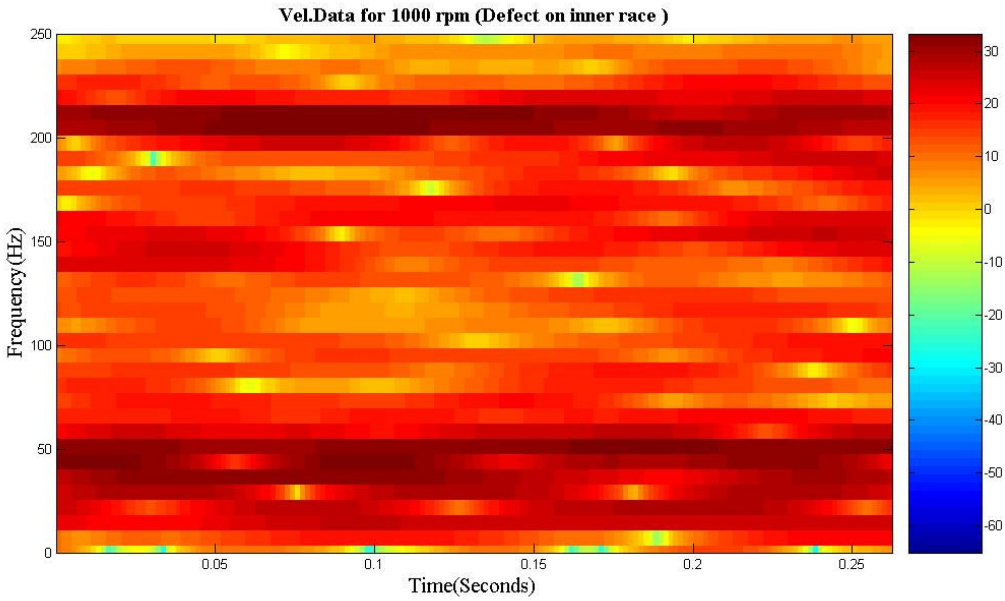

Figure 7.14 STFT of the velocity signal (shaft speed: 1000 rpm).

At 1250 rpm shaft speed, characteristic inner race fault frequency is 151 Hz. From Figure 7.15, it is not clear to see corresponding characteristic frequency component. There is no dark red area at that frequency in the spectrum.

.

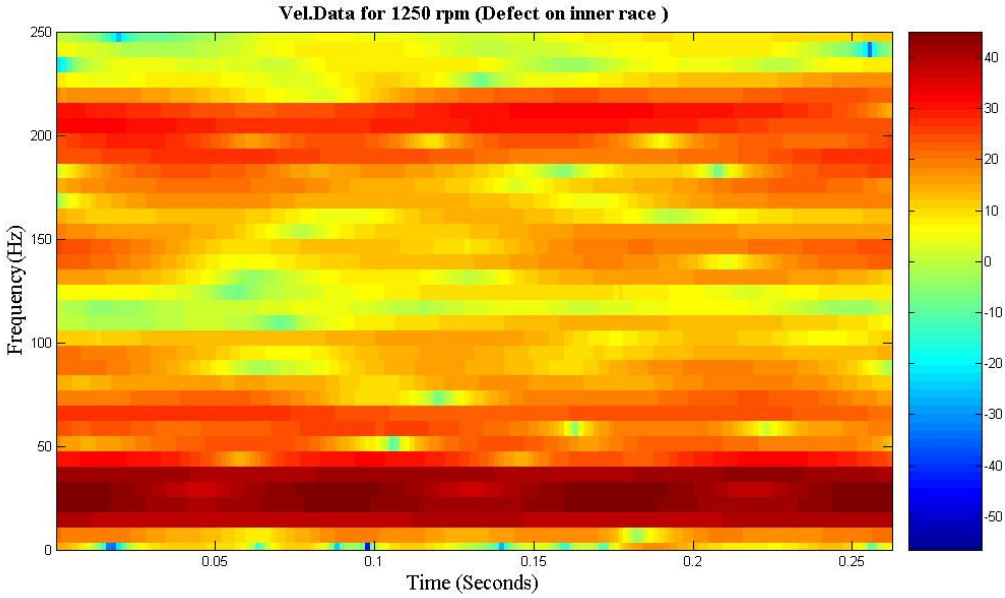

Figure 7.15 STFT of the velocity signal (shaft speed:1250 rpm).

At 1500 rpm shaft speed, characteristic inner race fault frequency is 182 Hz. From Figure 7.16, it is hard to see the characteristic fault frequency from the spectrum.

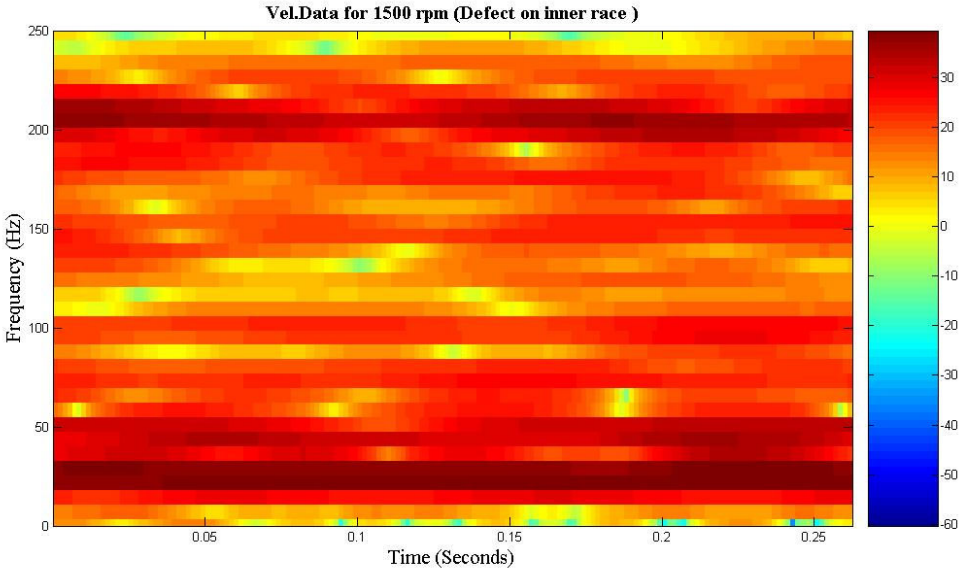

Figure 7.16 STFT of the velocity signal (shaft speed:1500 rpm).

At 1750 rpm shaft speed, characteristic inner race fault frequency is 212 Hz. From Figure 7.17, it is seen that there is a faulty condition between 0.15 s – 0.25 s time interval. However, around 30 Hz there is a frequency component (rotation speed), which has the highest amplitude in the spectrogram.

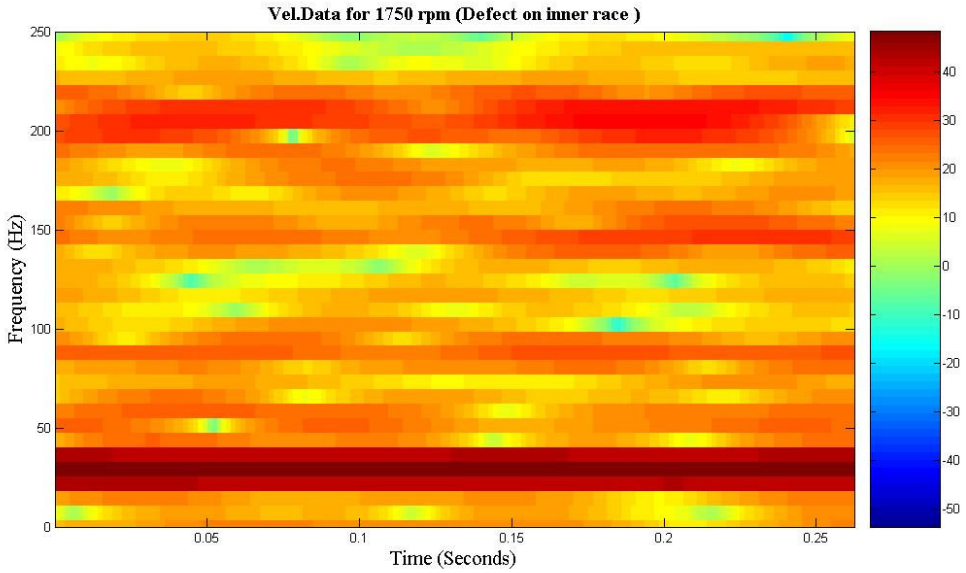

Figure 7.17 STFT of the velocity signal (shaft speed: 1750 rpm).

7.5.2 STFT of Acceleration Signal For Inner Race Defect Case

The short time Fourier transform of acceleration responses for the inner race defect cases are given from Figure 7.18 to Figure 7.22. In the transform, window length is chosen to get the optimum time and frequency resolution.

Analysis starts at 750 rpm shaft speed. In that shaft speed, characteristic inner race fault frequency is 91 Hz. From Figure 7.18, it is clearly seen that the darkest area is at that frequency.

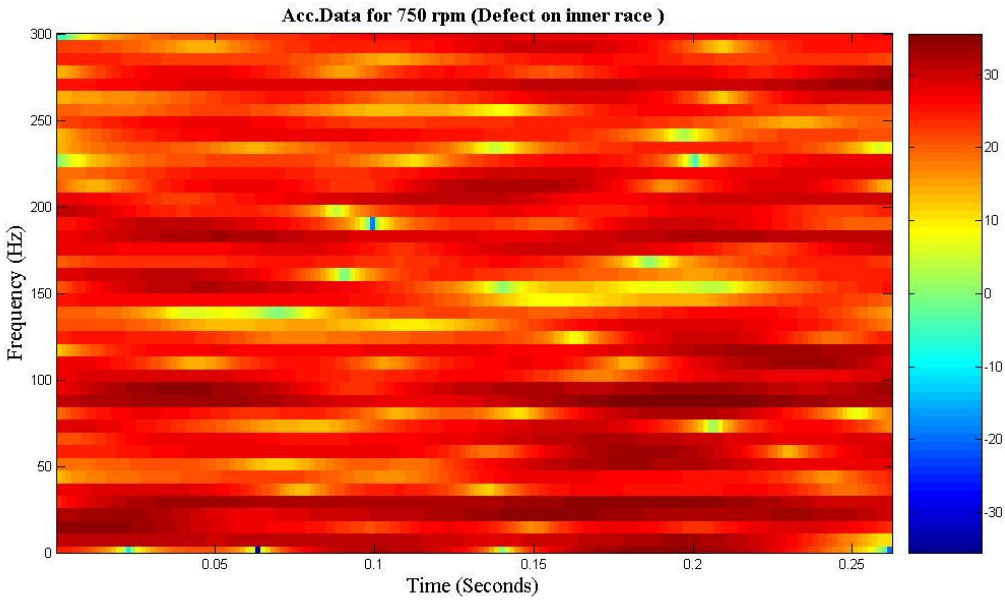

Figure 7.18 STFT of the acceleration signal (shaft speed: 750 rpm).

At 1000 rpm shaft speed, characteristic inner race fault frequency is 121 Hz and it is difficult to see the characteristic fault frequency from the spectrum.

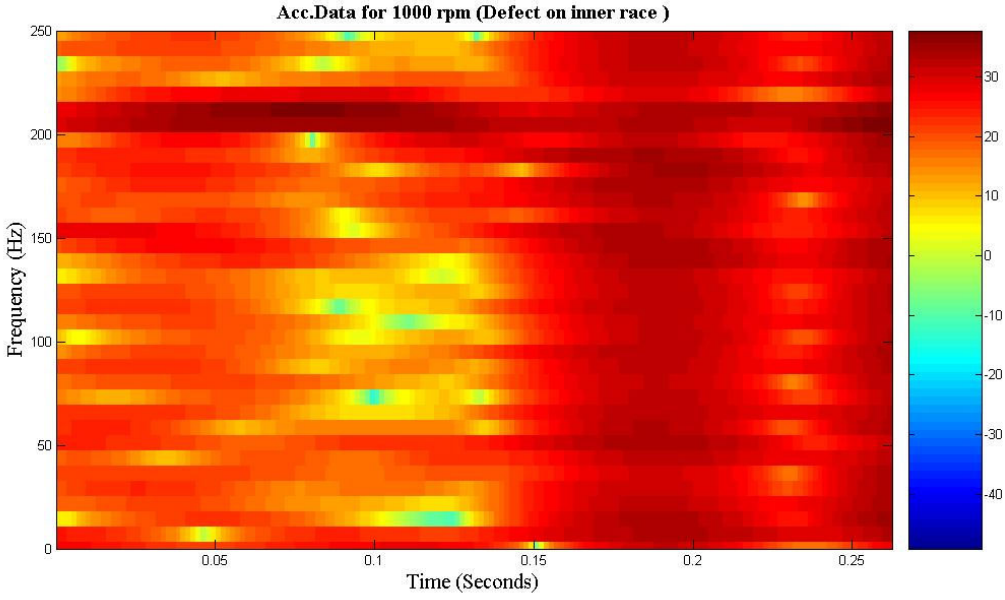

Figure 7.19 STFT of the acceleration signal (shaft speed: 1000 rpm).

At 1250 rpm shaft speed, characteristic inner race fault frequency is 151 Hz. From Figure 7.20, corresponding frequency components can be seen between 0-0.05 seconds time interval.

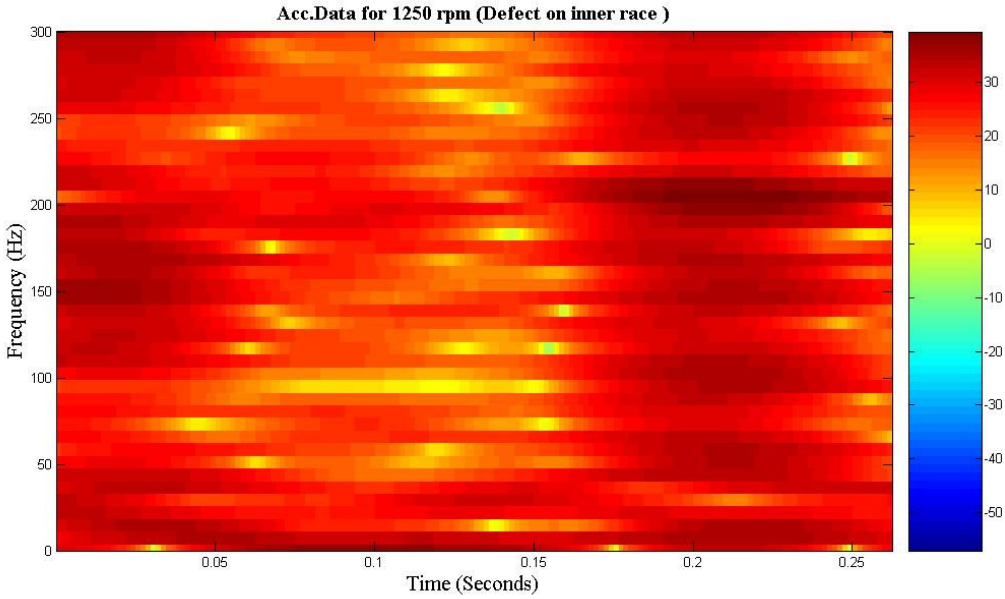

Figure 7.20 STFT of the acceleration signal (shaft speed: 1250 rpm).

At 1500-rpm shaft speed, characteristic inner race fault frequency is 182 Hz. From Figure 7.21, there are two frequency components which have the highest amplitudes. Moreover, it is again clearly seen that the one of the darkest area (182 Hz) is related with the corresponding frequency between 0-0.1 seconds time interval.

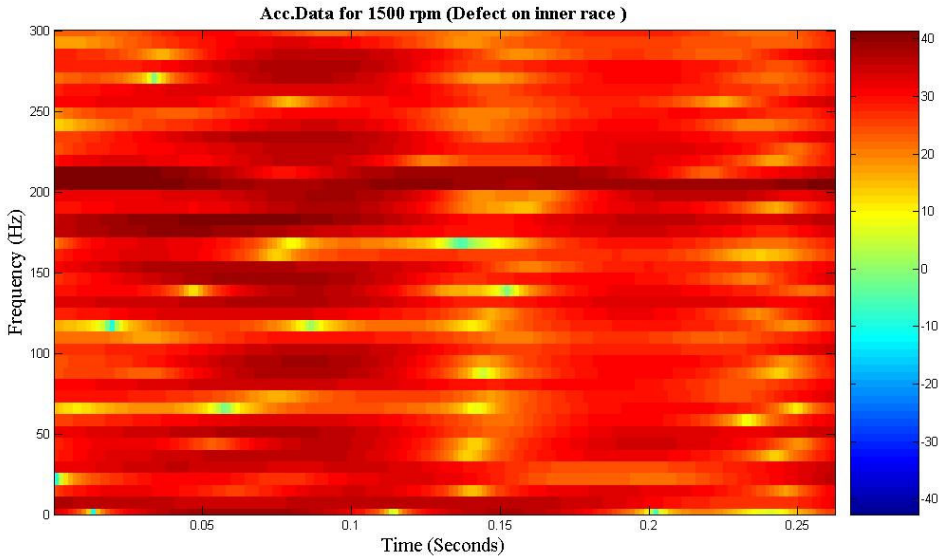

Figure 7.21 STFT of the acceleration signal (shaft speed : 1500 rpm).

At 1750 rpm shaft speed, characteristic inner race fault frequency is 212 Hz. Corresponding frequency component can be seen from Figure 7.22.

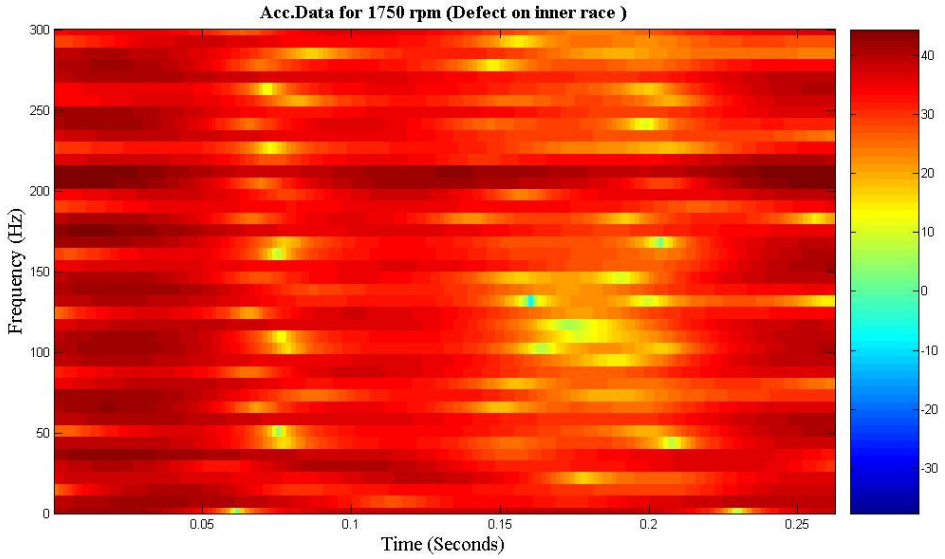

Figure 7.22 STFT of the acceleration signal (shaft speed : 1750 rpm).

CHAPTER EIGHT

WAVELET ANALYSIS

8.1 The Definition of Wavelet Transform

Wavelet is a mathematical function used to divide a given function or continuous-time signal into different scale components. Usually one can assign a frequency range to each scale component. Each scale component can then be studied with a resolution that matches its scale. A wavelet transform is the representation of a function by wavelets. The wavelets are scaled and translated copies (known as "daughter wavelets") of a finite-length or fast-decaying oscillating waveform (known as the "mother wavelet"). Wavelet transforms have advantages over traditional Fourier transforms for representing functions that have discontinuities and sharp peaks, and for accurately deconstructing and reconstructing finite, non-periodic and/or non-stationary signals. Moreover, wavelet transform provides time-frequency representation.

In this study, the continuous wavelet transform is used to overcome the resolution problem of short time Fourier transform. The wavelet analysis is done in a similar way to the short time Fourier transform analysis, in the sense that the signal is multiplied with the wavelet funcion, similar to the window function in the STFT, and the transform is computed separately for different segments of the time-domain signal. However, there are differences between the STFT and the CWT in such a manner that the Fourier transforms of the windowed signals are not taken, and therefore single peak will be seen corresponding to a sinusoid, i.e., negative frequencies are not computed and the width of the window is changed as the transform is computed for every single spectral component.

The continuous wavelet transform is defined as follows,

$$CWT_x(a,b) = \int_{-\infty}^{\infty} x(t) h^*_{b,a}(t) dt \tag{8.1}$$

$$h_{b,a}(t) = \frac{1}{\sqrt{a}} h\left(\frac{t-b}{a}\right) \tag{8.2}$$

Where a (a>0) and b denote dilation and translation parameters respectively and * represents complex conjugation. The family $h_{a,b}(t)$ is constructed by dilation and translation of a function h(t) (mother wavelet) (Öztürk, Yeşilyurt and Sabuncu, 2010).

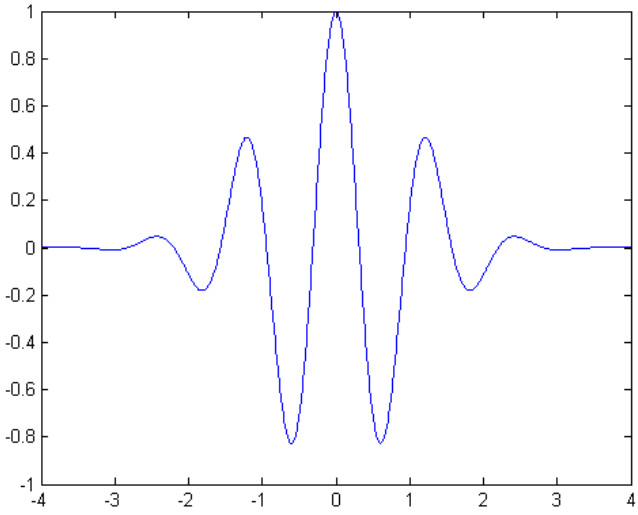

Figure 8.1 Morlet wavelet.

In this study, wavelet transform is performed by morlet wavelet as a mother wavelet (Figure 8.1.). Morlet wavelet in general defined as the equation below:

$$h(t) = e^{(j2\pi f_c t)} \cdot e^{(-t^2/2)} \tag{8.3}$$

where f_c is wavelet centre frequency.

8.2 Scale Frequency Relationship

In the wavelet transform, it is more convenient to use scale and time parameters. The parameter scale in the wavelet analysis is similar to the scale used in maps. As in the case of maps, high scales correspond to a non-detailed global view (of the signal), and low scales correspond to a detailed view. Similarly, in terms of frequency, low frequencies (high scales) correspond to a global information of a signal (that usually spans the entire signal), whereas high frequencies (low scales) correspond to a detailed information of a hidden pattern in the signal (that usually lasts a relatively short time). However, the question arise here how one can convert scale to frequency. The answer can only be given in a broad sense and it's better to speak about the pseudo-frequency corresponding to a scale.

The center frequency, f_c, of the wavelet can be calculated as below,

$$f_a = \frac{f_c}{a \cdot \Delta} \tag{8.4}$$

where,

a is a scale

Δ is the sampling period

f_a is the pseudo-frequency corresponding to the scale a, in Hz

f_c is the center frequency of a wavelet in Hz

In the wavelet transform, the mother wavelet (morlet) center frequency is taken as 0.796 Hz. Therefore, frequency-scale conversion calculations are made by using corresponding center frequency.

Table 8.1 Scale frequency conversion (shaft speed)

Shaft Speed (rpm)	Shaft Speed (Hz)	Scale Value(a)
750	12,50	163,02
1000	16,67	122,27
1250	20,83	97,81
1500	25,00	81,51
1750	29,17	69,87

Table 8.2 Scale frequency conversion (inner race fault characteristic frequency)

Shaft Speed (rpm)	Inner Race Fault Frequency (Hz)	Scale Value(a)
750	91,02	22,39
1000	121,36	16,79
1250	151,7	13,43
1500	182,04	11,19
1750	212,38	9,59

The tables (Table 1 & Table 2) are useful tool in interpretation of the wavelet scalograms. Because in the scalograms, scale and time parameters are configured and corresponding conversion will help to find fault frequencies.

8.3 CWT Application for Healthy Case

The Continuous Wavelet Transform is applied on the healthy condition acceleration data. The corresponding 2D and 3D scalograms are obtained by using MATLAB's *cwt* command. They can be used as a comparison tool in interpretation of the faulty condition scalograms.

From Figure 8.2 to Figure 8.6 it can be seen that healthy system has also some frequency components showing faults. However, their amplitudes are relatively small compared with the faulty case. For example, from Figure 8.2 it can be seen that coefficients peak value is nearly half of the faulty case.

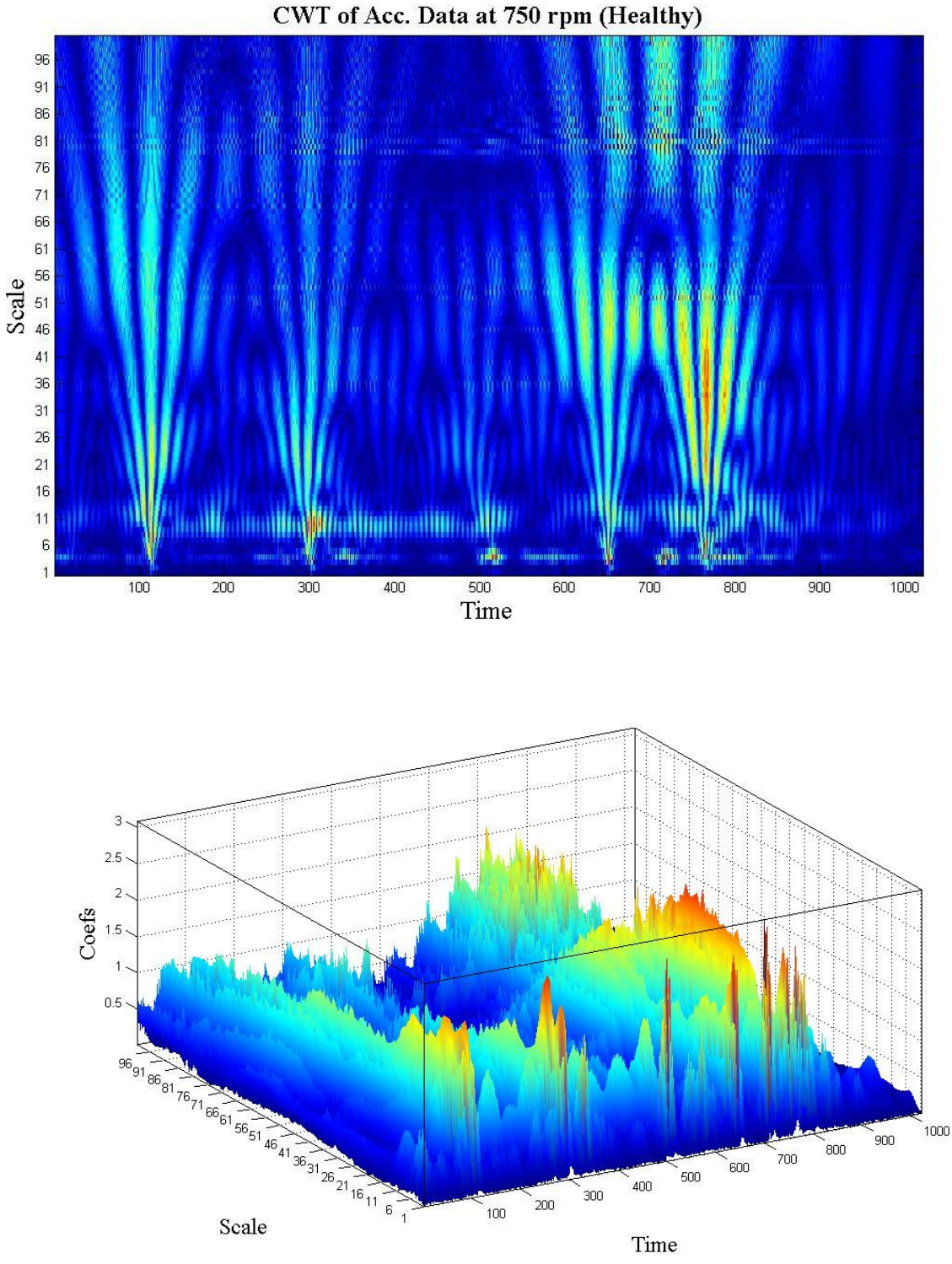

Figure 8.2 Scalogram of acceleration data for the healthy case at 750 rpm.

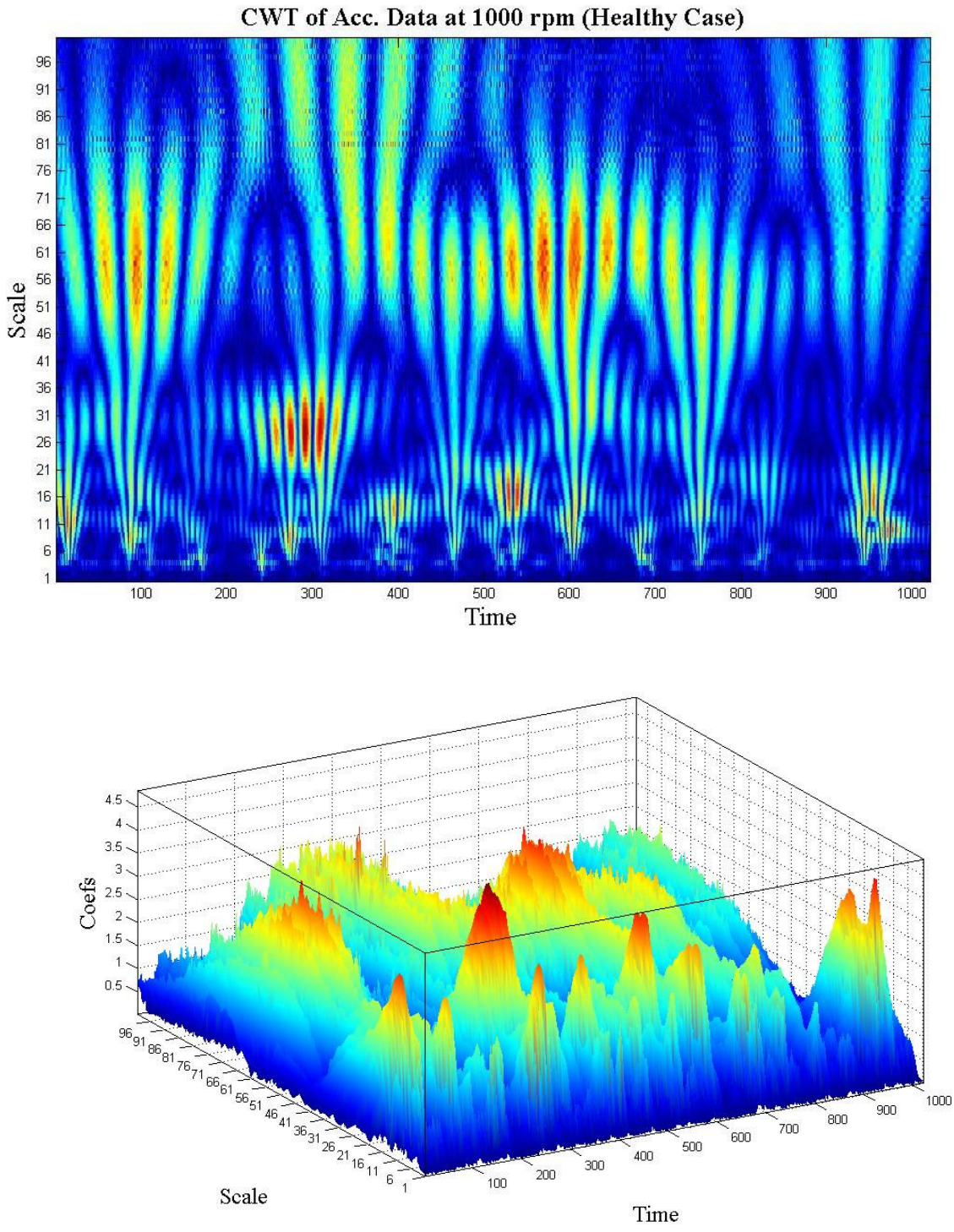

Figure 8.3 Scalogram of acceleration data for the healthy case at 1000 rpm.

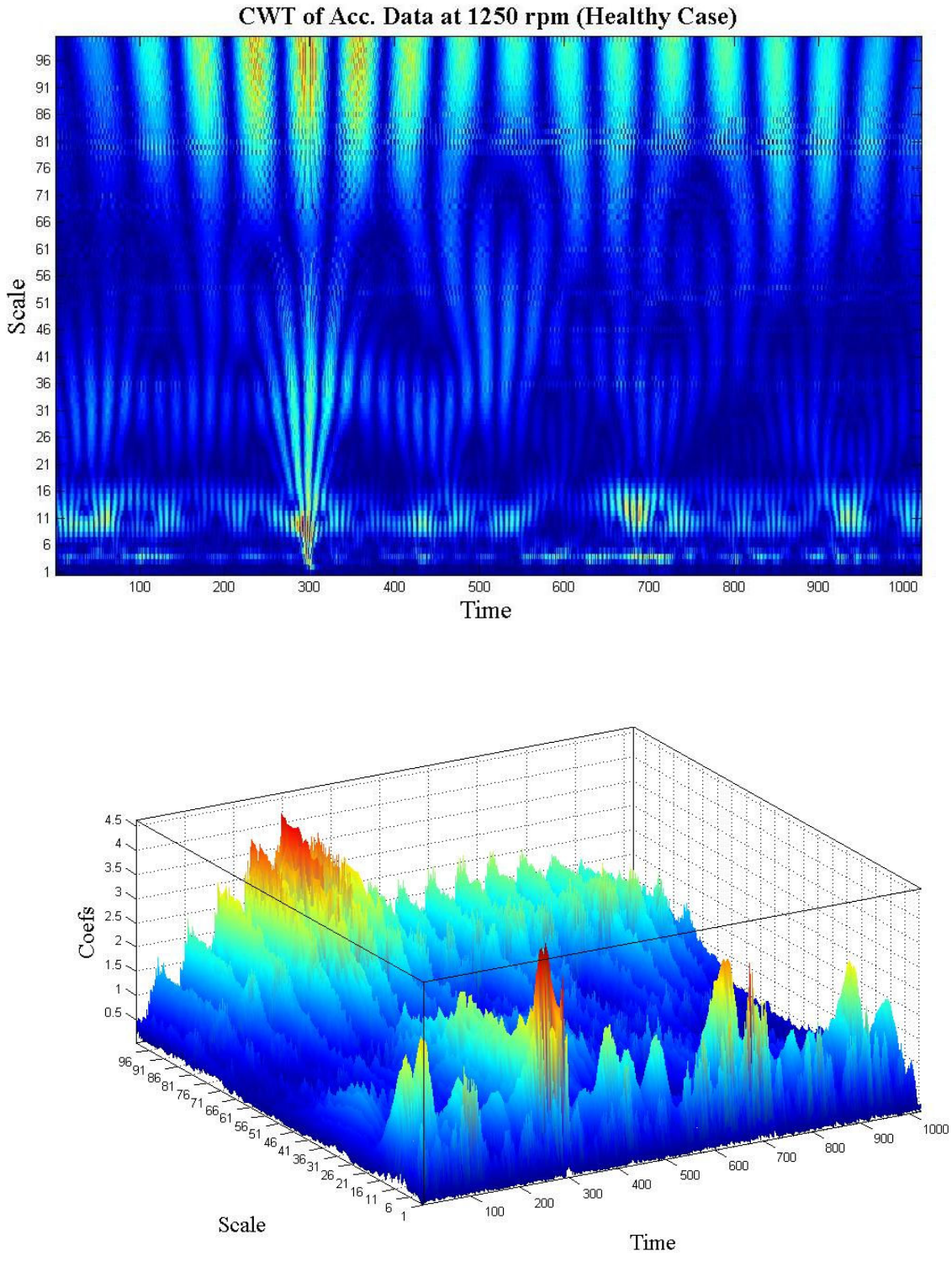

Figure 8.4 Scalogram of acceleration data for the healthy case at 1250 rpm.

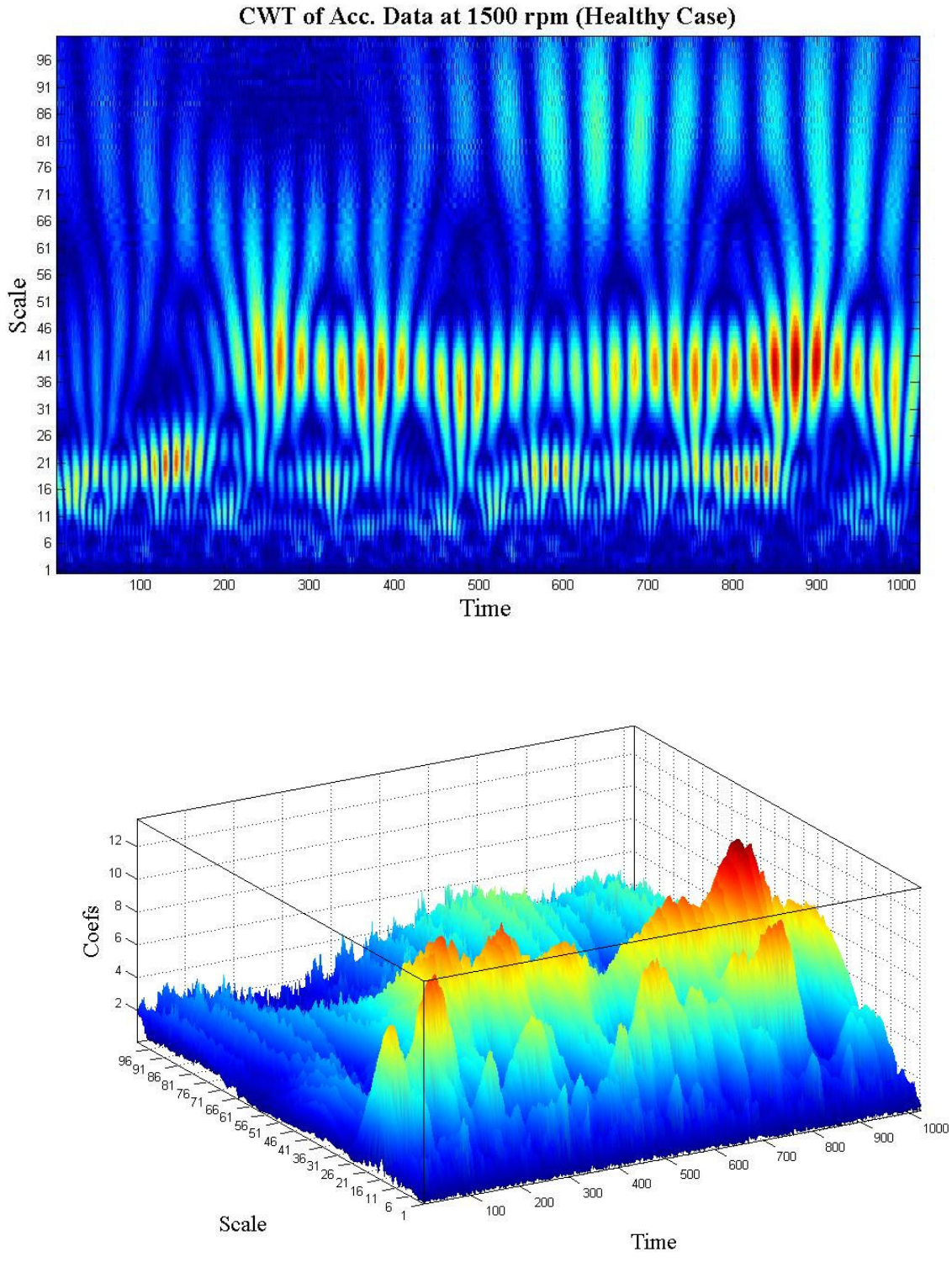

Figure 8.5 Scalogram of acceleration data for the healthy case at 1500 rpm.

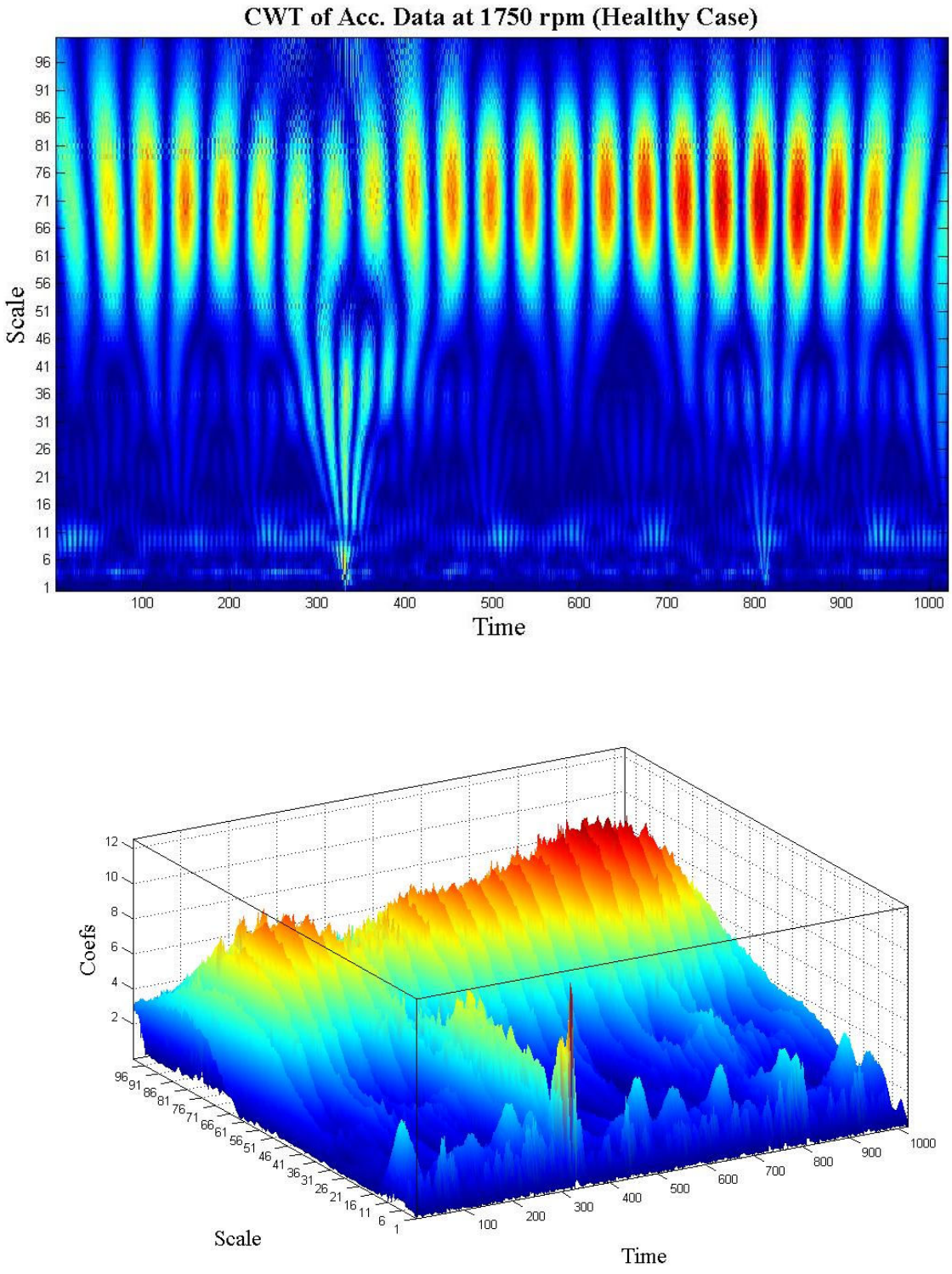

Figure 8.6 Scalogram of acceleration data for the healthy case at 1750 rpm.

8.4 CWT Application for Inner Race Fault Case

The Continuous Wavelet Transform is applied to inner race fault case's acceleration data. The corresponding 2D and 3D scalograms are obtained by using MATLAB's *cwt* command (from Figure 8.7 to Figure 8.11).

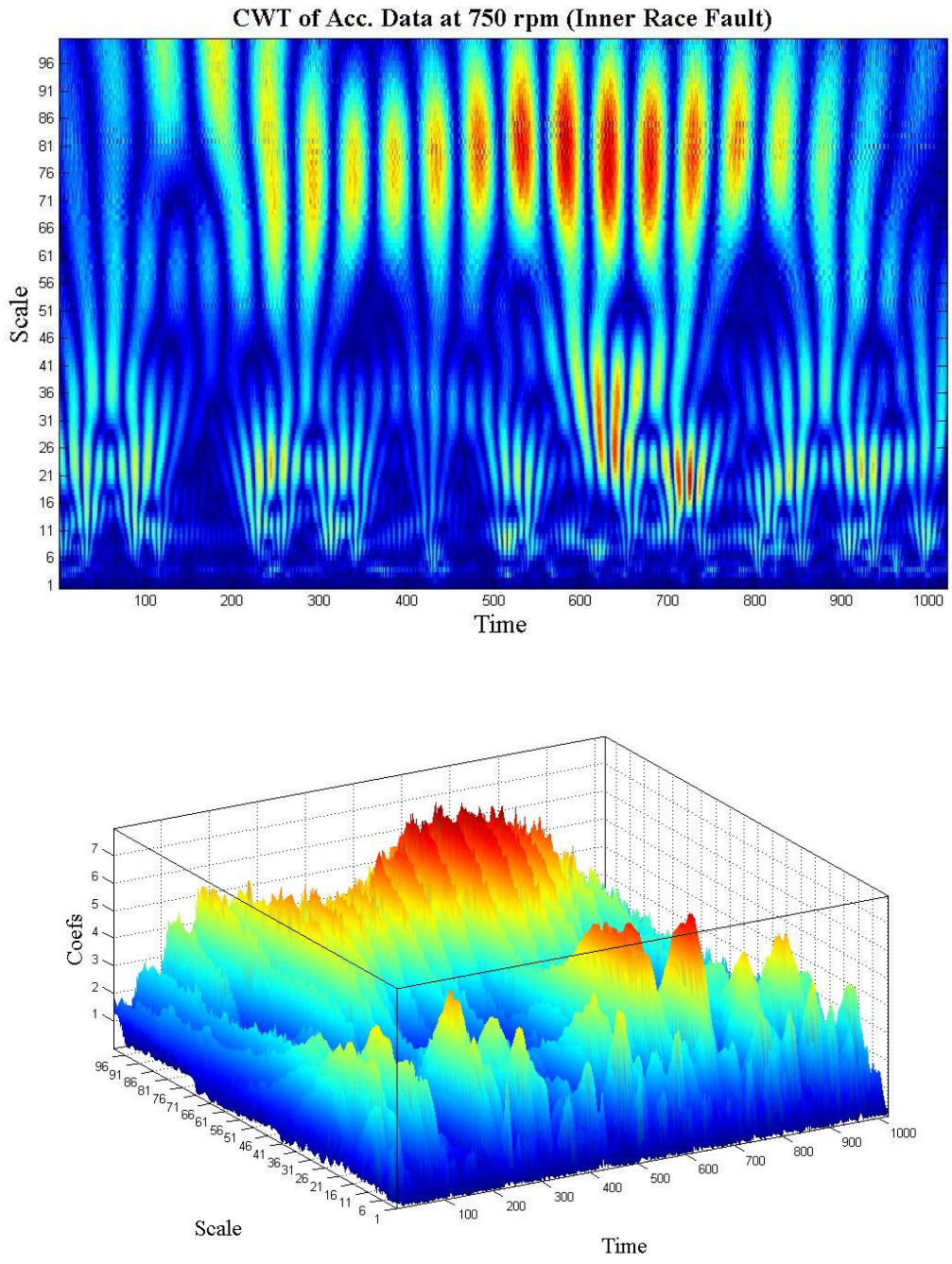

Figure 8.7 Scalogram of acceleration data for the inner race fault at 750 rpm.

At 750-rpm shaft speed, characteristic inner race fault frequency is 91 Hz. By using Table 8.2, it can be seen that this frequency corresponds to the scale value of 22. Corresponding fault frequency can be seen from Figure 8.7.

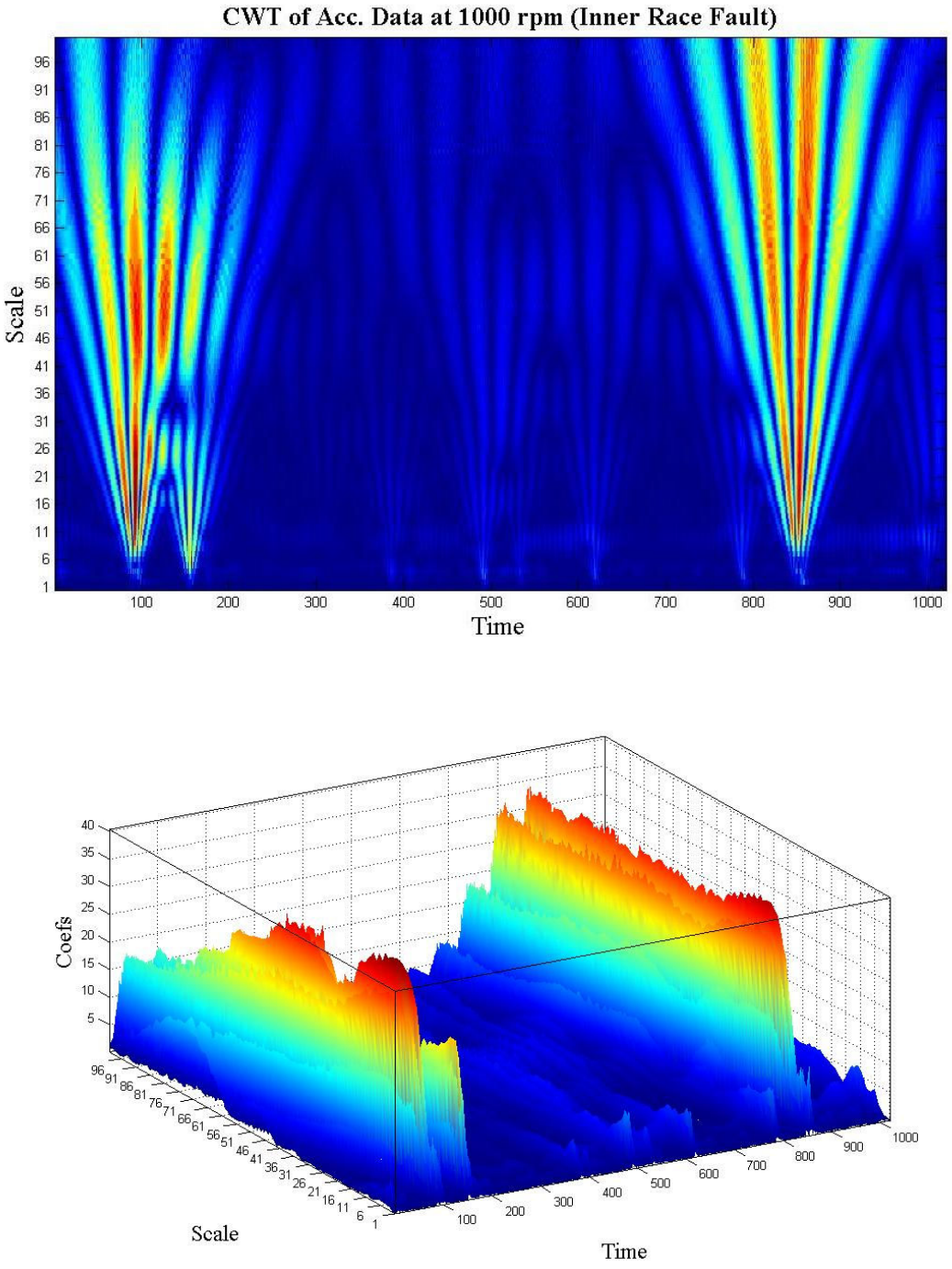

Figure 8.8 Scalogram of acceleration data for the inner race fault at 1000 rpm.

At 1000 rpm shaft speed, characteristic inner race fault frequency is 121 Hz. By using Table 8.2, it can be seen that this frequency corresponds to the scale value of 16. Corresponding fault frequency can be seen from Figure 8.8.

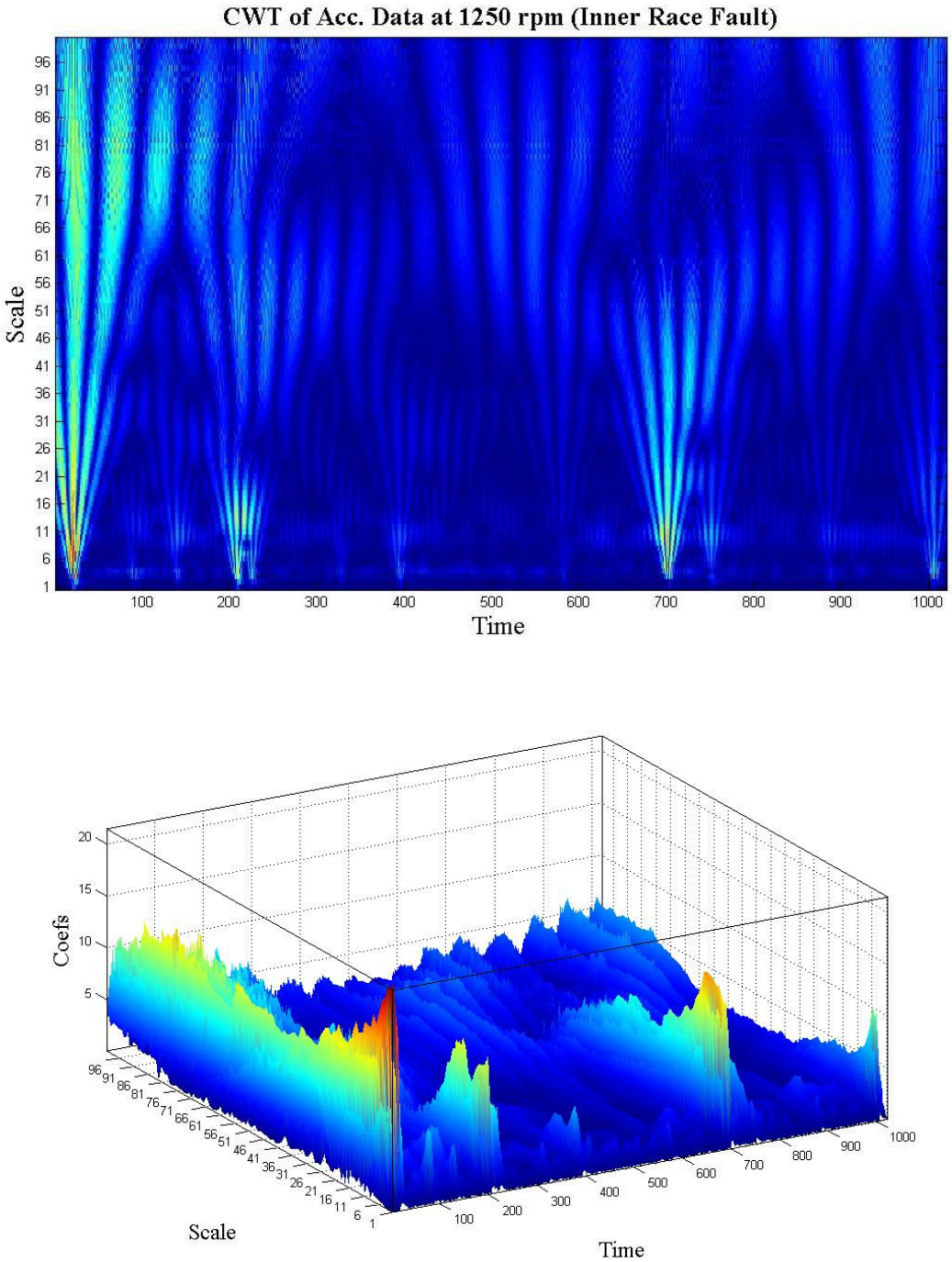

Figure 8.9 Scalogram of acceleration data for the inner race fault at 1250 rpm.

At 1250 rpm shaft speed, characteristic inner race fault frequency is 151 Hz. By using Table 8.2, it can be seen that this frequency corresponds to the scale value of 13. Corresponding fault frequency can be seen from Figure 8.9.

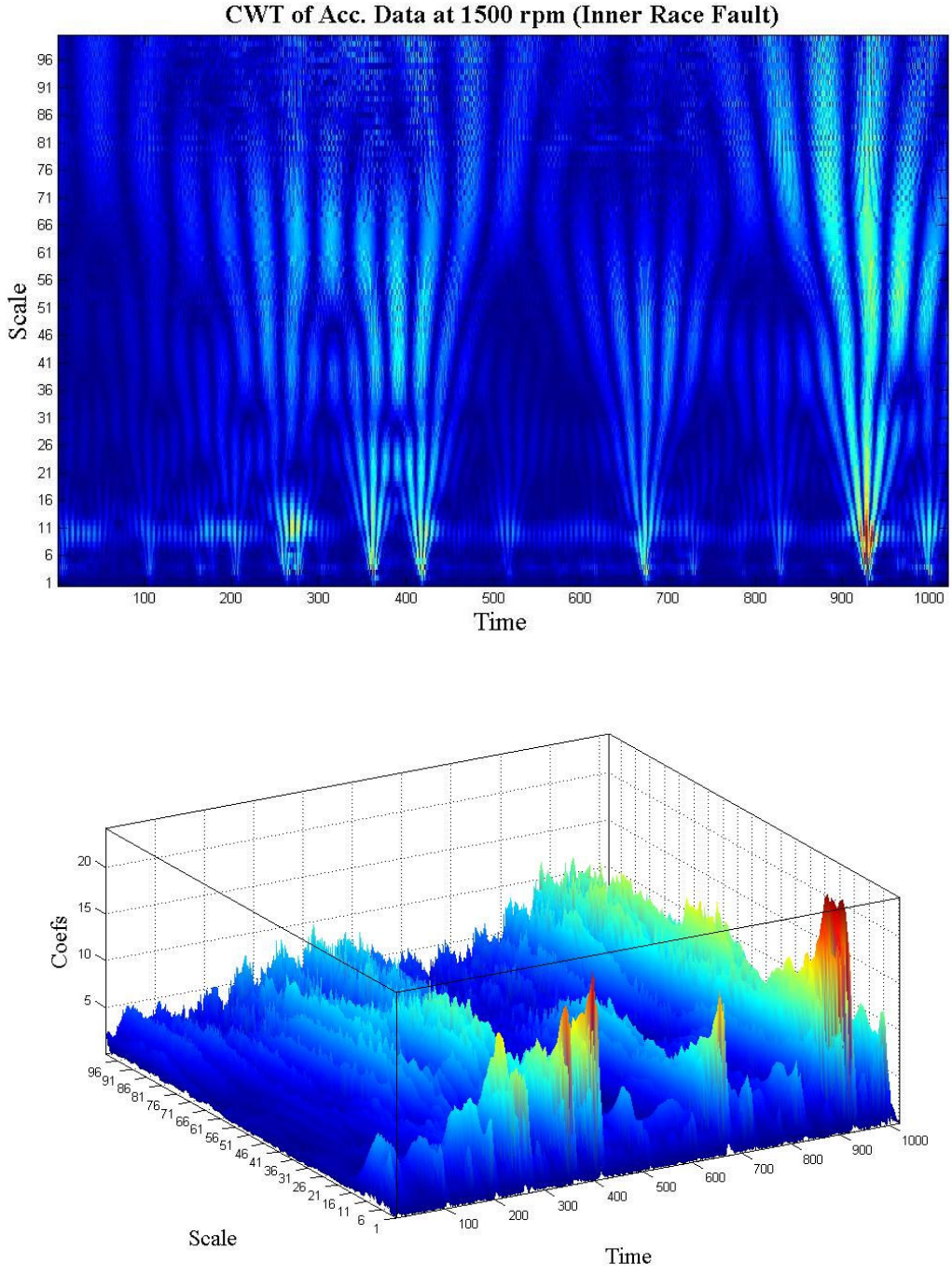

Figure 8.10 Scalogram of acceleration data for the inner race fault at 1500 rpm.

At 1500 rpm shaft speed, characteristic inner race fault frequency is 182 Hz. By using Table 8.2., it can be seen that this frequency corresponds to the scale value of 11. Corresponding fault frequency can be seen from Figure 8.10.

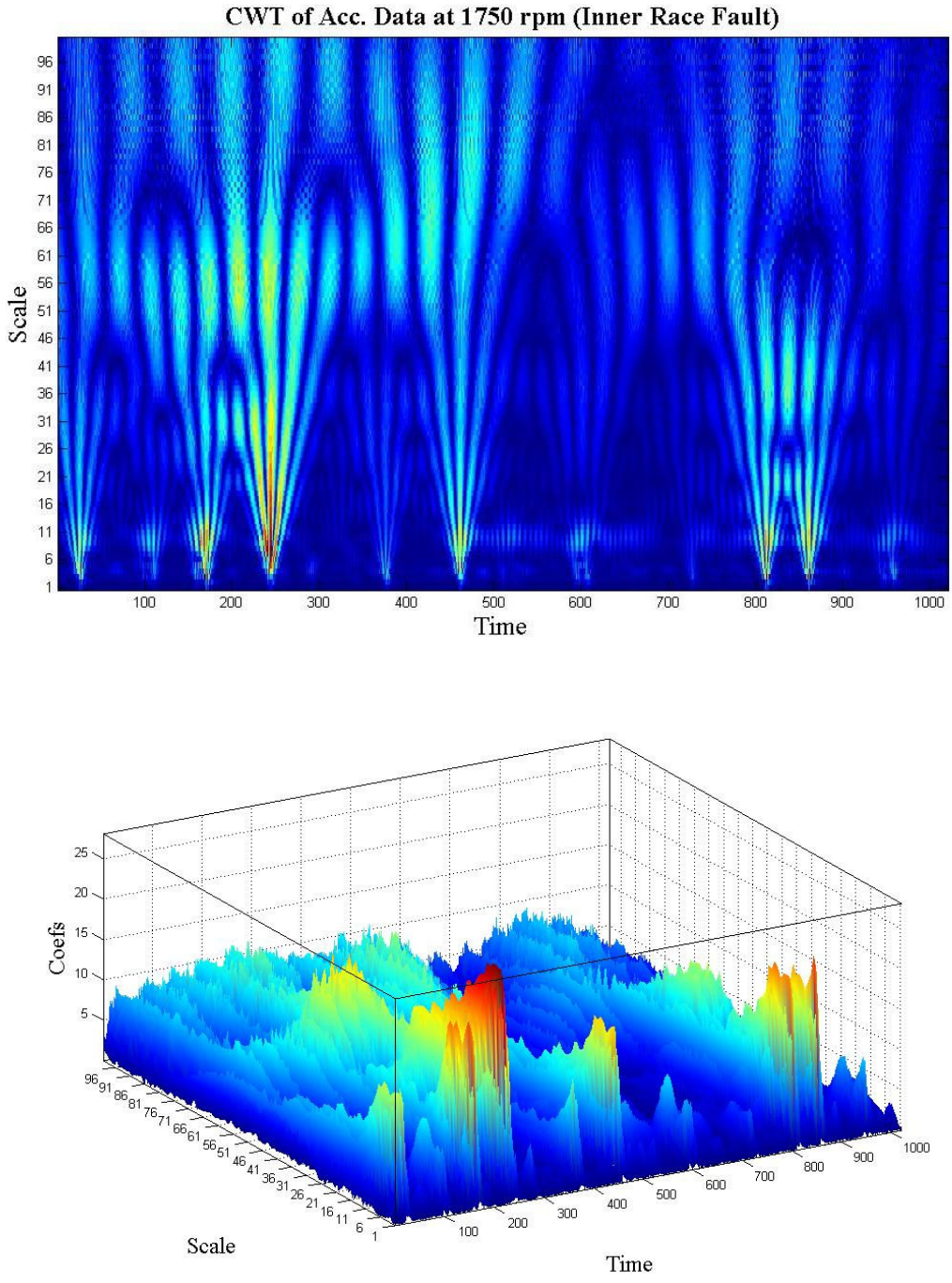

Figure 8.11 Scalogram of acceleration data for the inner race fault at 1750 rpm.

At 1750 rpm speed, inner race fault frequency is 212 Hz. and this frequency corresponds to the scale value of “9”. Corresponding fault frequency can be seen from Figure 8.11

In addition to acceleration data, velocity data’s scalograms are examined for the corresponding inner race fault detection. However, the velocity data are not successful for inner race fault as acceleration data. The characteristic frequency of the inner race fault cannot be seen from the Figure 8.12.

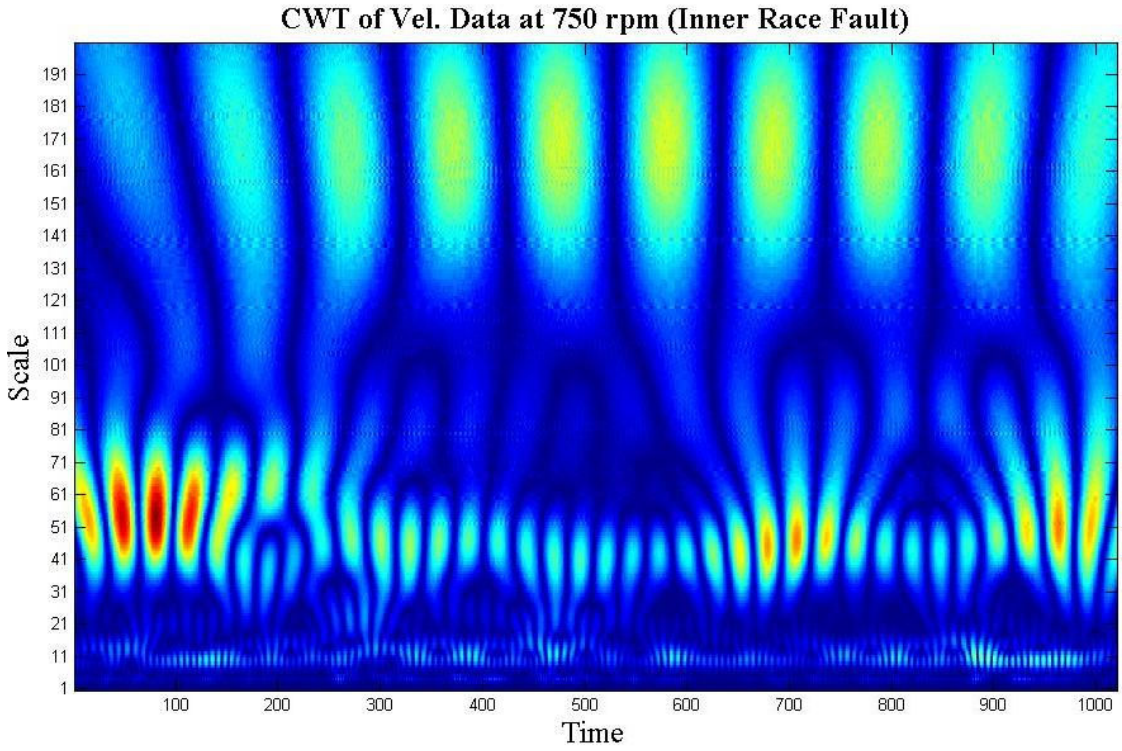

Figure 8.12 Scalogram of velocity data for the inner race fault at 750 rpm.

8.5 CWT Application for Inner Race Fault with Unbalance Case

The Continuous Wavelet Transform is applied on the inner race fault with unbalance case's velocity and acceleration data. The corresponding 2D and 3D scalograms are obtained by using MATLAB's *cwt* command (from Figure 8.13 to Figure 8.16).

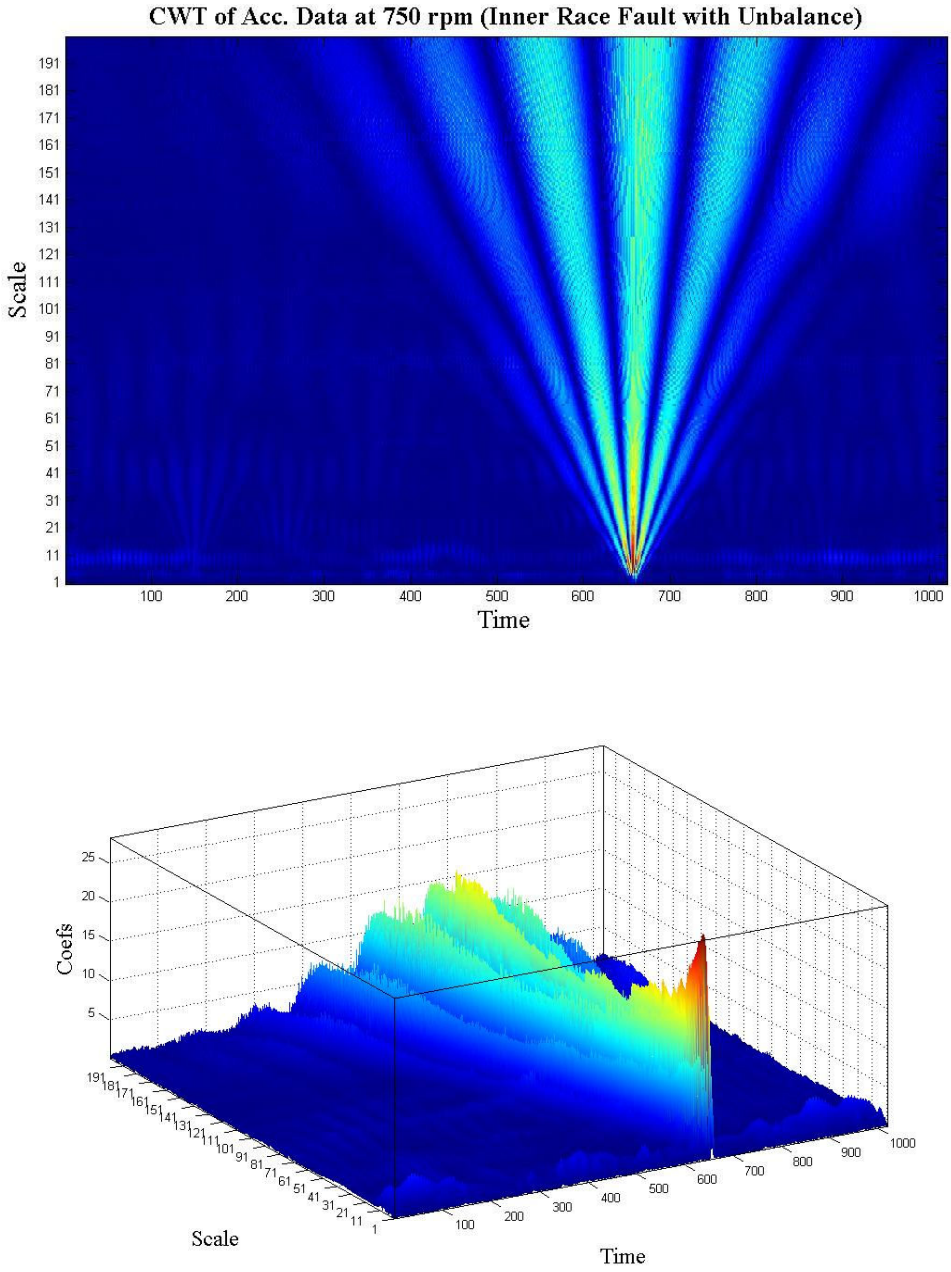

Figure 8.13 Scalogram of acceleration data for inner race fault with unbalance case at 750 rpm.

At 750 rpm shaft speed, characteristic inner race fault frequency is 91 Hz. and the corresponding scale value is 22. Moreover, by using Table 8.1 unbalance fault frequency (shaft rotating speed) is 12.5 Hz and corresponding scale value is 163. It is seen from Figure 8.14 (CWT of velocity data), inner race fault frequency cannot be seen; however, unbalance fault frequency can be seen clearly.

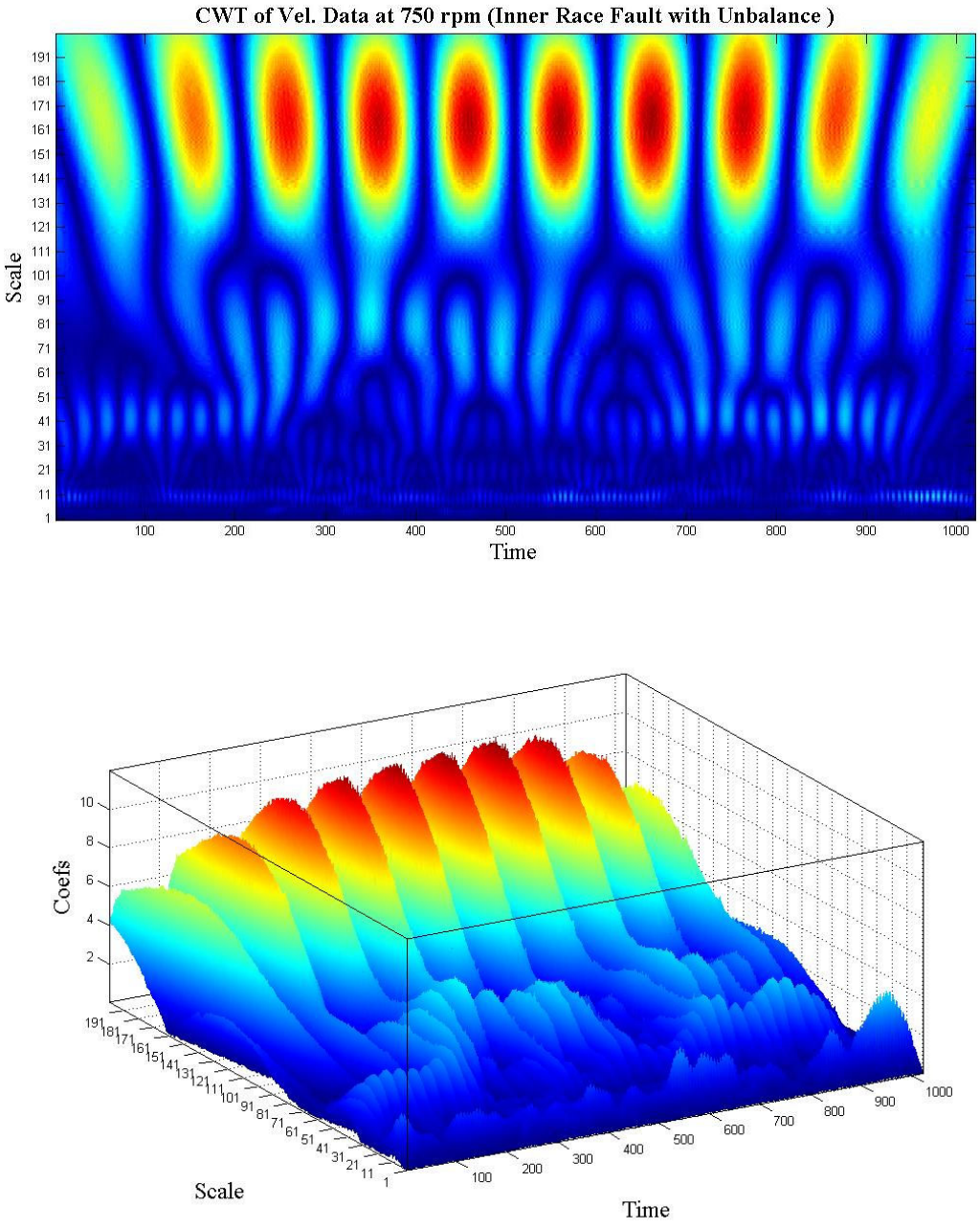

Figure 8.14 Scalogram of velocity data for the inner race fault with unbalance case at 750 rpm.

At 1500 rpm shaft speed, unbalance fault frequency is 25 Hz and inner race fault frequency is 182 Hz. From Table 8.1 and Table 8.2 their scale values are 82 and 11 respectively. After applying cwt to the acceleration data at 1500 rpm shaft speed, Figure 8.11 is obtained. The unbalance fault frequency and inner race characteristic frequency can be seen clearly in the corresponding scalogram.

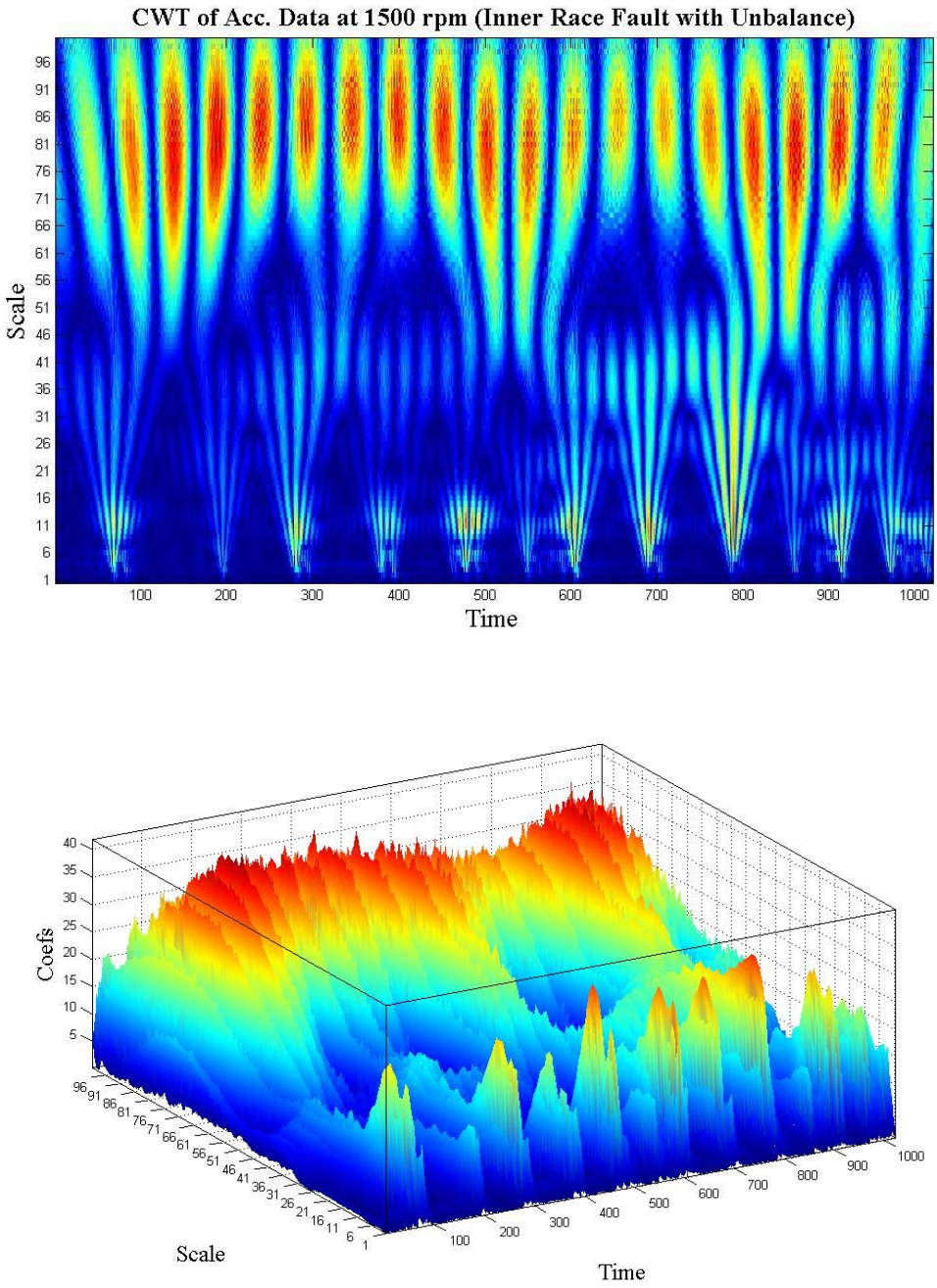

Figure 8.15 Scalogram of acc. data for inner race fault with unbalance case at 1500 rpm.

After applying cwt to the velocity data at 1500 rpm shaft speed, Figure 8.12 is obtained. The unbalance fault frequency can be seen clearly however, inner race characteristic frequency is not visible in the corresponding scalogram.

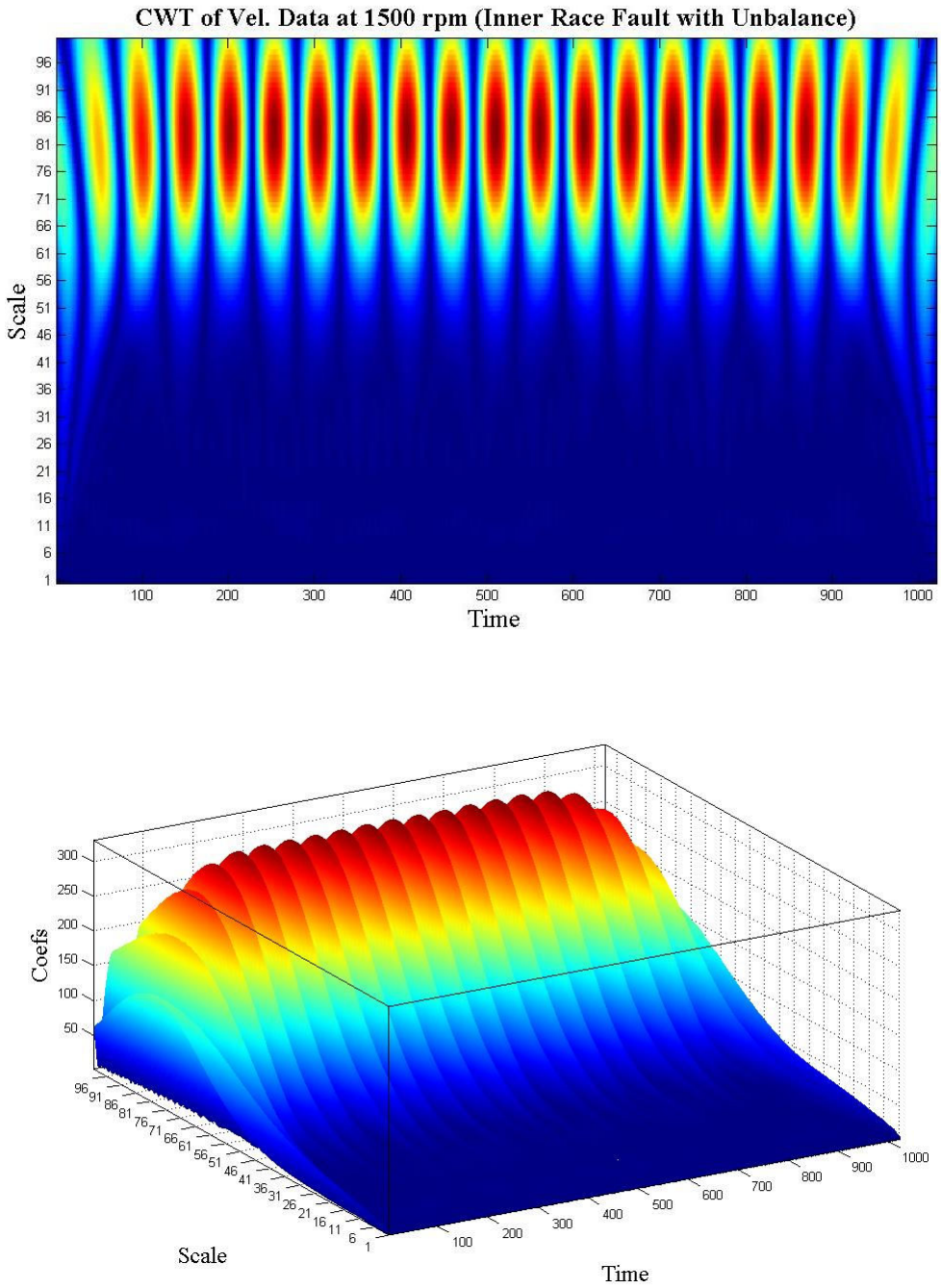

Figure 8.16 Scalogram of vel. data for inner race fault with unbalance case at 1500 rpm.

CHAPTER NINE
CONCLUSIONS

The condition of the rotating system having three main defects (shaft misalignment, unbalance, and inner race defect on cylindrical rolling bearings) is monitored experimentally by vibration analysis. Vibration measurements are performed at different rotational speeds and different fault conditions. The effectiveness of the time domain parameters on the fault diagnosis is investigated. Time domain parameters are applied to velocity and acceleration responses of the test apparatus for healthy and faulty cases and their ratios (faulty/healthy) are investigated. In the scope of this study, the curve length transform, which is a non-linear time based transform, is applied to the vibration signals. The effectiveness of the curve length transform on different kind of fault conditions is sought and scale factor effect on the curve length transform is determined. Furthermore, frequency analysis is performed on the vibration signals. Characteristic defect frequencies are sought on the frequency domain of the vibration signal. Furthermore, time-frequency representations of vibration signals are investigated by using STFT and Wavelet Transforms.

From the experimental results presented in this study, the following points of discussion are summarized:

- The velocity and acceleration responses of a structure including rolling element bearing can be used for defect detection with proper time domain parameters. The usage of acceleration response gives better results for shaft misalignment, inner race fault and their conjunctive conditions. However, velocity response gives better results for unbalance and unbalance & inner race combined fault conditions.

- Generally, the ability of showing faulty condition for time domain parameters changes with rotational speed.

- Standard deviation and peak to peak values give better results for detecting the three types of fault in raw vibration velocity data.

- Kurtosis and alfa give better results in run out and inner race fault cases for the raw vibration acceleration data. However, standard deviation and peak to peak gives better results for unbalance case in raw vibration acceleration data.
- In unbalance fault, velocity data give better results for detecting the fault.
- For run out and inner race fault, acceleration data give better results for detecting the fault.
- Generally, the curve length transform gives better results for detecting the defects.
- Kurtosis (kurt2) values give better results for detecting the faults for run out case after the curve length transform.
- 6^{th} normalized moment is much more sensitive than kurtosis in fault detection.
- The scale factor does not affect the faulty/healty ratio for run out and inner race fault case.
- Increase in the scale factor value causes the faulty/healthy ratio to increase at higher shaft speed for unbalance case.
- The characteristic fault frequency for inner race fault cannot be seen in FFT of velocity data, however can be clearly seen in FFT of acceleration data.
- The characteristic fault frequency for inner race fault cannot be seen in STFT of velocity data, however can be clearly seen in STFT of acceleration data.
- The short time Fourier transform gives an idea about the existence of a defect in the bearing, however the resolution problems in both time and frequency domains exist.

- The continuous wavelet transform gives better results about time instance and frequency of the fault.
- The characteristic inner race fault frequencies cannot be seen in CWT of velocity data; however it can be clearly seen in CWT of acceleration data.
- The coefficients obtained by CWT increase as the shaft speed increases both in inner race fault and unbalance condition.
- In the combined fault experiment (inner race with unbalance), at the low shaft speeds, acceleration signal shows only inner race fault and velocity signal shows only unbalance fault. At the high speeds, unbalance fault can be seen both in velocity and acceleration data.

REFERENCES

Al-Raheem, K.F., Roy, A., Ramachandran, K.P., Harrison, D.K., Grainger, S. (2007). *Rolling element bearing fault diagnosis using laplace-wavelet envelope power spectrum*. EURASIP Journal on Advances in Signal Processing, vol. 2007, Article ID 73629.

Chebil, J., Noel, G., Mesbah, M., Deriche, M. (2009). *Wavelet decomposition for the detection and diagnosis of faults in rolling element bearings.* JJMIE vol.3, no.4, 260-267

Condition Monitoring System. (n.d.). Retrieved July 10, 2010, from http://www.nordex-online.com/en/produkte-service/service/condition-monitoring-system.html.

Du, Q., Yang, S. (2006). *Improvements of the EMD method and applications in defect diagnosis of ball bearings*. Measurement Science and Technology, 17 2355-2361.

*FAG cylindrical roller bearings NU306-E-TVP2***.** Retrieved April 4, 2009, from http://medias.schaeffler.de/medias/en!hp.ec.br.zugprod/VRE3..-E*VRE306-E*NU3..-E*NU306-E-TVP2/.

Hariharan,V., Srinivasan,PSS. (2009). *Vibration analysis of misaligned shaft – ball bearing system.* India Journal of Science and Technology, Vol.2 No.9, 45-50.

Heng, R.B.W., & Nor, M.J.M. (1998). *Statictical analysis of sound and vibration signals for monitoring rolling.* Applied Acoustics, Vol.53, No. 1-3, pp.211-226.

Jardine, A.K.S., Lin, D., & Banjevic, D. (2006*). A review on machinery diagnostics and prognostics implementing condition-based maintenance*. Mechanical Systems and Signal Processing 20:1483-1510.

Kiral,Z., Karagülle,H. (2006). *Vibration analysis of rolling element bearings with various defects under the action of an unbalanced forces*. Mechanical System and Signal Processing, 20: 1967-1991.

Kumar, V., Gupta, S.P., Wadhwani,S. (2005). Wavelet based vibration monitoring for detection of faults in ball bearings of rotating machines.

Lebold, M., McClintic, K., Campell, R., Byington, C., & Maynard, K. (2000). *Review of vibration analysis methods for gearbox diagnostics and prognostics.* Proceedings of the 54th Meeting of the Society for Machinery Failure Preventation Technology, 623-634.

Liu, B., Ling, S.F., Gribonval, R. (2002). *Bearing failure detection using matching pursuit*. NDT & E International 35: 255-262.

Liu,J. (2008). *An intelligent system for bearing condition monitoring.* Ph. D. Thesis. The University of Waterloo, Canada.

Liu, J., Wang,W., Golnaraghi, F., Liu, K. (2008). *Wavelet spectrum analysis for bearing fault diagnostics*. Measurement Science and Technology 19 : 015105

Luo, G., Osypiw, D., Irle, M. (2003). *On-line vibration analysis with fast continuous wavelet algorithm for condition monitoring of bearings*. Journal of Vibration and Control: 931-947.

Miettinen, J., & Leinonen, P. (1999). *Monitoring of contaminants in a grease lubricated rolling bearing by acoustic emission in field environment*. Proceedings of the 2nd COST 516 Tribology Symposium. 243-252.

National Instruments Products for Wind Turbine Condition Monitoring. (n.d.). Retrieved June 5, 2010, from http://zone.ni.com/devzone/cda/tut/p/id/7676/.

Neter,J., Wasserman, W.,& Whitmore,G.A. (1988) *Applied statistics(*3rd ed.). United States of America: Allyn & Bacon, Inc.

Orhan,S., Aktürk,N., Çelik,V. (2006). *Vibration monitoring for defect diagnosis of rolling element bearings as a predictive maintenance tool: Comprehensive case studies*. NDT & E International 39: 293-298.

Ozturk, H., Yesilyurt, I., Sabuncu,M. (2010). *Detection and advancement monitoring of distributed pitting failure in gears.* J Nondestruct Eval 29 : 63-73.

Sendig911. (n.d.). Retrieved 2007, from http://www.sendig.com/old/E_E_911.html

Stack, J.R., Habetler, T.G., Harley, R.G. (2005). *Fault signature modeling and detection of inner race bearing faults*. Electric Machines and Drives, IEEE International Conference on May 2005.

Takeyasu, K., Higuchi, Y. (2006). *Analysis of the behavior of kurtosis and 6th normalized moment by simplified model and their application to machine diagnosis*. Osaka Prefecture University.

Tandon, N., Chouldhury,A. (1999). *A review of vibration and acoustic measurement methods for the detection of defects in rolling element bearings*. Tribology International, 32 469-480.

Tao, B., Zhu,L., Ding,H., Xiong,Y. (2007). *An alternative time-domain index for condition monitoring of rolling element bearings – A comparision study*. Reliability Engineering & System Safety 92 : 660-670.

Yen, G.G., Senior Member, IEEE, Lin, K.C. (2000). *Wavelet packet feature extraction for vibration monitoring*. IEEE Transactions on Industrial Electronics vol.47, no.3.

Zong,W.,Saeed M., Heldt T. (2006). *A QT interval detection algorithm based on ECG curve length transform*. IEEE International Conference on Computers in Cardiology, vol.33, pp. 377-380.

APPENDICES

List of Tables

Table 2.1 The distribution of the bearing failure(Lee,2000)……..18

Table 2.2 Types of bearing damages (Afshari, 1998)…….....20

Table 7.1 Geometrical parameters of FAG NU306-E-TVP2 ……63

Table 7.2 Inner Race Defect Frequencies of FAG NU306-E-TVP2……..63

Table 8.1 Scale Frequency Conversion (Shaft Speed)……80

Table 8.2 Scale Frequency Conversion (Inner Race Fault Characteristic Frequency)……..81